Programing strand displacement reaction pathways using small molecular DNA binders

By

Junpeng Xu

A Thesis Submitted to the Department of Chemistry

In Partial Fulfillment of the Requirements for the

Degree of Doctor of Philosophy

Faculty of Mathematics & Science, Brock University

St. Catharines, Ontario

Abstract

DNA has been used in nature as carriers of heredity information for billions of years. The last four decades have witnessed the success of DNA nanotechnology, an interdisciplinary research area in which DNA is used as a synthetic engineering tool rather than a carrier of genetic information. The growth of DNA nanotechnology crosses the boundaries between physics, chemistry, biology and computer science and enables DNA to function as an electronic component, substrate, drug delivery vector and data storage unit. The hybridization of DNA strictly follows the by Watson-Crick rule; thus, DNA base pairs are the most reliable and predictable building block in the true nanometer range. New methods and designs for controlling DNA hybridization have always provided the most essential momentum for the development of DNA nanotechnology.

When small molecules bind to the double helical structure of DNA, either through intercalation or minor groove binding, the stability and functionality of DNA may be significantly altered, which is a fundamental basis for many therapeutic and sensing applications. Herein, we reveal, for the first time, that small molecular DNA binders may also be used to program the reaction pathways of toehold-mediated DNA strand displacement, an elementary building block in DNA nanotechnology.

In this thesis, by combining experimental measurements and in silico simulations, we demonstrate that the Gibbs free energy of strand displacement can be tuned quantitatively according to the affinity, charge condition, and concentration of a given

DNA binder. Based on this finding, we developed a Binder-Induced Nucleic acid Displacement (BIND) technology that enables the interactions between DNA and small molecular binders to be comprehensively profiled. All critical thermodynamic parameters, including dissociation constant, binding site size, cooperativity, reaction enthalpy and entropy, as well as sequence selectivity can be obtained in a single, unbiased molecular platform without the need for any specialized equipment (Chapter 2). We also demonstrate that it is possible to program a single strand displacement reaction using two different binders in tandem. Using this principle, we further engineered two tandem BIND systems as high-throughput screening assays for discovering new DNA binders, through which 19 new DNA binders were successfully discovered from a library of 1170 compounds (Chapters 3 & 4). By programming strand displacement reaction pathways using DNA binders, BIND may inspire new designs and applications of DNA nanotechnology, as well as novel molecular tools for the comprehensive profiling and discovery of DNA-small molecule interactions.

Acknowledgement

I would like to express my thankfulness to my principal investigator, Dr. Feng Li for providing me with this exceptional tour in dynamic DNA nanotechnology guided by his insightfulness, perception, endurance, knowledge and unwavering encouragement in researching for unknown world. Thank you for being the guiding star on my way to success.

I would like to thank my family members: my mother, my step father and my father for supporting both financially and emotionally during my PhD program. In particular, my father might not be able to physically celebrate with me on the day when I decided to successfully defend my PhD thesis as he just passed away months ago. However, thank you for watching over me and I am sure that you will receive this good news at another world when the day comes.

I would like to thank my committee members: Dr. Van Der Est, Arthur and Lemaire, Martin for questioning, consulting and solving each problem with willingness and kindness. I would like to thank my colleagues and friends for their assistance and help. I would like to thank myself for not choosing the option of giving up whenever such an option is available. I truly enjoyed the PhD journey at Brock University, St. Catharines, Ontario, Canada.

Table of Contents

List of Figures

List of Tables

List of Equations

Equation 2.1 $CP \rightarrow C + P,\ K_D$

Equation 2.2 $C + I \rightarrow CI,\ K_H$

Equation 2.3 $CP + I \rightarrow CI + P,\ K_{S_N1}$

Equation 2.4 $CP + I \rightarrow CPI \rightarrow CI + P,\ K_{S_N2}$

Equation 2.5 $\Delta G^{\circ}_{BIND} = \Delta G^{\circ}_{ini} + \theta \cdot C_{Binder}$

Equation 2.6 $\Delta G^{\circ}_{BIND} = \Delta G^{\circ}_{ini} + (\theta - \xi) \cdot CBC + \xi \cdot C_{Binder}$

Equation 2.7 $^{v}/_{L} = K_a \,.\, {(1-nv)^n}/{(1-nv+v)^{n-1}}$

Equation 2.8 $^{v}/_{L} = \mathrm{K_a}(1-\mathrm{nv})\left[\frac{(2\omega-1)(1-\mathrm{nv})+\mathrm{v}-\mathrm{R}}{2(\omega-1)(1-\mathrm{nv})}\right]^{(n-1)}\left[\frac{1-(n+1)v+R}{2(1-nv)}\right]^2$

Equation 2.9 $ln\ K_a = -\frac{\Delta H}{RT} + \frac{\Delta S}{R}$

Equation 2.10 $Y = \frac{n\cdot(C_{binder}-C_{DNA}\cdot\frac{Y}{n})\cdot K_a\cdot(1-Y)^n}{(1-Y+\frac{Y}{n})^{(n-1)}}$

Equation 2.11 $Y = K_a(1-Y)(\frac{(2\cdot\omega-1)\cdot(1-\mathrm{Y})+\frac{Y}{n}-R}{2\cdot(\omega-1)\cdot(1-\mathrm{Y})})^{n-1}\left(\frac{1-(n+1)\cdot\frac{Y}{n}+R}{2\cdot(1-Y)}\right)^2\left(C_{binder} - \frac{Y\cdot C_{DNA}}{n}\right)n$

Equation 2.12 $ln\ K_a = -\frac{\Delta H}{RT} + \frac{\Delta S}{R}$

Equation 3.1 $Z' = 1 - \frac{3(\sigma_{P.C.}+\sigma_{N.C.})}{|\mu_{P.C.}-\mu_{N.C.}|}$

Equation 3.2 $Z = 1 - \frac{3(\sigma_{Sample}+\sigma_{P.C.})}{|\mu_{Sample}-\mu_{P.C.}|}$

Equation 3.3 $Y = \frac{n\cdot(C_{binder}-C_{DNA}\cdot\frac{Y}{n})\cdot K_a\cdot(1-Y)^n}{(1-Y+\frac{Y}{n})^{(n-1)}}$

Equation 3.4 $ln\ K_a = -\frac{\Delta H}{RT} + \frac{\Delta S}{R}$

Equation 4.1 $Y = \frac{n\cdot(C_{binder}-C_{DNA}\cdot\frac{Y}{n})\cdot K_a\cdot(1-Y)^n}{(1-Y+\frac{Y}{n})^{(n-1)}}$

Equation 4.2 $ln\ K_a = -\frac{\Delta H}{RT} + \frac{\Delta S}{R}$

List of Abbreviations

BIND	binder-induced nucleic acid displacement
HTS	high throughput screening
DNA	deoxynucleotide acid
RNA	ribonucleic acid
ssDNA	single-stranded DNA
dsDNA	double-stranded DNA
Da	Dalton
SG-I	SYBR Green I
SNVs	single-nucleotide-variants
TMSDs	toehold mediated strand displacement
SMFS	single-molecule force spectroscopy
PCR	polymerase chain reaction
MGB	minor groove binder
EB	ethidium bromide
PG	Pico Green
HPLC	high-performance liquid chromatography
UV/UV-Vis	ultra-violet/UV-Visible
ITC	isothermal titration calorimetry
DSC	differential scanning calorimetry
T_m	melting temperature
FRET	fluorescence resonance energy transfer
FID	fluorescent intercalator displacement
FIDA	fluorescence intensity distribution analysis
AI	artificial intelligence
TO	thiazole orange
DAPI	4’,6-diamidino-2-phenylindole
I	invading strand
P	protecting strand
C	complementary strand
8-HQ	8-hydroxyquinoline
CD	circular dichroism
NMR	nuclear magnetic resonance
FTIR	Fourier-transform infrared spectroscopy
DEG	DNA equalizer gate
MS	mass spectroscopy
CBC	critical binder concentration
IDT	Integrated DNA Technologies
NMEs	new molecular entities
BLAs	biologics license applications
BBB	blood-brain barrier
FDA	food & drug administration

PDB	protein data bank
PM1	1×PBS buffer with 1 mM $MgCl_2$
TE	1×Tris-EDTA buffer
SMFS	single-molecule force spectroscopy
WLK	worm-like chain
FJC	freely jointed chain
1-BQC	1-benzylquinolinium chloride

Chapter 1

Introduction of dynamic DNA nanotechnology responsive to nonnucleic acid inputs, DNA-small molecule interaction and small DNA binder HTS method

1.1 Dynamic DNA nanotechnology responsive to nonnucleic acid inputs

DNA nanotechnology is a multidiscipline field that combines chemical synthesis, molecular biology and computer science.[1] In this field, DNA is recognized as a nonbiological engineering material rather than a carrier of genetic information. Governed by the Watson-Crick base paring rule, nucleic acids possess high programmability and affordability, thus, DNA is the most reliable and manufacturable device on the true nanoscale among all biological and synthetic substances.

The DNA nanotechnology can be roughly divided into the following fields: structural DNA nanotechnology, in which two- and three-dimensional objectives of varying sizes and complexity are constructed through “bottom-up” DNA self-assembly,[2] and dynamic DNA nanotechnology, in which the nonequilibrium dynamics of DNA chemistry are emphasized to precisely program and control materials,[3] machineries,[4] or even the function and fate of living cells[5].

1.1.1 Overview of dynamic DNA nanotechnology

Dynamic DNA nanotechnology is built based on synthetic nucleic acid strand displacement reactions,[6] and the focus of this field is mainly on the hybridization/dehybridization process of DNA strands rather than their overall stable

structures at the final stage. This field can be roughly divided into the following areas: DNA nanomechanical devices and DNA strand displacement reaction networks. In 2000, Yurke et al. reported a DNA molecular machine that was fueled by itself.[7] This nanomachine was a DNA tweezer, while the exchange between the open and closed forms of the DNA nanostructure was governed by a pair of fully complementary DNA strands (Fig. 1). Dr. George Church and his research group provided another example in which dynamic DNA nanotechnology was applied to obtain a reconfigurable DNA nanostructure.[8] They designed a DNA origami clamp with two hinges. Each hinge consists of a pair of partially complementary DNA strands and one of them is a specific protein aptamer. When this specific protein key is in close contact with this payload delivery vector, the hinge disengages and releases the engulfed molecules such as gold nanoparticles or antibodies to the target site (Fig. 2). Nanorobot designs based on dynamic DNA nanotechnology can not only deliver their payload, but also sort randomly distributed cargos into ordered arrays. Dr. Lulu Qian reported a DNA nanomachine design with sorting ability.[9] In her design, two types of cargos (yellow and green) were conjugated with two sequences of single-stranded DNA (ssDNA) (yellow tail or green tail). By moving these two types of ssDNA together, they successfully sorted randomly distributed cargos into two piles of cargos (Fig. 3).

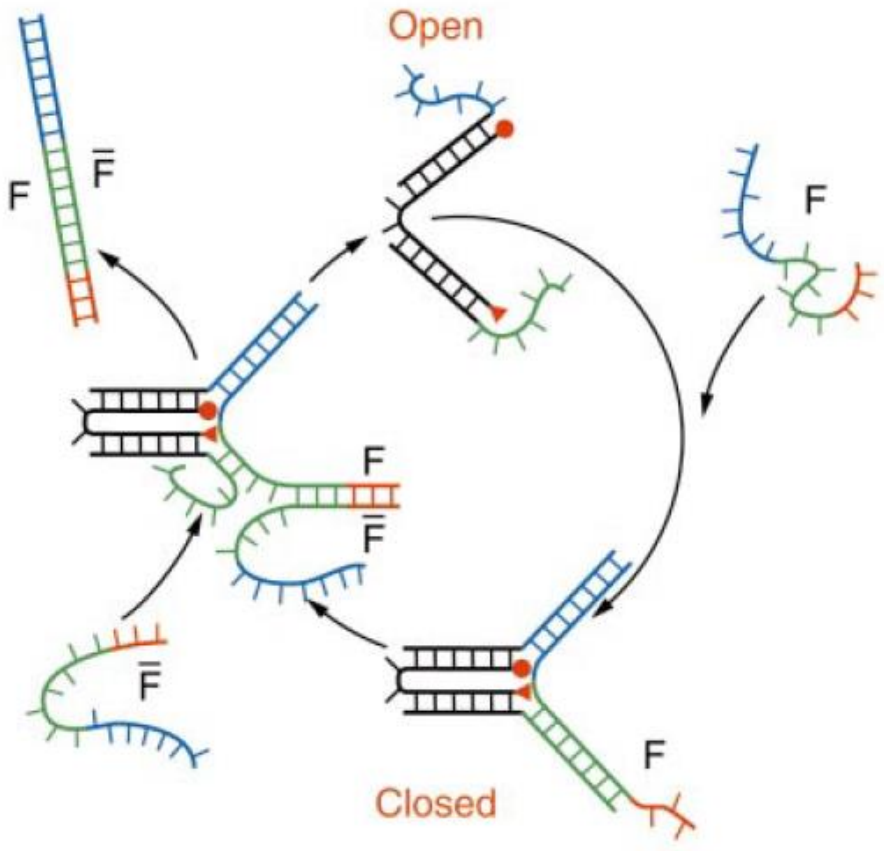

Fig. 1 | A switchable DNA tweezer governed by a pair of fully complementary DNA strands. The overall configuration of the DNA nanotweezer was determined by whether ssDNA F was hybridized at the 'blade' region. The open or closed status was reported by a fluorophore/quencher pair modified at the bottom of each 'blade'. The images (ref 7) were reproduced with permission.

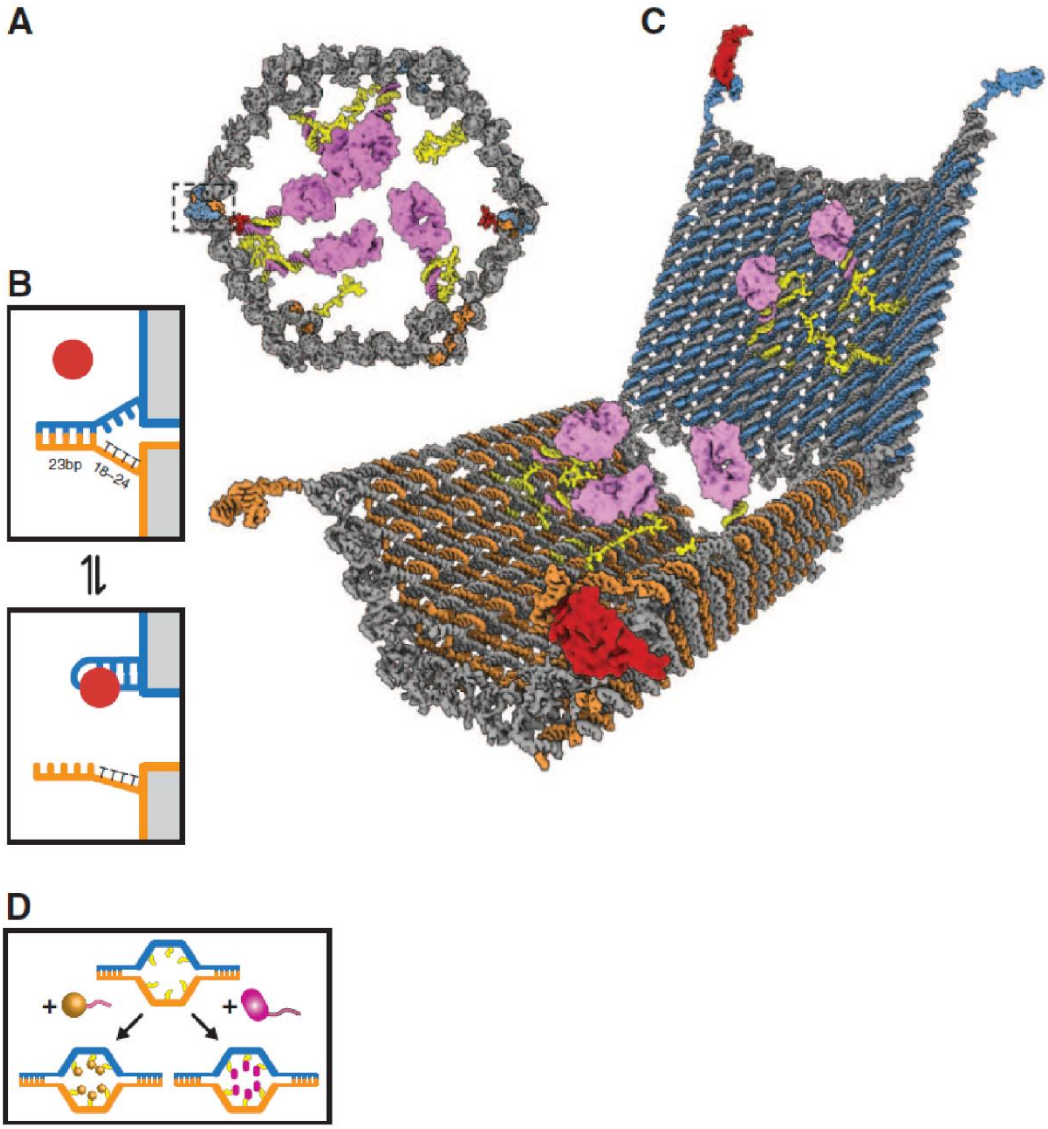

Fig. 2 | Design of a DNA nanorobot directed by two aptamer hinges. a. Front orthographic view of a drug loaded DNA nanorobot. The aptamer hinges were locked and framed on the graph. **b.** Aptamer hinge released by specific protein stimuli. **c.** Perspective view of a DNA nanorobot at open status with its payload ready to be released. **d.** These versatile drug loading and delivery vectors could be loaded with multiple payloads including gold nanoparticles or antibody Fab' fragments. The images (ref 8) were reproduced with permission.

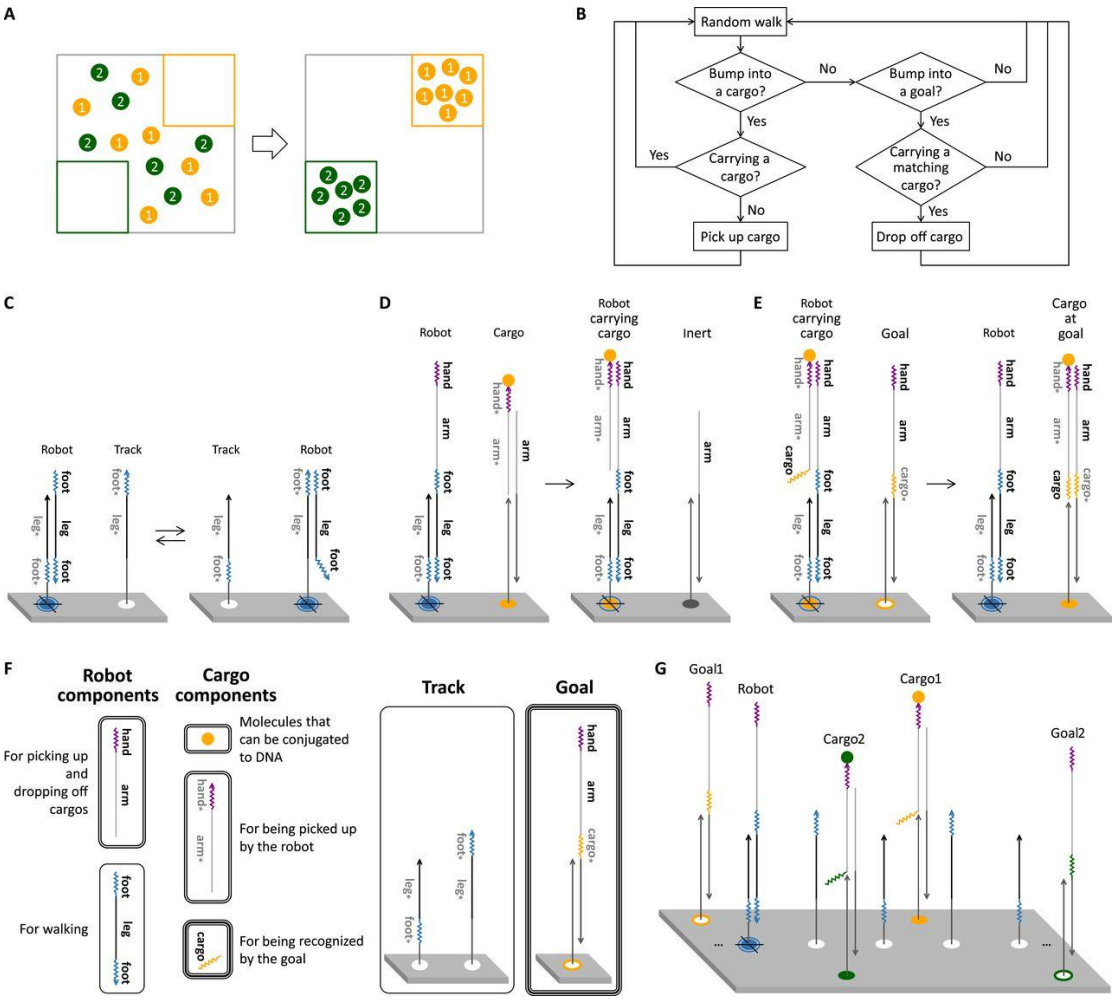

Fig. 3 | The cargo sorting and transportation algorithm of a DNA nanorobotic design. a. Schematic diagram of sorting randomly distributed molecules into piles at the upper-right and bottom-left corners. **b.** Flowchart of a single cargo-sorting mechanism. **c-e.** Algorithm of random walk (c), cargo loading (d) and cargo dropping (e) based on dynamic DNA nanotechnology design. **f.** Components of DNA robots, DNA cargo storing strands, DNA robot walk tracks and cargo dropping stations. **g.** The initial state of the cargo-sorting platform. The images (ref 9) were reproduced with permission.

DNA strand displacement reactions and reaction networks can be used to design various logic gates and DNA computing networks, which is another major aspect of dynamic DNA nanotechnology. Dr. Lulu Qian designed a DNA displacement reaction network that is capable of recognizing English letters and Arabic numbers, not only for printed versions, but also for corrupted versions of figures.[10] Even with vague writing,

the system could determine which figure was most likely to be expected by the writer with a parameter called the weighted sum (Fig. 4). On the other hand, diagnostics could also benefit from applying DNA computing networks. In recent years, Dr. Li and his colleagues designed a DNA equitizing gate (DEG)[11] to identify single-nucleotide variants (SNVs) and significantly expanded the narrow detection window between correct and spurious samples in which the SNVs were shown to have significant clinical implications and consequences and were usually hard to identify due to thermodynamical similarity (Fig. 5).

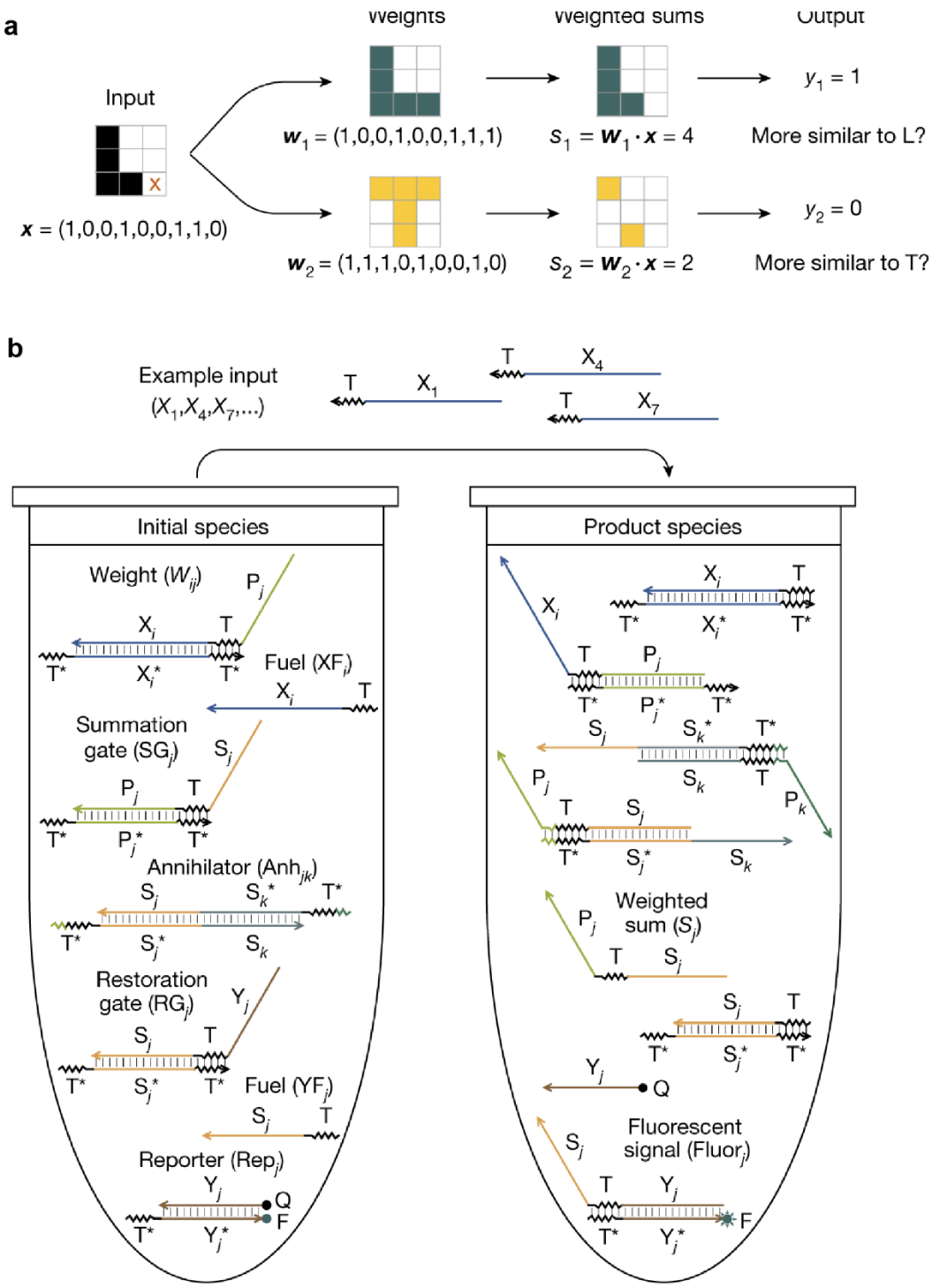

Fig. 4 | Application of the DNA strand displacement network in figure recognition. **a.** Illustration of using target patterns as weights to recognize a corrupted writing of 'L'. **b.** DNA strand displacement network in calculating the weighted sum for figure recognition purposes. The images (ref 10) were reproduced with permission.

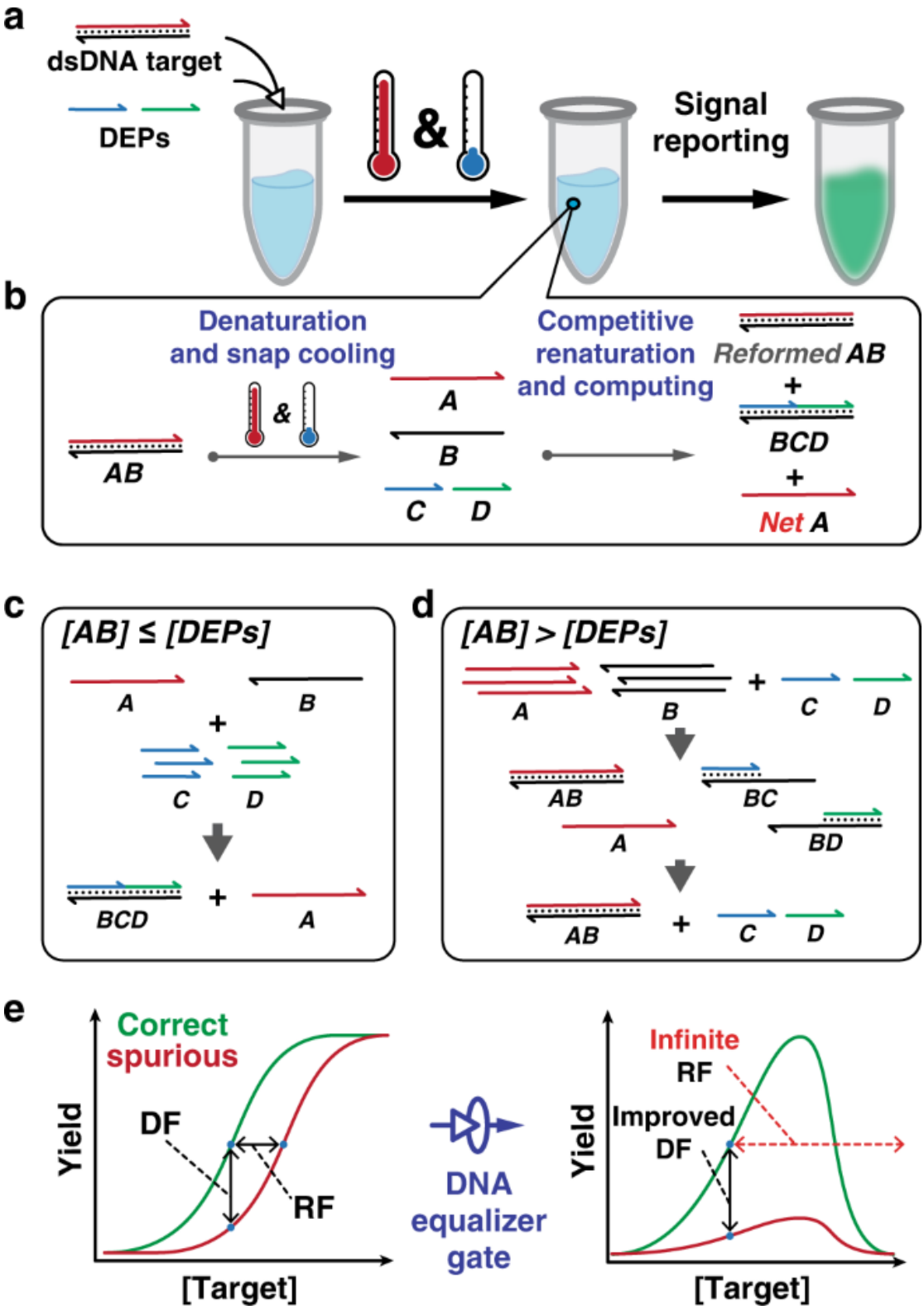

Fig. 5 | Algorithm of the DNA equalizer gate. a-b. The overall workflow of a DEG gate. **c-e.** DNA strand displacement reaction network applied in SNV detection and the DNA equalizer gate (DEGs) can expand the detection window of SNVs. The images (ref 11) were reproduced with permission.

1.1.2 Toehold-mediated DNA strand displacement

DNA strand displacement is among the most important foundations for dynamic manipulation of DNA nanotechnology.[12] In a hybridized DNA duplex, the introduction of the third invading strand binds to one of the prehybridized DNA single strands and replaces a prehybridized "incumbent" strand in a process called DNA strand displacement.[13]

Among all approaches designed to achieve a tunable DNA strand displacement, toehold mediated strand displacement (TMSD)[14] is the most widely applied and easily controlled method to isothermally complete a reaction displacing nucleic acid strands (Fig. 6). The 'toehold' represents a short and single-stranded overhang that can initiate the annealing between a newly introduced ssDNA input and the preannealed double-stranded DNA (dsDNA). The introduced ssDNA, also named invading strand (I) starts to displace the shorter strand (protecting strand, P) within the preannealed duplex after the hybridization of the toehold region is completed. The competition of displacement is named the branch migration process and is theoretically calculated and experimentally confirmed in a 'random walking' manner. The TMSD is finished when the protecting strand is discarded and the invading strand is fully hybridized with the substrate (complementary strand, C). The overall reaction is thermodynamically favored as more base pairs are formed.[15]

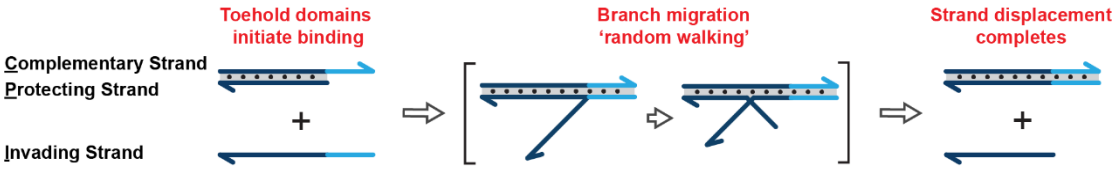

Fig. 6 | Traditional TMSD illustration. The TMSD initiated at the annealing of the I with CP duplex at toehold region, and progressed by the random walking fashion by the competition between the I and P, and completed by the dissociation of P with full hybridization between I and C (Xu et al. 2023, unpublished).

Since the development of TMSD in 2000, the success of dynamic DNA nanotechnology has been driven primarily by new strategies for activating toeholds. Unlike traditional TMSD where the toehold is unprotected and the binding of the invading strand with duplexed DNA overhang always happens almost instantly when the invader is injected. In the new toehold design, the invading strand can only interact with the toehold domain at close proximity when toehold protection is removed, resulting in programmed and timed activation of strand displacement such as remote toehold,[16] associative toehold,[17] allosteric toehold,[18] cooperative hybridization[19] (Fig. 7) as well as nonnucleic acid activated toehold systems such as photo[20] and enzymatic[21] regulation. We aim to construct a novel strand displacement system that is responsive to a new type of nonnucleic acid element by introducing duplexed DNA interacting small molecules into a traditional TMSD reaction.

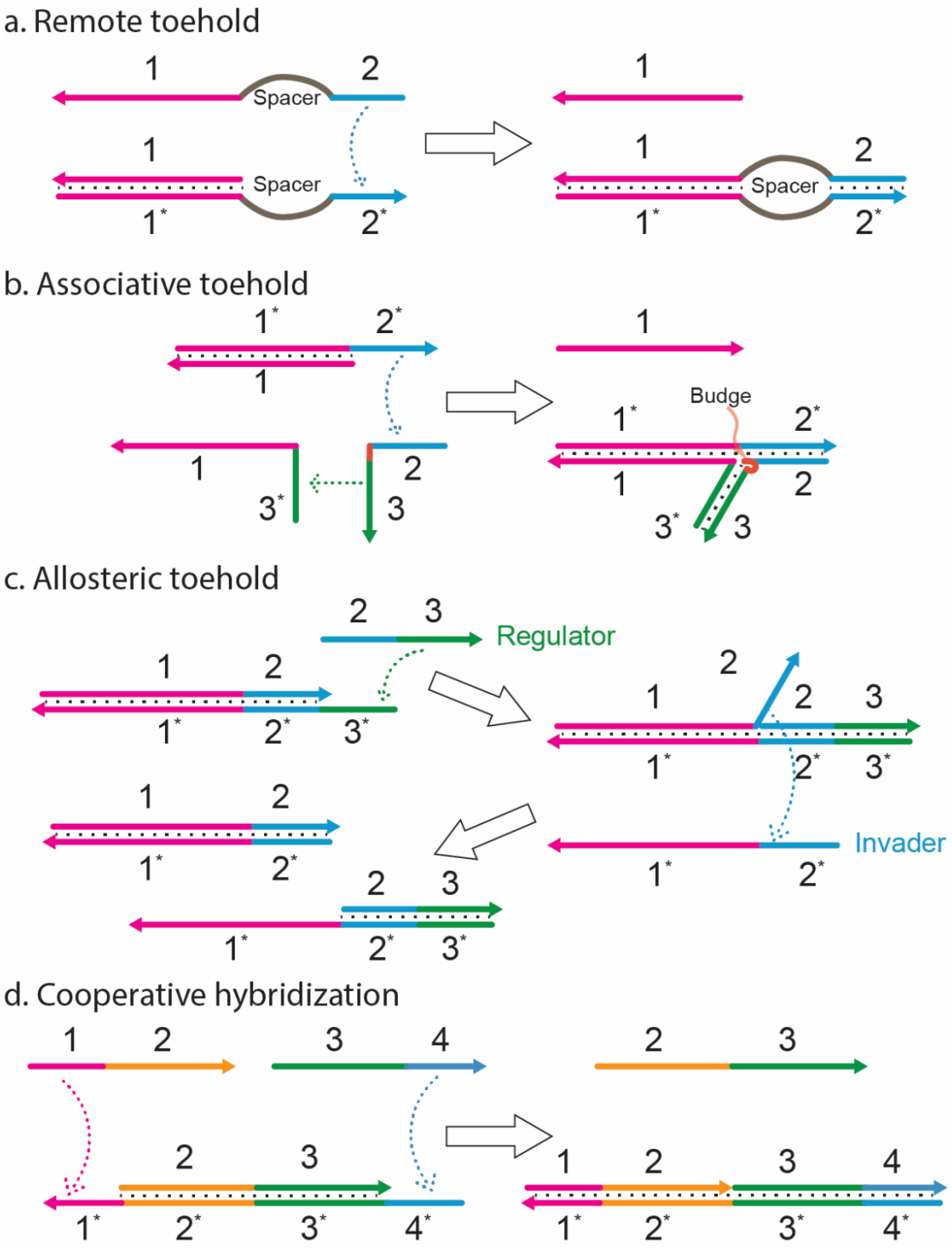

Fig. 7 | New strategies in toehold protection and activation. a-d. New toehold activation designs illustrated for remote toehold (a), associative toehold (b), allosteric toehold (c), cooperative hybridization (d) respectively (Xu et al. 2023, unpublished).

1.1.3 Strand displacement mediated by proximity binding

DNA strand displacement can be regulated by non-DNA species such as proteins, metal ions and other types of molecules through proximity binding.[22, 23] In brief, for a

partially or fully hybridized ssDNA (substrate), interacting with the third invading ssDNA (complementary to the abovementioned ssDNA) at close range will trigger an enhanced rate of strand exchange via DNA hybridization between the abovementioned ssDNA and the third invading strand as well as displacing of the protecting (incumbent) strand. This phenomenon occurs because the much-increased local concentration of the third invading strand shifts the equilibrium of DNA chemistry to the product (substrate and invading strand hybridization). In a protein directed DNA proximity binding,[24] two DNA motifs OT and C were both conjugated with a pair of affinity ligands to a specific target protein. The complementary region of OT was designed to have the same length and sequence as C and OT was prehybridized. When the target protein was absent, the displacement rate was extremely low. When the target protein was introduced and the two conjugated affinity ligands were associated with the protein therefore forcing C to be in close proximity with OT, the strand displacement rate was significantly enhanced as the local concentration of C was significantly increased (Fig. 8).

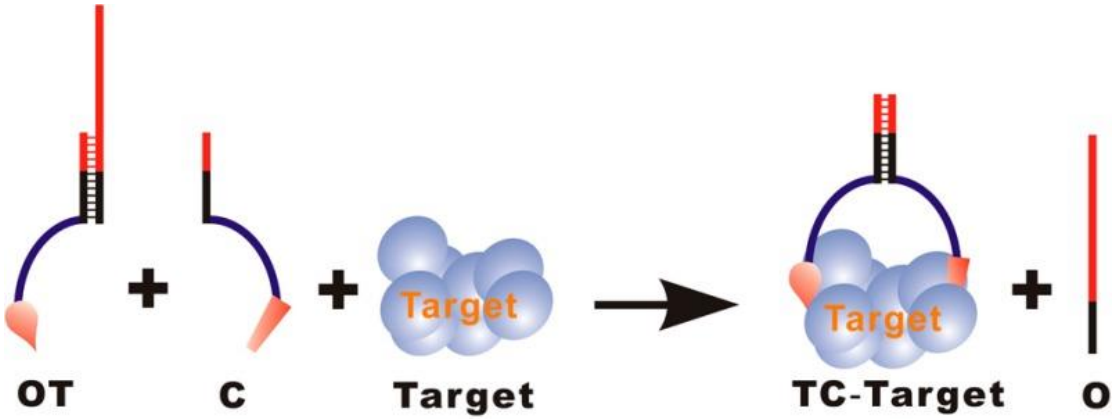

Fig. 8 | Protein binding-induced DNA strand displacement illustration. Displacement of C over O is significantly enhanced when its affinity ligand of C and OT binds at an epitope of the target protein to maintain proper distance. The images (ref 24) were reproduced with permission.

Metal ions could also trigger proximity binding, unlike conventional TMSD

design, the single strand overhang (toehold) was replaced by 8-hydroxyquinoline (8-HQ), which is a small molecule structure that is able to chelate several divalent metal ions.[25] The percentage of successful invasion was significantly increased when the invading strand was in close proximity with the prehybridized duplex in the presence of proper metal ions that chelated the pseudo toehold 8-HQ (Fig. 9).

Fig. 9 | DNA strand displacement mediated by metal-ligand complexation. The presence of divalent metal ions stabilizes the chelator structure thus mediating the overall strand displacement. The images (ref 25) were reproduced with permission.

1.1.4 Strand displacement mediated by functional nucleic acids

DNA strand displacement could also be triggered by functional nucleic acids such as aptamers or DNAzymes. In an aptamer triggered displacement design,[26] modified with green donor fluorophore (green circle) and red acceptor fluorophore (red circle), was treated with or without adenosine in an aqueous solution. The adenosine within the reacting mixture bound with its aptamer sequence (long strand) and forced this strand to dissociate from its capturing strand (short strand), then and subsequently regulated the overall strand displacement of DNA (Fig. 10).

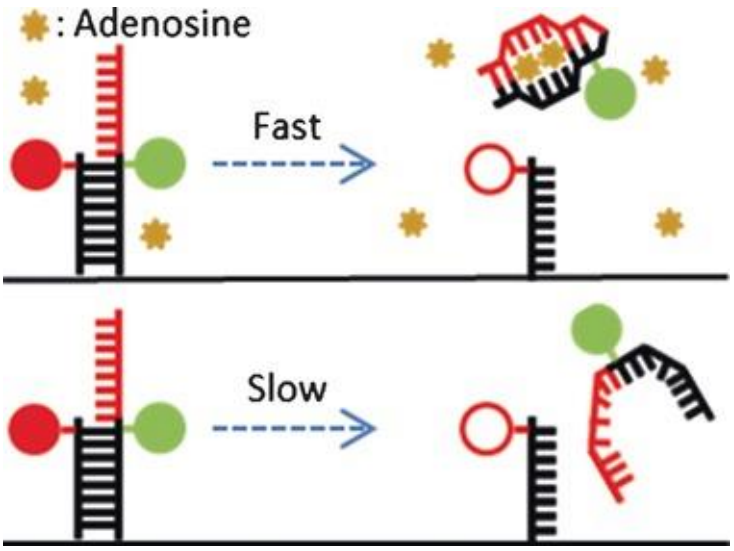

Fig. 10 | DNA strand displacement mediated by aptamer. The presence of adenosine forces the aptamer sequence (long strand) to dissociate from its capturing strand (short strand), while simultaneous dehybridization of the duplexed structure without adenosine in this system is slow. The kinetics are monitored by the Cy3-Cy5 fluorescence resonance energy transfer (FRET) method. The images (ref 26) were reproduced with permission.

Another example is a DNAzyme-regulated strand displacement reaction.[27] Initially, the system consisted of A/A' with an H1 hairpin in which the DNAzyme cleaving site was located at the middle of the hairpin loop. The introduction of T1 displaced A' through conventional TMSD and completed the formation of the DNAzyme, and hybridization of the hairpin loop with duplex A/T1 positioned the hairpin cleaving site at a proper location for A/T1 cleavage. The H1 hairpin was then scissored at the middle and H1a and H1b disengaged. The dissociated H1a displaced A from T1 via another TMSD reaction and depleted the newly formed DNAzyme (Fig. 11).

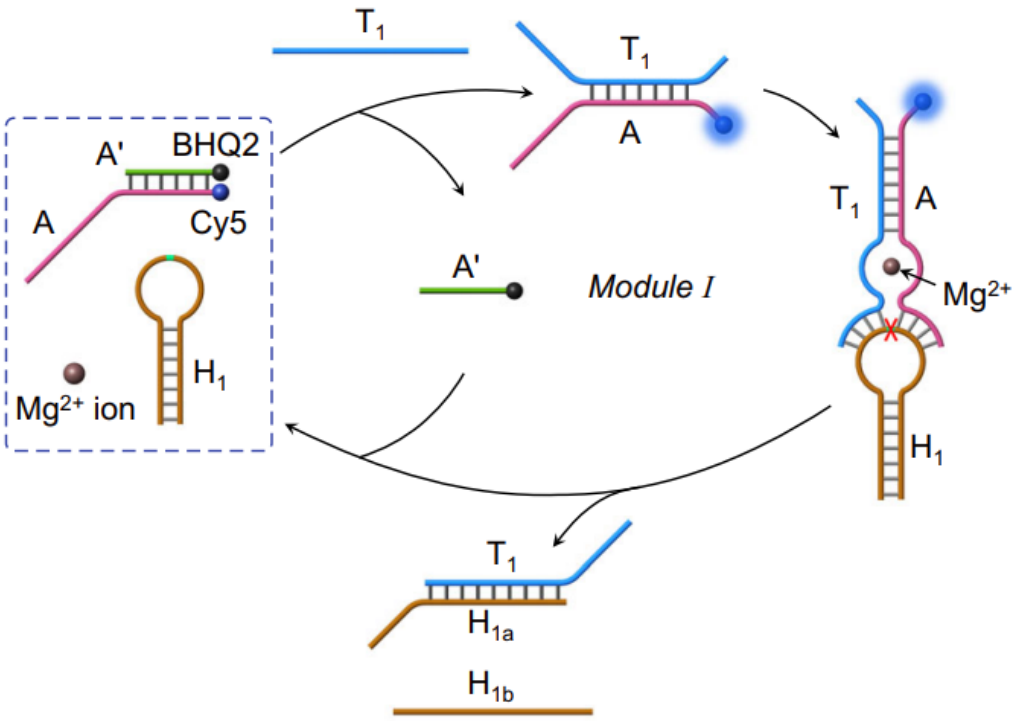

Fig. 11 | A DNAzyme regulated strand displacement reaction. The pathway for the formation-depletion of DNAzyme is illustrated above. The image (ref 27) was reproduced with permission.

Overall, dynamic DNA nanotechnology is thriving, as new methods to mediate DNA strand displacement are being discovered, as well as new concepts for tuning DNA strand displacement based on new toehold designs for nonnucleic-acid molecule stimuli as well as functional nucleic acids. These achievements expanded our toolbox in shaping and utilizing these nucleic acid-based nanotechnologies.

1.2 DNA-small molecule interactions

Small DNA binders are a group of small molecules that interact with DNA, especially dsDNA via electrostatic, hydrophobic, allosteric, hydrogen bonding and/or van der Waals interactions. These binding interactions may distort the DNA structure and alter the small molecule structure, showing great promise in both DNA tracing and disease curing applications.[28]

1.2.1 Overview of dsDNA-small molecule interaction

Quite a few dsDNA binding small molecules are ancient drugs. The application of quinine (later identified as a DNA intercalator) for antiparasitic purposes can be traced back to the early 1630s when Cinchona bark was documented to treat malaria by physicians.[29] Actinomycin D, the first compound isolated from soil microbe *Streptomyces* species in the 1940s, possesses anticancer properties.[30] Roughly ten years later, the first chemotherapy drug was discovered, which belongs to the family of anthracyclines: daunorubicin was discovered from the same strain of species and remained one of the pillars of chemotherapeutic treatment.[31] Since then, more than a thousand anthracyclines and their derivatives have been researched biomedically and clinically for antineoplastic purpose, such as doxorubicin, idarubicin and pirarubicin.[32] Apart from the cytotoxicity application, many duplexed DNA binding small molecules were also used for DNA tracing purposes; SYBR GREEN I (SG-I),[33] ethidium bromide (EB),[34] thiazole orange (TO)[35] and Hoechst 33258[36] were widely applied for DNA quantification, and 4',6-diamidino-2-phenylindole (DAPI) was also used as cell nucleus locating agent due to its DNA binding and nucleus membrane penetrating properties.[37]

1.2.2 Mechanism of dsDNA-small molecule interactions

The mechanism of dsDNA-small molecule interactions can be categorized into the following types: major groove binding, minor groove binding, electrostatic/allosteric binding and intercalation (Fig. 12). Groove binders are a class of small molecules that bind to DNA major grooves or minor grooves. Compounds less than 1000 Dalton (Da)

usually preferred to bind into DNA minor grooves rather than major grooves because minor grooves are usually narrower and shallower. Minor groove binders often have crescent shapes to fit the DNA minor groove structure while major groove binders are more structurally versatile. Electrostatic/allosteric binding is the weakest interaction among the four and is often involved in the interaction of DNA with mono- or di-valent metal ions. A DNA intercalating agent usually possesses a planar polyaromatic system characterized by the insertion of a polyaromatic ring between base pairs. The process of base pair stacking occurs perpendicular to the DNA backbone without destroying hydrogen bonds between the DNA bases, unwinds the DNA double helical structure, elongates the neighboring base pairs and increases the DNA contour length. The ability to discriminate the binding fashion between small molecules and target DNAs is critical for rational design/modification and tuning the overall dsDNA-small molecule interaction.[38]

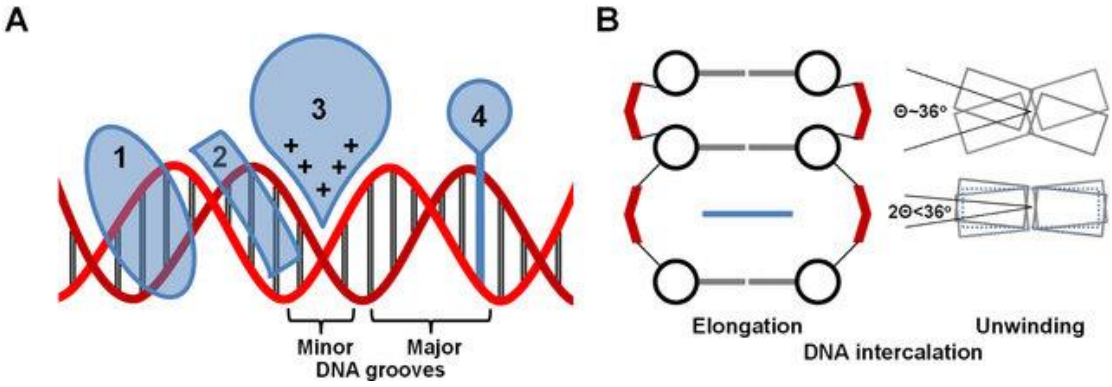

Fig. 12 | Illustrations of different DNA binding modes. a. Small molecules interact with DNA via 1) major groove binding, 2) minor groove binding, 3) electrostatic/allosteric binding and 4) intercalation. **b.** The DNA intercalator elongates the DNA base pairs and unwinds the overall DNA duplexed structure. The images (ref 38) were reproduced with permission.

1.2.3 Functionality of dsDNA binders

The “central dogma” describes that DNA is transcribed to RNA and then RNA translates to protein; therefore, DNA interference may be deemed the highest controller of protein production. The small molecule-DNA interaction can thus disrupt vital biological activities, such as protein recognition, protein synthesis and DNA duplication, which serves the fundamental basis for many anticancer, antimicrobial and antiparasitic pharmaceuticals.[39] Binder-DNA interactions could also be applied as chemical probes for sensing, imaging and quantifying nucleic acids in diverse settings.[40-44] Recent advances in designing, screening and understanding novel DNA binders not only promoted our knowledge of their essential roles in critical biological processes, such as DNA replication,[45] DNA damage[46-48] and transcriptional regulation,[49] but also resulted in exciting novel applications ranging from guiding the differentiation of pluripotent stem cells,[50] to epigenetic regulation,[51, 52] and inducing trinucleotide-repeat contraction (Fig. 13a and 13b).[53] Beyond their important roles in biological systems, DNA binders have also been increasingly applied in artificial systems for constructing and controlling DNA origami assembly and conformation,[54] stabilizing DNA nanostructures against low-magnesium buffers[55] and nuclease degradation,[56] modulating the bond strength of DNA-nanoparticle superlattices[57] and constructing DNA-based rectifier (Fig. 13c)[58] and excitonic circuits.[59]

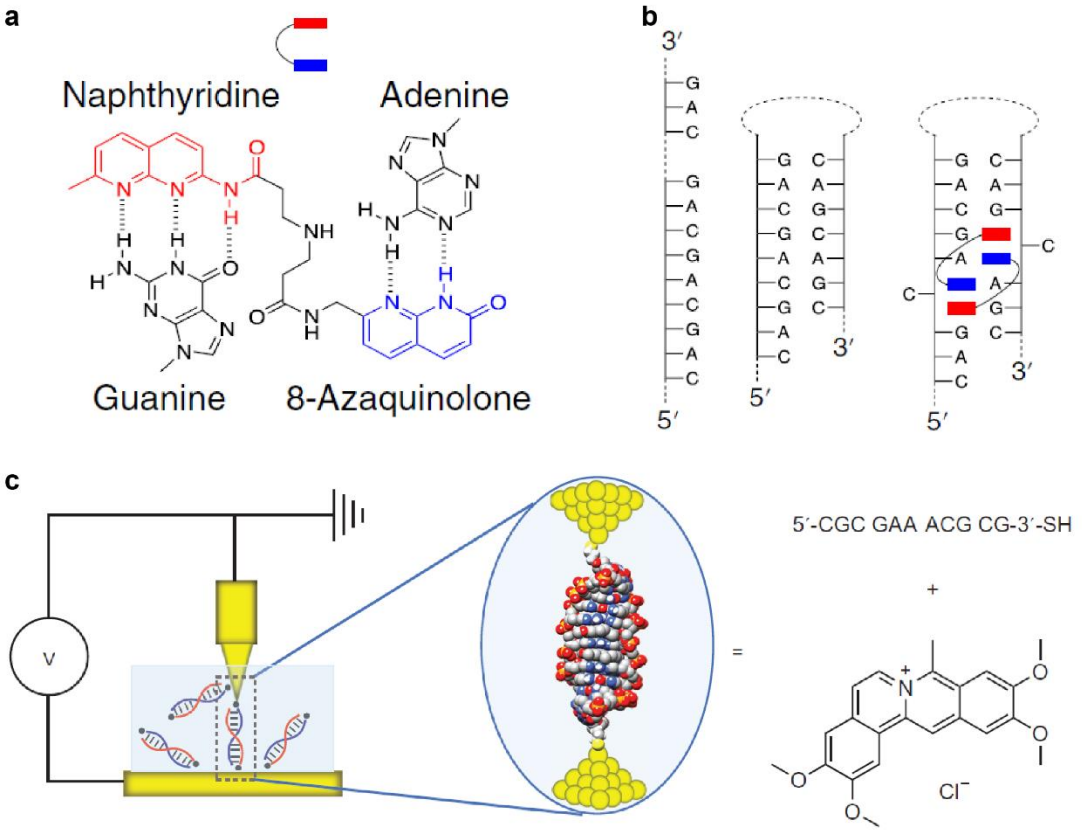

Fig. 13 | Application of small DNA binder at a biological and a nonbiological field. a-b. The structure of the ds-DNA interacting small molecule naphthyridine-8-azaquinolone (a) and its mechanism in inducing trinucleotide-repeat (CAG) contraction (b). **c.** The small DNA binder coralyne is applied to bind with the dsDNA strand and the bound DNA duplexed structure can be used as a rectifier. The images (ref 53 & 58) were reproduced with permission.

1.2.4 Techniques used to characterize dsDNA-small molecule interactions

dsDNA-small molecule interactions are most widely characterized by spectroscopic approaches.[60] Quite a few small molecule binders undergo fluorescence alternation after fitting themselves within DNA and this structural change can be monitored through fluorimetry.[61-63] The spectroscopic property changes due to binder-DNA conjugation can also be analyzed and quantified by ultraviolet-visible (UV-vis) absorption spectroscopy (Fig. 14)[64] and circular dichroism (CD).[65] Other spectroscopic techniques including H^1 nuclear magnetic resonance (NMR),[66] Fourier-transform

infrared spectroscopy (FTIR)[67] and mass spectrometry (MS)[68] have also been used to obtain vital information on binder-DNA interactions.

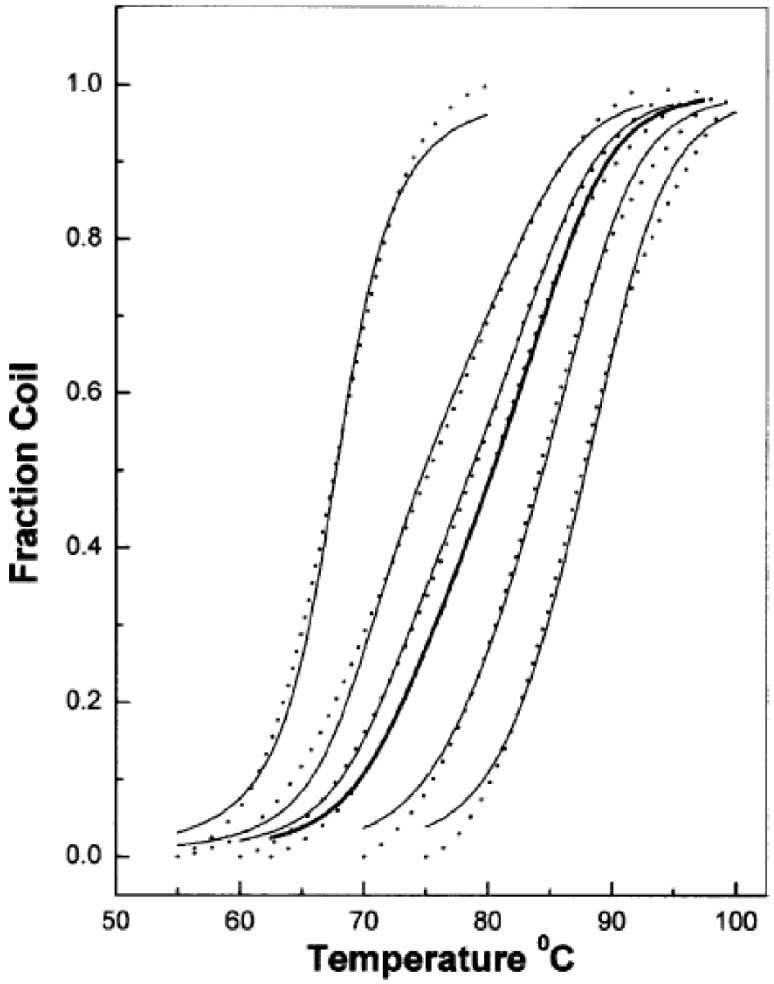

[DNA] (M bp)	[echino] (M)	K (M^{-1})	n (bp)	$[echino]_{sim}$ (M)	σ
5.0×10^{-5}	0	0	0	0	2.8×10^{-3}
5.0×10^{-5}	2.5×10^{-6}	4.5×10^{5}	5.3	2.9×10^{-6}	2.3×10^{-3}
5.0×10^{-5}	4.0×10^{-6}	4.5×10^{5}	5.3	4.2×10^{-6}	2.4×10^{-3}
5.0×10^{-5}	5.0×10^{-6}	4.6×10^{5}	5.3	4.9×10^{-6}	2.4×10^{-3}
5.0×10^{-5}	1.0×10^{-5}	4.5×10^{5}	5.3	7.3×10^{-6}	2.7×10^{-3}
5.0×10^{-5}	2.0×10^{-5}	4.5×10^{5}	5.3	1.05×10^{-5}	3.4×10^{-3}

Fig. 14 | Parsing DNA-binder interaction with DNA denaturation research. Analyzing DNA-binder interactions with melting analysis were a rigorous yet laborious method. Fixed concentrations of DNA with varying concentrations of ligands were mixed and examined in a UV-vis spectroscopic machine for complete melting curve analysis. The dashed lines are the experimental results and the solid lines are the best fit via successive approximation. The ligand concentration was usually altered for simulation for best fitting, and σ was the nucleation parameter for simulation with varying range. In all, human artifacts must be considered for the best fitting results. The images (ref 64) were reproduced with permission.

DNA denaturation studies are another method to obtain binding parameters based on McGhee's theory of the helix-coil transition of DNA.[69] Instruments that are extremely sensitive to tiny amounts of heat transfer can monitor bind-DNA interactions so that both isothermal titration calorimetry (ITC)[70] and differential scanning calorimetry (DSC)[71] can provide complete thermodynamic profiles as well as binding affinity.

The state-of-the-art technology of single-molecule force spectroscopy (SMFS) focuses on the duplexed DNA transition between worm-like chains (WLC) and freely jointed chains (FJC) to calculate the energy needed to obtain the force-induced melting transition of unbound and bound DNA, and binding affinity could be obtained with force/extension data analysis (Fig. 15).[72, 73]

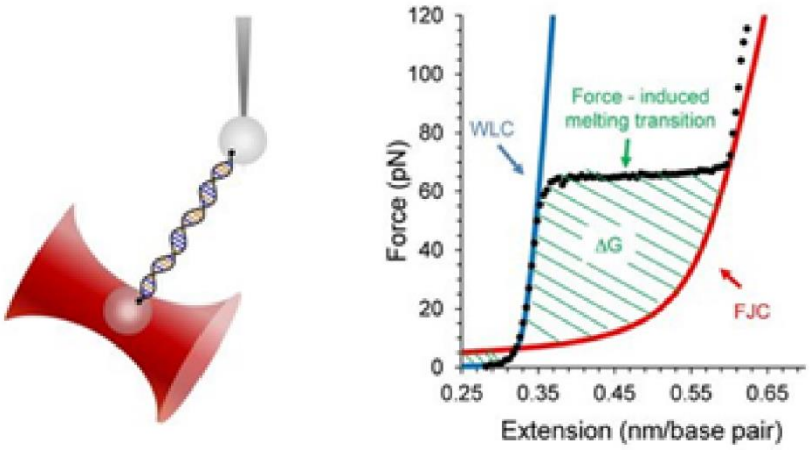

Fig. 15 | Parsing DNA melting transition using SMFS. The cartoon illustrates a DNA strand with two bead modifications at both ends, one bead is trapped by a dual-beam optical tweezers and the other bead is held by a micropipette tip (left). A typical dsDNA stretching curve with WLC indicates a helical structure and FJC indicates the coil structure. The area between the WLC and FJC is the energy required to introduce force mediated DNA melting transition. The images (ref 73) were reproduced with permission.

Although these techniques allow the binding affinities and thermodynamic signatures to be accurately characterized, they can seldom provide sequence selectivity

data. Sequence selectivity was usually reported by competition dialysis (Fig. 16)[74] and fluorescent intercalator displacement (FID)[75] assays. In the competition dialysis assay, DNA with different sequences was separated by semipermeable membrane and then soaked with binder-containing buffers, and the number of bound binders was spectroscopically monitored the next day in each DispoDialyzer. FID assays monitor the reduction in prebound binder on each DNA strand upon interacting with the second kind of binder (to be ranked with sequence selectivity), the more prebound binder is displaced, the stronger the affinity between the second binder and the DNA sequence.

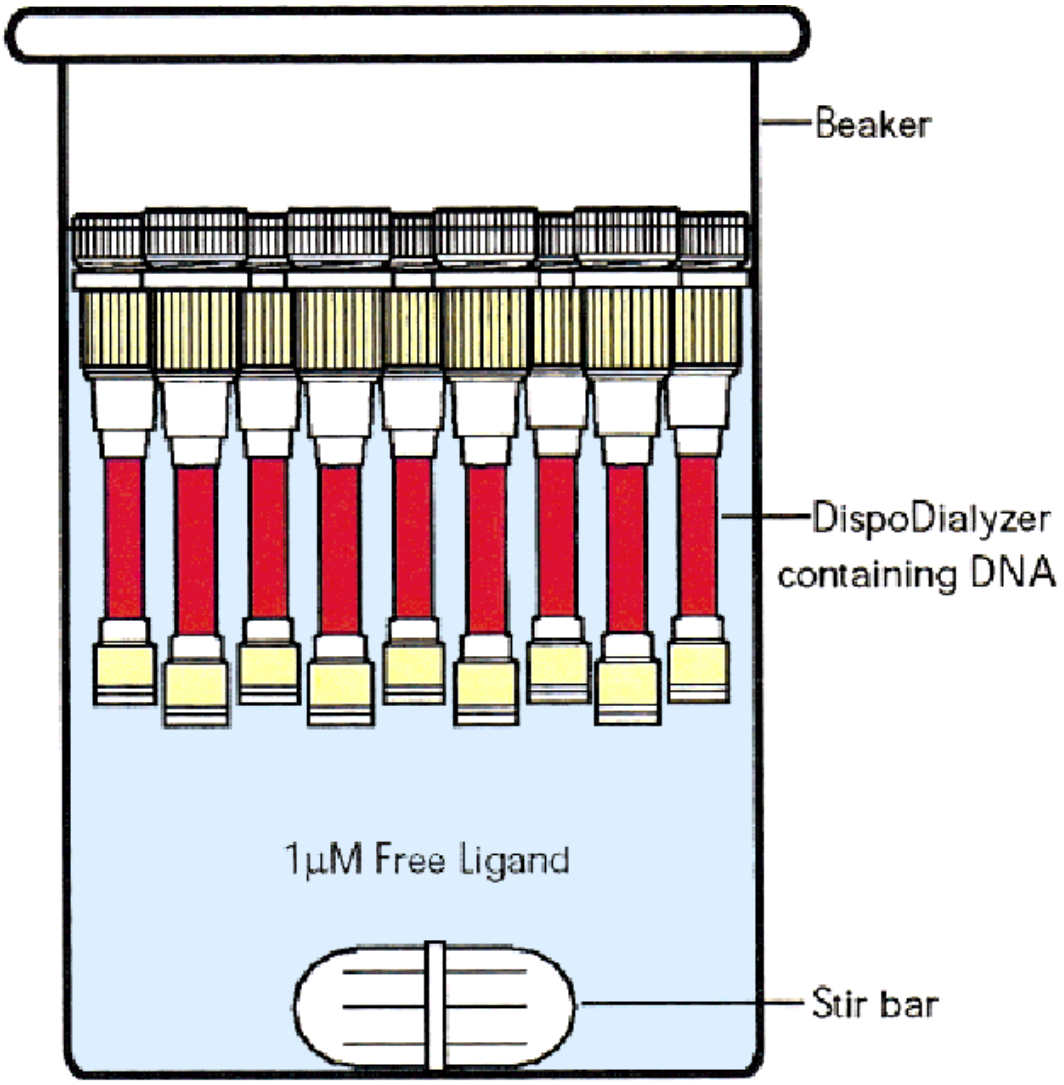

Fig. 16 | A competition dialysis assay determining DNA sequence selectivity. Different sequences of DNA are stored inside semipermeable membranes where small molecules can freely penetrate between these membranes. A stir bar was applied to increase free ligand penetration through the semipermeable membrane, and the amount of ligand binding in each DispoDialyzer containing DNA was monitored spectroscopically the next day. The images were reproduced with permission.

dsDNA small molecule interactions can also be characterized by other methods such as crystallography,[76] intrinsic viscosity,[77] cyclic voltammetry[78] and enzyme digestion[79] and each of these approaches exibits its own advantages in specific scenarios, but many characterization methods can only report information on a specific aspect of the ds-DNA small molecule interaction, sometimes multiple approaches must

be combined to generate a full picture of the dsDNA-small molecule interaction profile including binding affinity, thermodynamic signature and sequence selectivity.

1.3 HTS of small molecular binders for dsDNA

1.3.1 Introduction to the HTS method

HTS is the most commonly applied approach to discover bioactive compounds of a biological/chemical targets.[80-82] On average, over 10 years are needed to introduce a licensed drug into market, which cost approximately around 1 billion US dollars. Therefore, methods to identify, modify characterize and synthesize lead compounds with reduced cost and shortened intervals are always in high demand. HTS technology is capable of screening up to 1,000,000 compounds of interest per day, even taking the bottom line of a qualified HTS with a scanning rate of 10,000/day, the workload of a basic HTS instrument is equal to 10,000-man hours of laboratory work daily.

FRET, fluorescence intensity distribution analysis (FIDA), NMR and multiple biological or chemical assays are commonly used as HTS techniques. The focus on improving current HTS approaches can be summarized into the following categories: automation, miniaturization and coupling with artificial intelligence (AI).

HTS identifies potential ‘hits’ on a functional activity basis rather than known mechanics of drug-target interactions via in-silico prediction and simulation, which dramatically increases the structural diversity compared to drug leads designed from structure-based rational design. It is worthy clarifying that the HTS approach itself is not sufficient to “confirm” a candidate compound with a desired function, rather, it is sufficient to “deny” a biochemical structure with little or no effects, saving time that

would have been wasted on parsing candidates without the expected binding ability. HTS identified potential bioactive compounds usually require fine characterization methods, such as single-molecule analysis or cytotoxicity studies to confirm the final drug activity

1.3.2 Current small DNA binder HTS approaches

Visualizing small molecule-DNA interactions is challenging. First, 3D structural information from imaging methods including NMR and X-ray crystallization is lacking for nucleic acids.[83] Second, most computer-assisted docking techniques do not recognize DNA structures as flexible bodies[84] which further impairs the ability to predict small molecule-DNA interactions. The lack of a miniaturized and prior knowledge free characterization method for small molecule-DNA interactions further hampers the application of the HTS method for such binding activity.

To satisfy a non-AI-assisted HTS design identifying duplexed DNA interacting small molecules, the assay must meet at least the following criteria: prior information independent and human analysis free.[85] It is worth mentioning that all methods of characterizing the binding affinity of small DNA binders are not suitable for HTS application in searching for small molecules that interact with ds-DNA, on the one hand, the spectroscopy measure requires structural knowledge in advance which excludes its possibility to become an HTS assay. On the other hand, it is very challenging to apply an HTS assay based on a characterization approach that is designed to elucidate individual samples or molecules (calorimetry and atomic force spectroscopy). Although

DNA binders are an important source of anticancer and anti-infective drugs, HTS approaches for finding new binders have been very limited. To date, fluorescent intercalator displacement (FID) is the only HTS assay for DNA binders.[86] The mechanism behind this assay allows DNA intercalators such as EB or thiazole orange (TO) to prebind with DNA duplexed structures. Then the drug candidates are introduced, and the prebound binder's fluorescence is monitored. Successful drug binding will replace partial preintercalated binders, thus attenuating their fluorescence intensity. However, such a method is subject to low screening efficiency and significant screening bias because the fluorescence of preintercalated binder and drug must not overlap, and the method relies on the competitive binding between the binder and the indicator (Fig. 17).

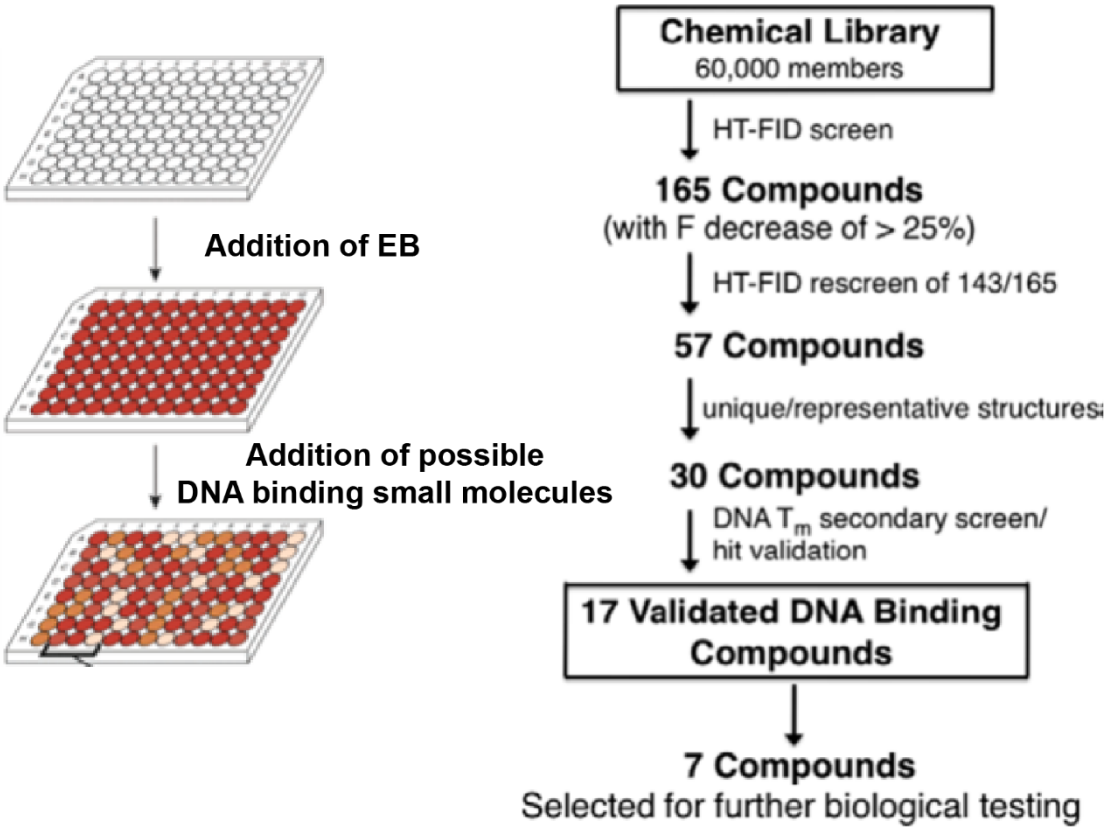

Fig. 17 | Algorithm and workflow of FID HTS identifying duplexed DNA interacting small molecules. EB is prebound with dsDNA in each well of the 96-well plate, and the addition of a DNA binder will displace partial prebound EB molecules thus introducing EB fluorescence attenuation while the EB-bound DNA interacting with nonbinding small molecules will keep the EB fluorescence unchanged (left). A typical flowchart of such HTS is listed (right). The images (ref 86) were reproduced with permission.

1.4 Objectives and hypothesis

The overall objective and hypothesis are to systematically design a method that can directly regulate elementary DNA reactions (strand displacement) with dsDNA interacting small molecules, one kind of nonnucleic acid molecule. Since the DNA strand displacements are individually governed by the presence of small DNA binders, their binding parameters might also be returned retrospectively by the extent of DNA strand displacement directed by those molecules. Finally, the observation of DNA

strand displacement reactions requires no prior information on the small DNA binder itself, and we can possibly build non-AI-assisted HTS assays for the discovery of small DNA binders based on this type of brand-new elementary DNA strand displacement reaction.

The first project was our theoretical study of fundamental BIND reactions. We systemically constructed a theory that illustrated how a duplexed DNA-interacting small agent could direct DNA strand displacement, a TMSD without a counterion effect exerted by mono- or divalent metal ions. Then we used BIND to comprehensively characterize different binder-DNA interactions with binding affinity, thermodynamic signature and sequence selectivity. We found that all BIND parsed parameters agreed well with previous works.

The second project was an HTS assay identifying novel DNA binding small molecules. Since BIND is uniquely introduced by DNA binding agents, we successfully designed an HTS assay and found 8 possible binders from a bioactive pool of 700 compounds provided by Pfizer. We then parsed the strongest hit with BIND as well as traditional methods, performed computer-assisted docking and examined its biological activity via a cytotoxicity study (MTT assay). Compared to the conventional FID HTS assay, BIND HTS was more sensitive and produced less screening bias.

The last project was to design and apply an orthogonal bias-free HTS assay that merged BIND and FID techniques together, since applying BIND HTS individually excluded the possibility of identifying uncharged binders. We carefully upgraded BIND HTS with an FID module and successfully identified a total of 20 possible binders

including 2 possible neutral binders in a pool of 1170 compounds provided by Pfizer. One of the possible charged binders as well as two possible neutral binders were characterized. The possible charged binder was characterized by BIND, DNA melting analysis computer assisted docking and cytotoxicity studies, the two possible neutral binders were parsed by DNA denaturation research, UV-vis absorption spectroscopy and cytotoxicity studies.

1. Seeman, N.C. & Sleiman, H.F. DNA nanotechnology. *Nature Reviews Materials* **3** (2017).
2. Zhang, F., Nangreave, J., Liu, Y. & Yan, H. Structural DNA nanotechnology: state of the art and future perspective. *J Am Chem Soc* **136**, 11198-11211 (2014).
3. Liu, X. et al. Complex silica composite nanomaterials templated with DNA origami. *Nature* **559**, 593-598 (2018).
4. Lu, C.H., Willner, B. & Willner, I. DNA nanotechnology: from sensing and DNA machines to drug-delivery systems. *ACS Nano* **7**, 8320-8332 (2013).
5. Song, T. et al. Programming DNA-Based Biomolecular Reaction Networks on Cancer Cell Membranes. *J Am Chem Soc* **141**, 16539-16543 (2019).
6. Simmel, F.C., Yurke, B. & Singh, H.R. Principles and Applications of Nucleic Acid Strand Displacement Reactions. *Chem Rev* **119**, 6326-6369 (2019).
7. Yurke, B., Turberfield, A.J., Mills, A.P., Jr., Simmel, F.C. & Neumann, J.L. A DNA-fuelled molecular machine made of DNA. *Nature* **406**, 605-608 (2000).
8. Douglas, S.M., Bachelet, I. & Church, G.M. A logic-gated nanorobot for targeted transport of molecular payloads. *Science* **335**, 831-834 (2012).
9. Thubagere, A.J. et al. A cargo-sorting DNA robot. *Science* **357** (2017).
10. Cherry, K.M. & Qian, L. Scaling up molecular pattern recognition with DNA-based winner-take-all neural networks. *Nature* **559**, 370-376 (2018).
11. Wang, G.A. et al. Expanding detection windows for discriminating single nucleotide variants using rationally designed DNA equalizer probes. *Nat Commun* **11**, 5473 (2020).
12. Zhang, D.Y. & Seelig, G. Dynamic DNA nanotechnology using strand-displacement reactions. *Nat Chem* **3**, 103-113 (2011).
13. Irmisch, P., Ouldridge, T.E. & Seidel, R. Modeling DNA-Strand Displacement Reactions in the Presence of Base-Pair Mismatches. *J Am Chem Soc* **142**, 11451-11463 (2020).
14. Del Grosso, E. et al. Dissipative Control over the Toehold-Mediated DNA Strand Displacement Reaction. *Angew Chem Int Ed Engl* **61**, e202201929 (2022).
15. Machinek, R.R., Ouldridge, T.E., Haley, N.E., Bath, J. & Turberfield, A.J. Programmable energy landscapes for kinetic control of DNA strand displacement. *Nat Commun* **5**, 5324 (2014).
16. Genot, A.J., Zhang, D.Y., Bath, J. & Turberfield, A.J. Remote toehold: a mechanism for

flexible control of DNA hybridization kinetics. *J Am Chem Soc* **133**, 2177-2182 (2011).
17. Chen, X. Expanding the rule set of DNA circuitry with associative toehold activation. *J Am Chem Soc* **134**, 263-271 (2012).
18. Yang, X., Tang, Y., Traynor, S.M. & Li, F. Regulation of DNA Strand Displacement Using an Allosteric DNA Toehold. *J Am Chem Soc* **138**, 14076-14082 (2016).
19. Zhang, D.Y. Cooperative hybridization of oligonucleotides. *J Am Chem Soc* **133**, 1077-1086 (2011).
20. Nakamura, S., Hashimoto, H., Kobayashi, S. & Fujimoto, K. Photochemical Acceleration of DNA Strand Displacement by Using Ultrafast DNA Photo-crosslinking. *Chembiochem* **18**, 1984-1989 (2017).
21. Li, C. et al. Flexible regulation of DNA displacement reaction through nucleic acid-recognition enzyme and its application in keypad lock system and biosensing. *Sci Rep* **7**, 10017 (2017).
22. Fan, S. et al. Proximity-Induced Pattern Operations in Reconfigurable DNA Origami Domino Array. *J Am Chem Soc* **142**, 14566-14573 (2020).
23. Xie, Y., Niu, F., Yu, A. & Lai, G. Proximity Binding-Triggered Assembly of Two MNAzymes for Catalyzed Release of G-Quadruplex DNAzymes and an Ultrasensitive Homogeneous Bioassay of Platelet-Derived Growth Factor. *Anal Chem* **92**, 593-598 (2020).
24. Li, F. et al. Dynamic DNA Assemblies Mediated by Binding-Induced DNA Strand Displacement. *Journal of the American Chemical Society* **135**, 2443-2446 (2013).
25. Wang, L.L. et al. Controllable DNA strand displacement by independent metal-ligand complexation. *Chem Sci* **12**, 8698-8705 (2021).
26. Monserud, J.H., Macri, K.M. & Schwartz, D.K. Toehold-Mediated Displacement of an Adenosine-Binding Aptamer from a DNA Duplex by its Ligand. *Angew Chem Int Ed Engl* **55**, 13710-13713 (2016).
27. Wang, J., Li, Z. & Willner, I. Cascaded dissipative DNAzyme-driven layered networks guide transient replication of coded-strands as gene models. *Nat Commun* **13**, 4414 (2022).
28. Double-helix disruption. *Nat Chem* **4**, 587 (2012).
29. Achan, J. et al. Quinine, an old anti-malarial drug in a modern world: role in the treatment of malaria. *Malar J* **10**, 144 (2011).
30. Finocchiaro, G. Actinomycin D: a new opening for an old drug. *Neuro Oncol* **22**, 1235-1236 (2020).
31. Blair, H.A. Daunorubicin/Cytarabine Liposome: A Review in Acute Myeloid Leukaemia. *Drugs* **78**, 1903-1910 (2018).
32. Martins-Teixeira, M.B. & Carvalho, I. Antitumour Anthracyclines: Progress and Perspectives. *ChemMedChem* **15**, 933-948 (2020).
33. Dragan, A.I. et al. SYBR Green I: fluorescence properties and interaction with DNA. *J Fluoresc* **22**, 1189-1199 (2012).
34. Galindo-Murillo, R. & Cheatham, T.E. Ethidium bromide interactions with DNA: an exploration of a classic DNA-ligand complex with unbiased molecular dynamics simulations. *Nucleic Acids Res* **49**, 3735-3747 (2021).
35. O'Neil, C.S., Beach, J.L. & Gruber, T.D. DNA Electrophoresis Using Thiazole Orange Instead of Ethidium Bromide or Alternative Dyes. *J Vis Exp* (2019).
36. Zhang, X.X., Brantley, S.L., Corcelli, S.A. & Tokmakoff, A. DNA minor-groove binder

Hoechst 33258 destabilizes base-pairing adjacent to its binding site. *Commun Biol* **3**, 525 (2020).

37. Le Gresley, A., Gudivaka, V., Carrington, S., Sinclair, A. & Brown, J.E. Synthesis, analysis and biological evaluation of novel indolquinonecryptolepine analogues as potential anti-tumour agents. *Org Biomol Chem* **14**, 3069-3079 (2016).
38. Almaqwashi, A.A., Paramanathan, T., Rouzina, I. & Williams, M.C. Mechanisms of small molecule-DNA interactions probed by single-molecule force spectroscopy. *Nucleic Acids Res* **44**, 3971-3988 (2016).
39. Chaires, J.B. A small molecule--DNA binding landscape. *Biopolymers* **103**, 473-479 (2015).
40. Gao, Y. et al. Dual-Color Emissive AIEgen for Specific and Label-Free Double-Stranded DNA Recognition and Single-Nucleotide Polymorphisms Detection. *Journal of the American Chemical Society* **141**, 20097-20106 (2019).
41. Uno, K., Sugimoto, N. & Sato, Y. N-aryl pyrido cyanine derivatives are nuclear and organelle DNA markers for two-photon and super-resolution imaging. *Nat Commun* **12**, 2650 (2021).
42. Newton, M.D., Fairbanks, S.D., Thomas, J.A. & Rueda, D.S. A Minimal Load-and-Lock Ru(II) Luminescent DNA Probe. *Angew Chem Int Ed Engl* **60**, 20952-20959 (2021).
43. Niyazi, H. et al. Crystal structures of Lambda-[Ru(phen)(2)dppz](2)(+) with oligonucleotides containing TA/TA and AT/AT steps show two intercalation modes. *Nat Chem* **4**, 621-628 (2012).
44. Song, H., Kaiser, J.T. & Barton, J.K. Crystal structure of Delta-[Ru(bpy)(2)dppz](2)(+) bound to mismatched DNA reveals side-by-side metalloinsertion and intercalation. *Nat Chem* **4**, 615-620 (2012).
45. Biebricher, A.S. et al. The impact of DNA intercalators on DNA and DNA-processing enzymes elucidated through force-dependent binding kinetics. *Nat Commun* **6**, 7304 (2015).
46. Wilson, M.R. et al. The human gut bacterial genotoxin colibactin alkylates DNA. *Science* **363** (2019).
47. Li, Z.R. et al. Macrocyclic colibactin induces DNA double-strand breaks via copper-mediated oxidative cleavage. *Nat Chem* **11**, 880-889 (2019).
48. Dziubanska-Kusibab, P.J. et al. Colibactin DNA-damage signature indicates mutational impact in colorectal cancer. *Nat Med* **26**, 1063-1069 (2020).
49. Trigo, J. et al. Lurbinectedin as second-line treatment for patients with small-cell lung cancer: a single-arm, open-label, phase 2 basket trial. *The Lancet Oncology* **21**, 645-654 (2020).
50. Taniguchi, J. et al. A synthetic DNA-binding inhibitor of SOX2 guides human induced pluripotent stem cells to differentiate into mesoderm. *Nucleic Acids Res* **45**, 9219-9228 (2017).
51. Taniguchi, J. et al. Biomimetic Artificial Epigenetic Code for Targeted Acetylation of Histones. *J Am Chem Soc* **140**, 7108-7115 (2018).
52. Yu, Z. et al. Pip-HoGu: An Artificial Assembly with Cooperative DNA Recognition Capable of Mimicking Transcription Factor Pairs. *J Am Chem Soc* **140**, 2426-2429 (2018).
53. Nakamori, M. et al. A slipped-CAG DNA-binding small molecule induces trinucleotide-repeat contractions in vivo. *Nat Genet* **52**, 146-159 (2020).

54. Chen, H. et al. Dynamic and Progressive Control of DNA Origami Conformation by Modulating DNA Helicity with Chemical Adducts. *ACS Nano* **10**, 4989-4996 (2016).
55. Lee, C., Kim, Y.J., Kim, K.S., Lee, J.Y. & Kim, D.N. Modulating the chemo-mechanical response of structured DNA assemblies through binding molecules. *Nucleic Acids Res* **49**, 12591-12599 (2021).
56. Wamhoff, E.C. et al. Controlling Nuclease Degradation of Wireframe DNA Origami with Minor Groove Binders. *ACS Nano* (2022).
57. Seo, S.E. et al. Modulating the Bond Strength of DNA-Nanoparticle Superlattices. *ACS Nano* **10**, 1771-1779 (2016).
58. Guo, C. et al. Molecular rectifier composed of DNA with high rectification ratio enabled by intercalation. *Nat Chem* **8**, 484-490 (2016).
59. Boulais, E. et al. Programmed coherent coupling in a synthetic DNA-based excitonic circuit. *Nat Mater* **17**, 159-166 (2018).
60. Magdy, G., Shaldam, M.A., Belal, F. & Elmansi, H. Multi-spectroscopic, thermodynamic, and molecular docking/dynamic approaches for characterization of the binding interaction between calf thymus DNA and palbociclib. *Sci Rep* **12**, 14723 (2022).
61. Kapuscinski, J. & Szer, W. Interactions of 4', 6-diamidine-2-phenylindole with synthetic polynucleotides. *Nucleic Acids Res* **6**, 3519-3534 (1979).
62. Airoldi, M., Barone, G., Gennaro, G., Giuliani, A.M. & Giustini, M. Interaction of doxorubicin with polynucleotides. A spectroscopic study. *Biochemistry* **53**, 2197-2207 (2014).
63. Pohl, F.M., Jovin, T.M., Baehr, W. & Holbrook, J.J. Ethidium bromide as a cooperative effector of a DNA structure. *Proc Natl Acad Sci U S A* **69**, 3805-3809 (1972).
64. Leng, F., Chaires, J.B. & Waring, M.J. Energetics of echinomycin binding to DNA. *Nucleic Acids Res* **31**, 6191-6197 (2003).
65. Pilch, D.S., Kirolos, M.A., Liu, X., Plum, G.E. & Breslauer, K.J. Berenil [1,3-bis(4'-amidinophenyl)triazene] binding to DNA duplexes and to a RNA duplex: evidence for both intercalative and minor groove binding properties. *Biochemistry* **34**, 9962-9976 (1995).
66. Wilson, W.D. et al. DNA sequence dependent binding modes of 4',6-diamidino-2-phenylindole (DAPI). *Biochemistry* **29**, 8452-8461 (1990).
67. Jangir, D.K., Tyagi, G., Mehrotra, R. & Kundu, S. Carboplatin interaction with calf-thymus DNA: A FTIR spectroscopic approach. *Journal of Molecular Structure* **969**, 126-129 (2010).
68. Beck, J.L. et al. Probing DNA selectivity of ruthenium metallointercalators using ESI mass spectrometry. *Chem Commun (Camb)*, 626-627 (2003).
69. McGhee, J.D. Theoretical calculations of the helix-coil transition of DNA in the presence of large, cooperatively binding ligands. *Biopolymers* **15**, 1345-1375 (1976).
70. Kumar, S., Xue, L. & Arya, D.P. Neomycin-neomycin dimer: an all-carbohydrate scaffold with high affinity for AT-rich DNA duplexes. *J Am Chem Soc* **133**, 7361-7375 (2011).
71. Leng, F., Priebe, W. & Chaires, J.B. Ultratight DNA binding of a new bisintercalating anthracycline antibiotic. *Biochemistry* **37**, 1743-1753 (1998).
72. Lipfert, J., Klijnhout, S. & Dekker, N.H. Torsional sensing of small-molecule binding using magnetic tweezers. *Nucleic Acids Res* **38**, 7122-7132 (2010).
73. Vladescu, I.D., McCauley, M.J., Nunez, M.E., Rouzina, I. & Williams, M.C. Quantifying force-dependent and zero-force DNA intercalation by single-molecule stretching. *Nat Methods*

4, 517-522 (2007).
74. Ren, J. & Chaires, J.B. Sequence and structural selectivity of nucleic acid binding ligands. *Biochemistry* **38**, 16067-16075 (1999).
75. Boger, D.L., Fink, B.E., Brunette, S.R., Tse, W.C. & Hedrick, M.P. A simple, high-resolution method for establishing DNA binding affinity and sequence selectivity. *J Am Chem Soc* **123**, 5878-5891 (2001).
76. Brown, D.G., Sanderson, M.R., Garman, E. & Neidle, S. Crystal structure of a berenil-d(CGCAAATTTGCG) complex: An example of drug-DNA recognition based on sequence-dependent structural features. *Journal of molecular biology* **226**, 481-490 (1992).
77. Wu, J. et al. A class of novel carboline intercalators: Their synthesis, in vitro anti-proliferation, in vivo anti-tumor action, and 3D QSAR analysis. *Bioorg Med Chem* **18**, 6220-6229 (2010).
78. Guin, P.S. & Das, S. Exploration of Electrochemical Intermediates of the Anticancer Drug Doxorubicin Hydrochloride Using Cyclic Voltammetry and Simulation Studies with an Evaluation for Its Interaction with DNA. *International Journal of Electrochemistry* **2014**, 1-8 (2014).
79. Ellis, T., Evans, D.A., Martin, C.R. & Hartley, J.A. A 96-well DNase I footprinting screen for drug-DNA interactions. *Nucleic Acids Res* **35**, e89 (2007).
80. Macarron, R. et al. Impact of high-throughput screening in biomedical research. *Nat Rev Drug Discov* **10**, 188-195 (2011).
81. Blay, V., Tolani, B., Ho, S.P. & Arkin, M.R. High-Throughput Screening: today's biochemical and cell-based approaches. *Drug Discov Today* **25**, 1807-1821 (2020).
82. Mishra, K.P., Ganju, L., Sairam, M., Banerjee, P.K. & Sawhney, R.C. A review of high throughput technology for the screening of natural products. *Biomed Pharmacother* **62**, 94-98 (2008).
83. Campagne, S., Gervais, V. & Milon, A. Nuclear magnetic resonance analysis of protein-DNA interactions. *J R Soc Interface* **8**, 1065-1078 (2011).
84. van Dijk, M., van Dijk, A.D., Hsu, V., Boelens, R. & Bonvin, A.M. Information-driven protein-DNA docking using HADDOCK: it is a matter of flexibility. *Nucleic Acids Res* **34**, 3317-3325 (2006).
85. Kato, R. et al. Novel strategy for protein exploration: high-throughput screening assisted with fuzzy neural network. *J Mol Biol* **351**, 683-692 (2005).
86. Glass, L.S., Bapat, A., Kelley, M.R., Georgiadis, M.M. & Long, E.C. Semi-automated high-throughput fluorescent intercalator displacement-based discovery of cytotoxic DNA binding agents from a large compound library. *Bioorg Med Chem Lett* **20**, 1685-1688 (2010).

Chapter 2

Programming strand displacement reaction pathways using small molecular DNA binders

Contribution statement

I performed all the experimental work while Wang built the mathematical models, and Gao performed molecular docking; we both participated into the experimental design and data analysis.

2.1 Introduction

Dynamic DNA nanotechnology prospers through last several decades, among which the TMSD remains the most effective and easy-to-use pathway to achieve desired DNA structures via a strand exchanging approach isothermally. Building upon the highly predictable and programmable Watson-Crick base pairing rule, the field of DNA nanotechnology[1, 2] has made profound impact to material science[3-9], synthetic biology[10, 11], and medicine[12-14]. While structural DNA nanotechnology constructs two- and three-dimensional objectives of varying sizes and complexity through "bottom-up" DNA self-assembly[15, 16], dynamic DNA nanotechnology[17] emphasizes on the non-equilibrium dynamics of DNA chemistry, through which materials[18], machineries[19], or even the function and fate of living cells[20] can be precisely programmed and controlled. To further expand the functionality of dynamic DNA nanotechnology, it is critical to diversify the DNA chemistry to include non-nucleic-acid species, such as proteins and

small molecules. So far, such stimuli-responsive DNA nanotechnology is typically achieved by hardwiring functional motifs, such as aptamers[21, 22], antibodies[23, 24], DNAzymes[25] and i-motifs[26, 27], into existing DNA reactions. Here, we introduce an alternative binder-induced nucleic acid strand displacement (BIND) approach that programs the reaction pathways of elementary toehold-mediated strand displacement (TMSD) reactions using small molecular DNA binders.

First introduced by Yurke et.al in 2000[28], TMSD has become the most widely used elementary reaction in dynamic DNA nanotechnology. Mechanistically, TMSD can be considered as a S_N2 reaction, which is initiated at a short complementary single-stranded DNA (ssDNA) toehold domain and progresses through a branch migration process to displace a pre-hybridized DNA strand. In this reaction pathway, metal cations, such as Mg2+, play critical roles for stabilizing the initial duplex as well as the triplex intermediate against the repulsion caused by the dense negative charges of phosphorate backbones (Fig. 1b)[29]. In a BIND reaction system, TMSD is placed in a solution containing no metal cations or very low concentrations of monovalent metal cations (< 40 mM) to maintain the charge repulsion, so that the dominant reaction pathway becomes S_N1 (Fig. 1c)[30]. At this stage, the addition of low concentrations of dsDNA binders suppresses the S_N1 reaction pathway by stabilizing the duplex reactant through specific DNA-binder interactions and thus reduce the yield of the overall strand displacement in a dose-response manner (Fig. 1d). Once fully occupying the initial pre-hybridized DNA duplex, free DNA binders then facilitate the docking of the toehold domain and thus promote stand displacement via a S_N2 reaction pathway (Fig. 1e). By

programing the reaction pathways of TMSD using small molecular DNA binders, we demonstrate both in-silico and experimentally that unique reaction isotherms can be achieved in response to different types of DNA binders. More importantly, critical binding parameters of DNA-binder interactions, including binding constant (Kd), binding site size (n), cooperativity (ω), enthalpic (ΔH) and entropic (-TΔS) contributions, as well as sequence selectivity, can be accurately profiled using BIND.

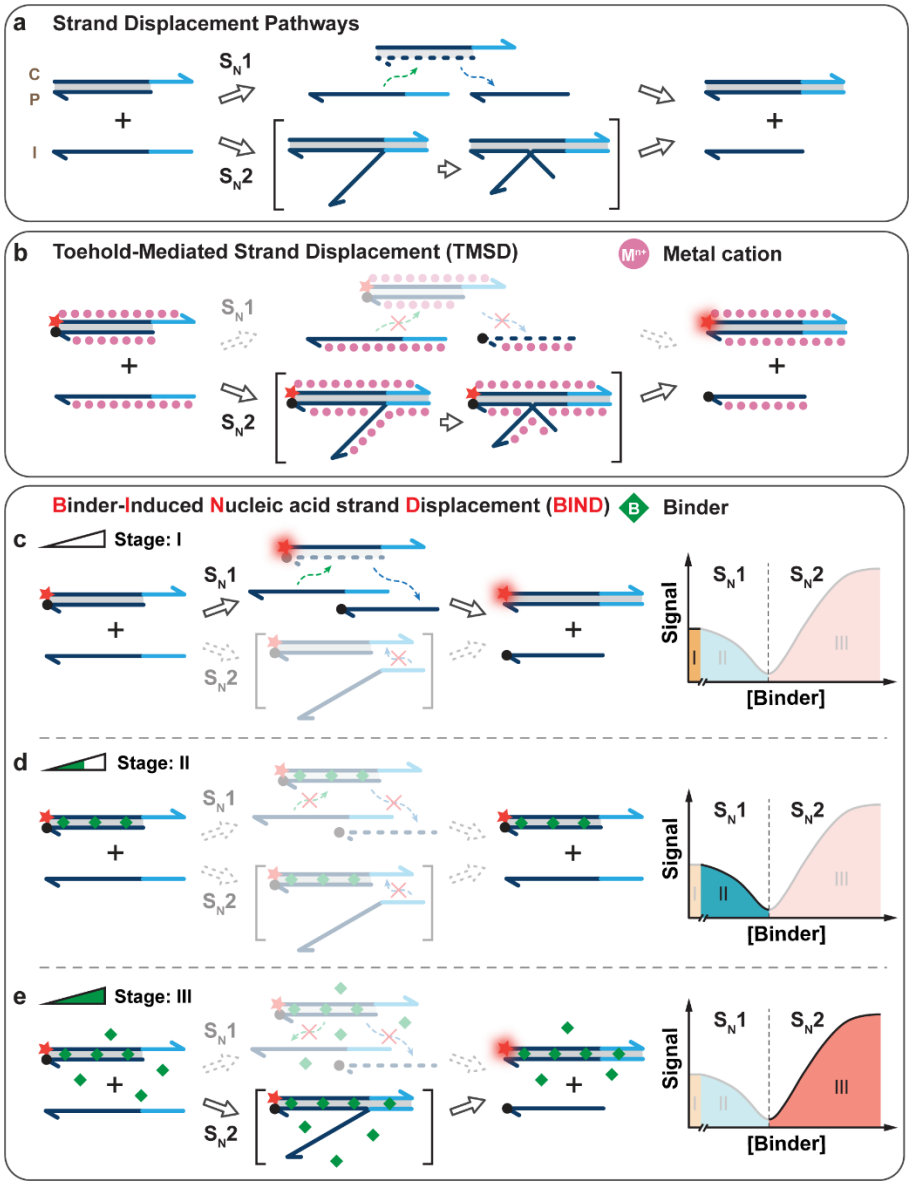

Fig. 1 | Reaction pathways for DNA strand displacement reactions. a. Schematic illustration of two possible reaction pathways (S_N1 and S_N2) for a typical toehold-mediated strand displacement reaction. **b.** Conventional strand displacement reaction is

dominated by S_N2 reaction pathway, where metal cations help stabilize the triplex intermediate. **c.** Activation of the S_N1 reaction pathway by placing the displacement reaction in a buffer containing no or very low concentrations of metal ions. **d.** Inhibition of both reaction pathways in response to low concentrations of DNA binders in BIND. **e.** Activation of the S_N2 reaction pathway in response to high concentrations of DNA binders in BIND.

2.2 Result and Discussion

2.2.1 Theoretical

BIND is a DNA strand displacement reaction with programmable reaction pathways in response to small molecular DNA binders. Because the prehybridized DNA duplex (CP) is destabilized by the strong charge repulsion, the displacement between CP and the invader strand (I) involves the dissociation of CP (reaction 1) and subsequent hybridization between C and I (reaction 2), corresponding to a classic S_N1 reaction pathway (Fig. 1c):

$$CP \rightarrow C + P,\ K_D \tag{1}$$

$$C + I \rightarrow CI,\ K_H \tag{2}$$

$$CP + I \rightarrow CI + P,\ K_{S_N1} \tag{3}$$

where K_D, K_H, and K_{S_N1} stand for equilibrium constants of CP dissociation, hybridization of C and I, and the overall S_N1 reaction pathway, respectively, and $K_{S_N1} = K_D \times K_H$. In our study, all three initial equilibrium constants in the absence of any binder were determined experimentally for a representative strand displacement reaction in a Tris-EDTA (TE) buffer containing no metal cations. The initial reaction free energy ΔG°_{ini} of the strand displacement was then determined to be 0.33 kcal/mol. Upon the addition of SYBR Green I (SG-I, K_d = 7.1 nM) as a model DNA binder, I observed sharp decreases in the reaction yields against increasing concentration of SG-

I until reaching a critical binder concentration (CBC) at which the CP duplex was fully occupied (Fig. 2). Further raising the concentration of SG-I above CBC, I observed the acceleration of strand displacement through a S_N2 reaction pathway (Fig. 2):

$$CP + I \rightarrow CPI \rightarrow CI + P,\ K_{S_N2} \tag{4}$$

where K_{S_N2} stands for equilibrium constant of the S_N2 reaction pathway. This observation suggests that high concentrations of free SG-I could facilitate the toehold docking which initiates the process of branch migration and strand displacement.

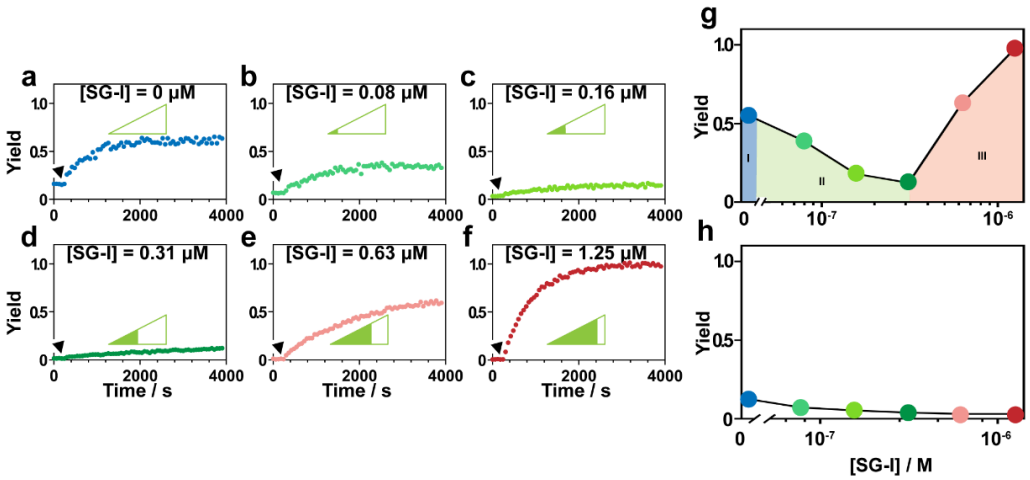

Fig. 2 | Kinetic and thermodynamic BIND profile for SG-I. (**a-f**) Representative kinetic profiles of strand displacement reactions in the absence (**a**) and increasing concentrations of SG-I (**b-f**). **g.** Thermodynamic profile of SG-I-mediated BIND reaction by plotting the strand displacement reaction yields at equilibrium against increasing concentrations of SG-I. **h.** Effect of increasing concentration of SG-I to the stability of CP duplex in the absence of the invader.

To quantitatively understand how SG-I programs the BIND reaction, I next developed a theoretical model that considers both S_N1 and S_N2 reaction pathways for the strand displacement. A theoretical model for BIND was established by considering the strand displacement to be an S_N1 reaction in the absence of the binder or the binder concentration was below the critical binder concentration (CBC). When the binder

concentration was greater than CBC, the reaction was considered to go through an S_N2 strand displacement reaction pathway. To quantitatively profile BIND, Dr. Wang and I established a workflow for extracting critical thermodynamic parameters by combining experimental measurement and theoretical fitting (Fig. 3). We first derived the initial values of K_D and K_H in the absence of any binder by fitting the experimental data. Equilibrium constants when binder concentration equals to CBC were also determined. K_D values in the presence of binders with concentrations below CBC were then determined by fitting experimental data in a dissociation reaction of CP in the presence of binders but absence of the invader I (Fig. 2h). K_H and the overall strand displacement equilibriumK_{S_N1} could then be determined by fitting the strand displacement reaction using the S_N1 reaction mechanism and experimentally determined reaction yield in the presence of a given concentration of binder (Eq. 1 and 2). By further determining the Gibbs free energy of the reaction using the equilibrium constant (Fig. 3), we observed a linear relationship between ΔG_{S_N1} and the concentrations of DNA binders (Fig. 4). The similar mathematical treatment at the S_N2 region also revealed a linear relationship of ΔG_{S_N2} against binder concentration above CBC (Fig. 4 and Eq. 4). The graphic illustration of in-silico simulation was shown below:

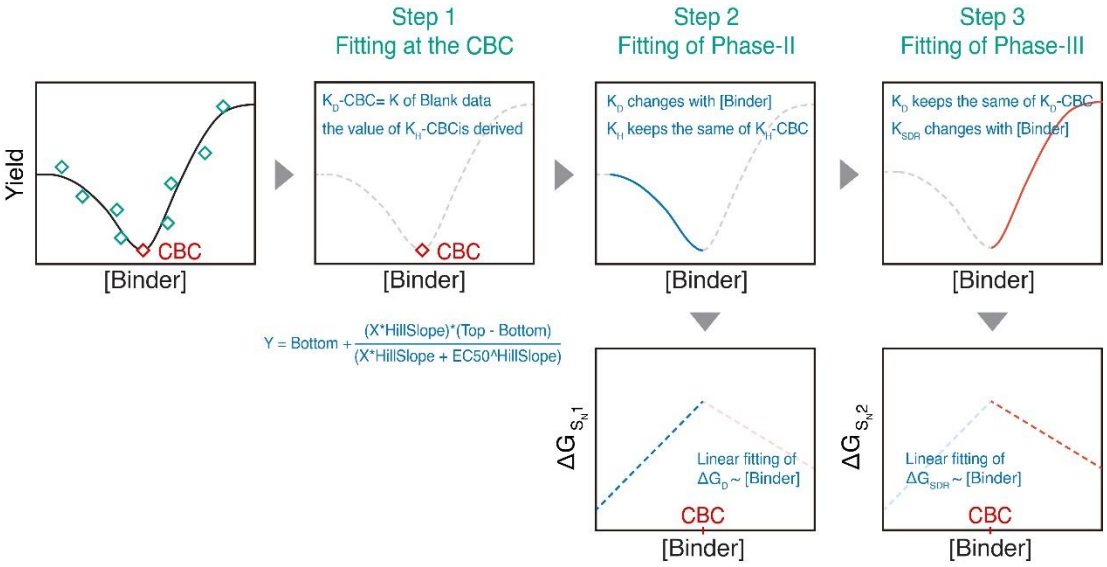

Fig. 3 | Schematic illustration of the workflow for data fitting and simulation against the theoretical model.

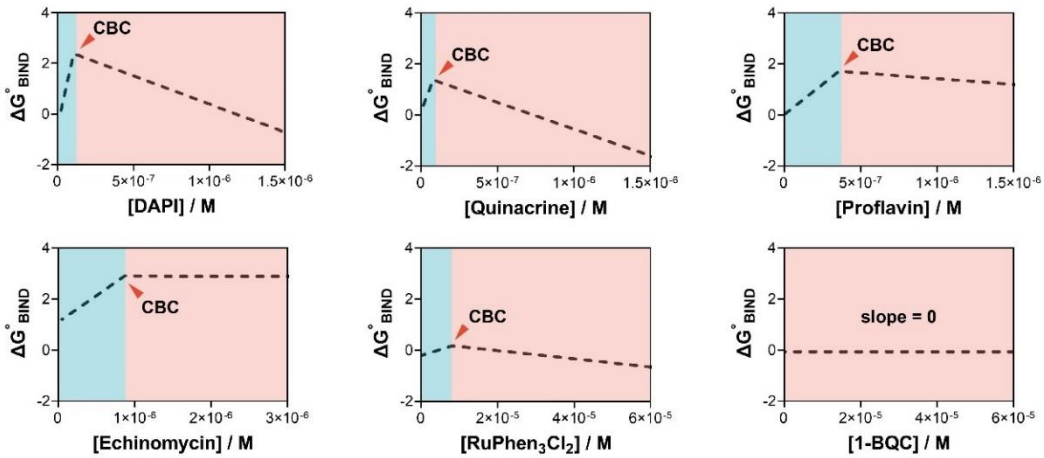

Fig. 4 | Quantitative profiles of ΔG°_{BIND} as a function of increasing concentrations of binders. Linear relationships were established for representative binders, including DAPI, Quinacrine, Proflavin, Echinomycin, and $RuPhen_3Cl_2$, as well as a positively charged non-binder, 1-benzylquinolinium chloride (1-BQC).

Dr. Wang and I then fit experimental data in Fig. 2a into the model to determine the quantitative relationship between SG-I concentration and the overall equilibrium constant K_{BIND} (Fig. 5a and 5b) as well as the reaction free energy ΔG°_{BIND} (Fig. 5c). Interestingly, SG-I was found to program ΔG°_{BIND} in a linear fashion at both S_N1 and

S_N2 regions (Fig. 5c). We further confirmed this quantitative relationship was generalizable to other DNA binders regardless their binding modes to DNA (intercalator or groove binder) (Fig. 4). ΔG°_{BIND} can thus be expressed in the following equations and BIND becomes predictable at any given binder concentration:

$$\Delta G^{\circ}_{BIND} = \Delta G^{\circ}_{ini} + \theta \cdot C_{Binder}, (C_{Binder} \leq CBC, \text{S}_N1 \text{ reaction pathway}) \quad (5)$$

$$\Delta G^{\circ}_{BIND} = \Delta G^{\circ}_{ini} + (\theta - \xi) \cdot CBC + \xi \cdot C_{Binder}, (C_{Binder} > CBC, \text{S}_N2 \text{ reaction pathway}) \quad (6)$$

where ΔG°_{BIND} is the reaction free energy of the overall BIND reaction, ΔG°_{ini} is the initial reaction free energy in the absence of DNA binders, C_{Binder} is the concentration of DNA binder, θ is an activity coefficient for inhibiting strand displacement, and ξ is an activity coefficient for promoting strand displacement. Both θ and ξ are intrinsic properties for a given DNA binder and can be determined quantitatively as the slopes at the S_N1 pathway region and S_N2 pathway region, respectively.

By plotting θ and ξ against binders with increasing binding affinities, Dr. Wang and I found that θ was determined solely by the binding strength of DNA binders (Fig. 5d), whereas ξ was determined by both affinity and the charge condition (Fig. 5e). For example, Echinomycin is a much stronger binder than $Ru(Phen)_3Cl_2$ but showed much less promotion to strand displacement at the S_N2 pathway because it is a neutral binder. Using 1-benzylquinolinium chloride (1-BQC) as a positively charged non-binder, we also confirmed that BIND is highly binder-specific in both S_N1 and S_N2 reaction pathways. Therefore, four classes of distinct BIND profiles can be established according to small molecules with varying combination of affinities and charge

conditions, including strong and positively charged binders ($\theta > 0, \xi < 0$) (Fig. 5f), strong neutral binders ($\theta > 0, \xi = 0$) (Fig. 5g), weak and positively charged binders ($\theta = 0, \xi < 0$) (Fig. 5h), and non-binders ($\theta = 0, \xi = 0$) (Fig. 5i). The theoretically predicted profiles were further confirmed experimentally using representative compounds, including Berenil (Fig. 5j), Echinomycin (Fig. 5k), $Ru(Phen)_3Cl_2$ (Fig. 5l), and 1-BCQ (Fig. 5m).

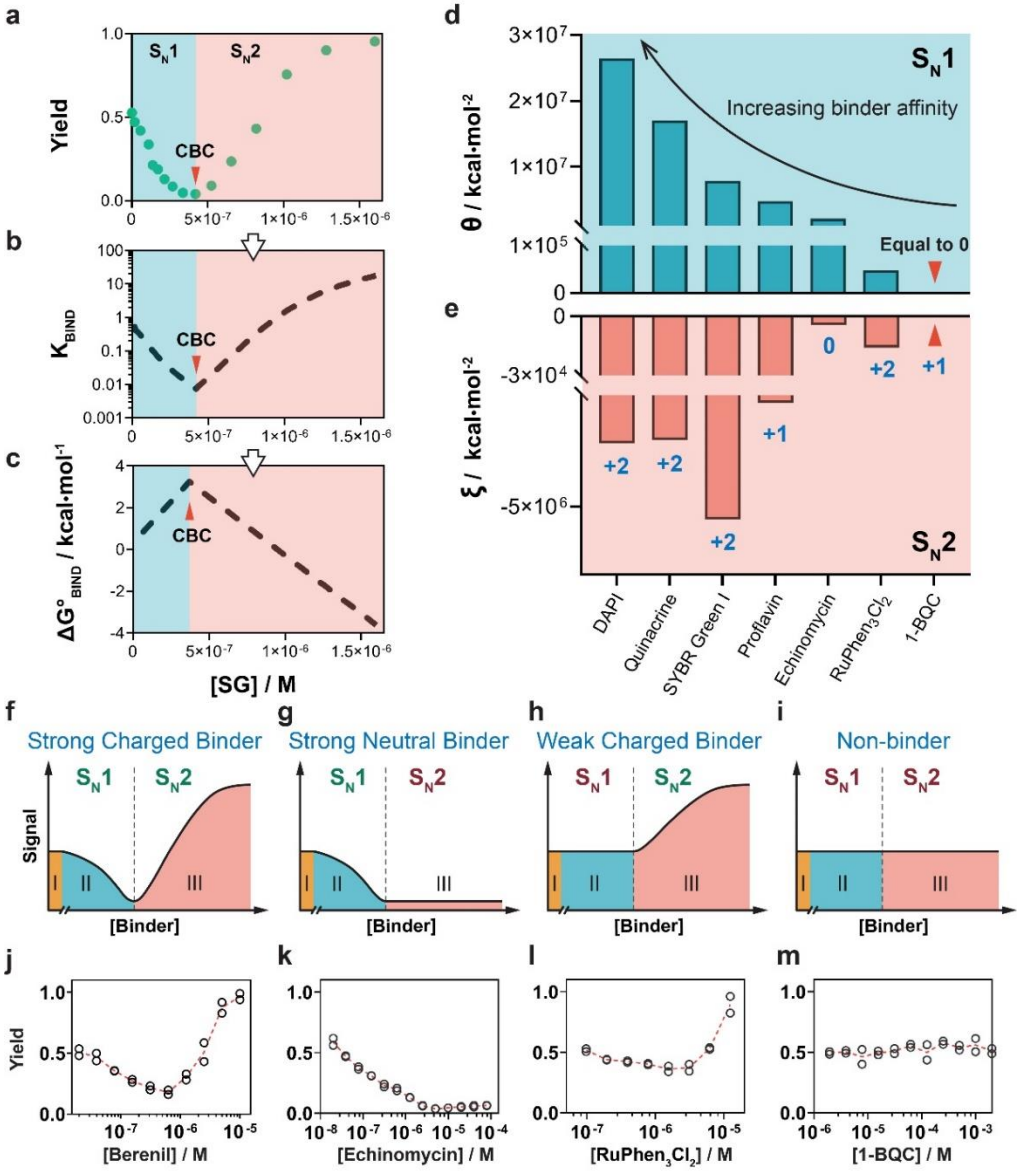

Fig. 5 | BIND profiles in response to binder affinity and charge condition. a. A typical BIND curve established by plotting strand displacement reaction yields against the concentrations of SG-I. **b.** Quantitative relationship between K_{BIND} and SG-I

concentration achieved by fitting experimental data into a theoretical model of BIND. **c.** A further mathematical conversion revealed the linear relationship between ΔG°_{BIND} and SG-I concentration. **d. e.** Changes of activity coefficients $\boldsymbol{\theta}$ at the S_N1 region (**d**) and $\boldsymbol{\xi}$ at the S_N2 region (**e**) in response to binders with varying binding affinities and charge conditions. **f-i.** Schematic illustration of four distinct BIND profiles against positively charged strong binders (**f**), strong neural binders (**g**), positively charged weak binders (**h**), and non-binders (**i**). **j.** Experimentally established BIND profile for a representative positively charged strong binder, SG-I. **k.** Experimentally established BIND profile for a strong, neutral binder, Echinomycin. **l.** Experimentally established BIND profile for a representative positively charged weak binder, $RuPhen_3Cl_3$. **m.** Experimentally established BIND profile for a representative positively charged nonbinder, 1-BQC.

2.2.2 Profiling DNA-Binder interactions using BIND.

I next employed BIND to quantitatively profile the affinities of DNA-binder interactions. Because the fluorescence signal is generated by externally labeled fluorophore-quencher pairs and strand displacement reactions, BIND does not rely on the intrinsic fluorescent properties of DNA binders and is thus a universal assay generalizable to all DNA binders. Experimentally, the binding isotherm was established by plotting the attenuated fluorescent signals against binder concentrations at the region of S_N1 reaction pathway, where 0% and 100% occupancies were established at binder concentrations of zero (F_0) and CBC (F_{CBC}), respectively (Fig. 6).

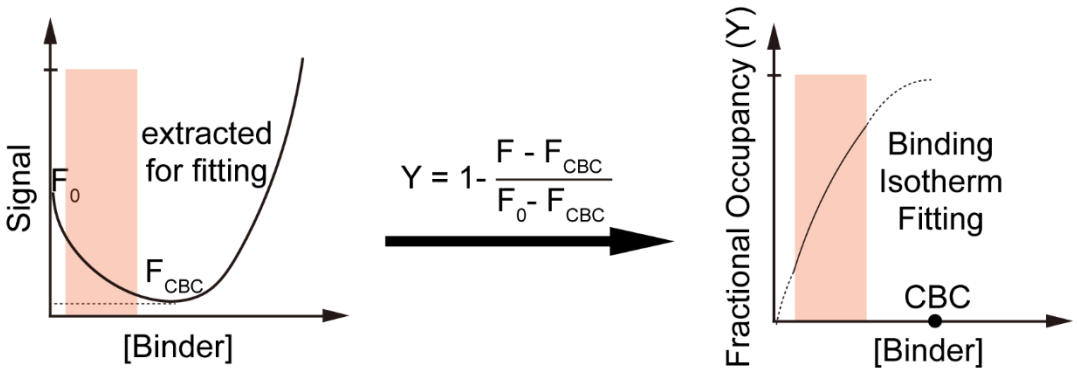

Fig. 6 | Schematic illustration the mathematical transformation to determine the binding affinity of varying binders using BIND. The fractional occupancy from 35% and 85% was determined to be the optimal range for determining critical binding parameters, including dissociation constants, and binding site sizes.

Both binding constants (Ka and Kd) and the binding site size (n) were determined by fitting the binding curves at the S_N1 region against the lattice-ligand model developed by McGhee and Von Hippel.

$$v/L = K_a \cdot (1 - nv)^n / (1 - nv + v)^{n-1} \quad (7)$$

where v was the number of bound ligands per DNA bp, L was the concentration of unbound ligand in the solution, K_a was the association constant and n was the binding site size.

A head-to-head comparison between BIND and classic fluorescence turn-on assay for measuring binding affinities of SG-I to dsDNA revealed highly consistent values in both Kd (7.0 nM *vs.* 9.3 nM) and n (2.6 *vs.* 2.4), confirming the feasibility of BIND for profiling the binding properties of small molecular DNA binders (Fig. 7).

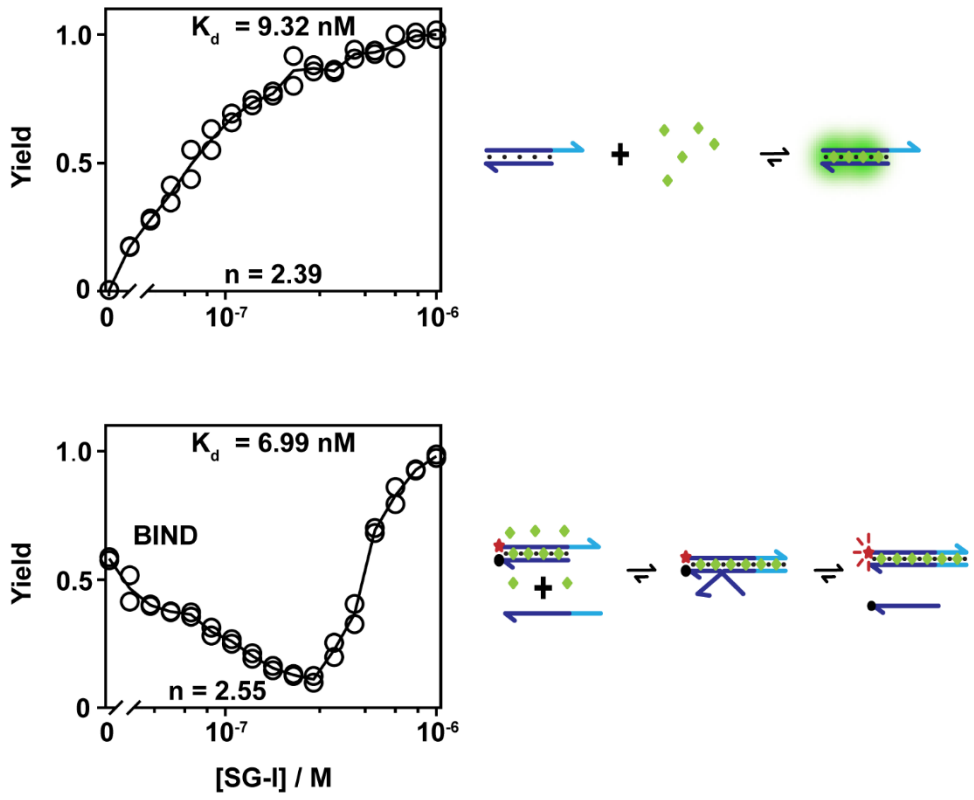

Fig. 7 | A head-to-head comparation between the classic fluorescence turn-on assay

(top) and BIND (bottom) for determining the K_d and binding site size of SG-I. To ensure a fair comparison, the same CP duplex with fixed concentration of 20 nM was used for both assays and highly consistent K_d and n values were reported within both parsing methods.

I further expanded the validation of BIND against 16 known DNA binders with reported K_d ranging from 0.4 nM to 250 μM (Fig. 8).

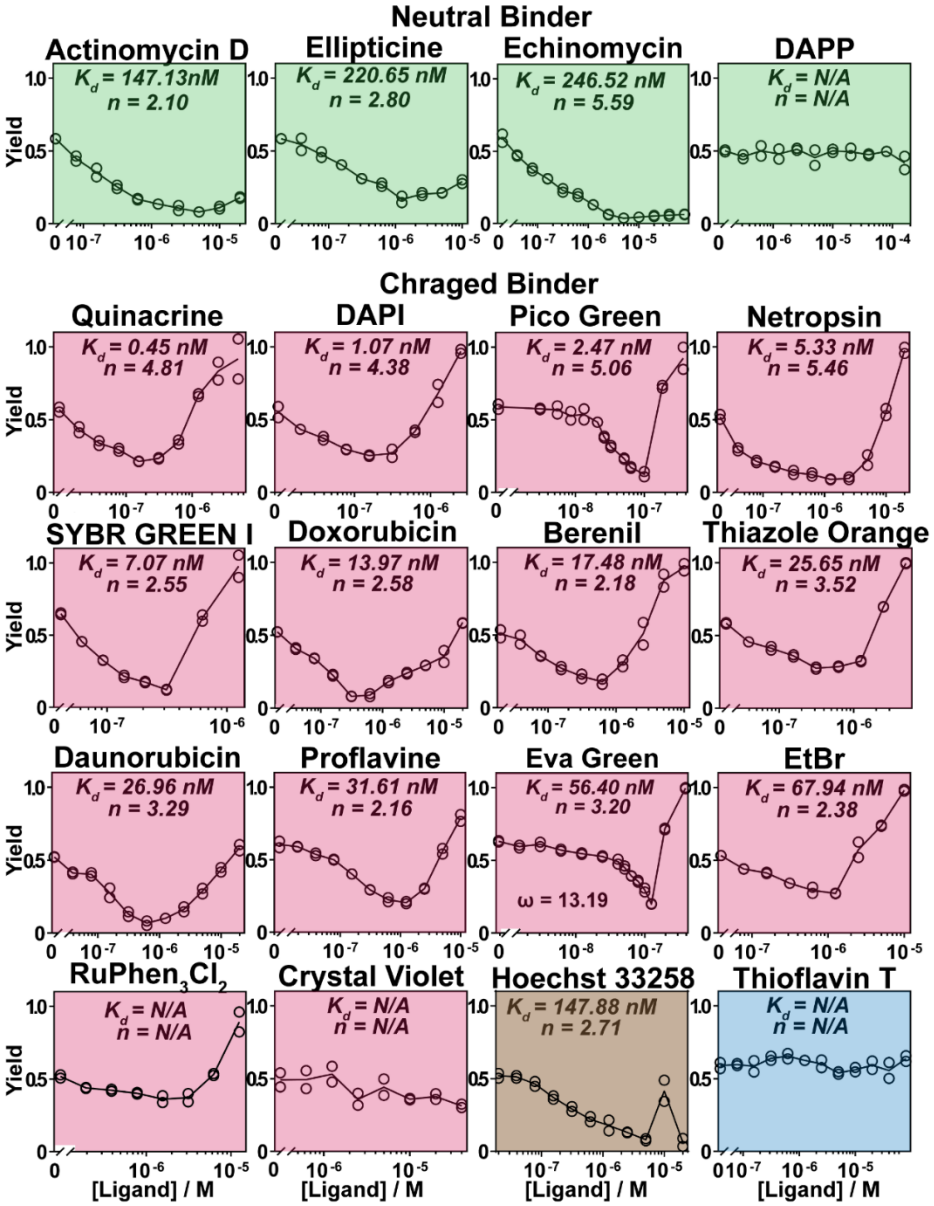

Fig. 8 | BIND curves for representative small molecular DNA binders and non-binders. Binding dissociation constants and binding site sizes were calculated via BIND curves. Hoechst 33258 shows a sharp drop of fluorescence signal at high binder concentrations, which was a result of strong inner filter effect for the high concentration of Hoechst 33258 dye when concentration exceeds 10 μM.

Values of K_d and n were successfully determined for all 16 binders using BIND, regardless the binding modes (7 intercalators, 8 groove binders and 1 unknown mode) and charge condition (13 positively charged binders and 3 neutral binders), which were highly consistent with reported values determined at similar conditions (Table 1, Fig. 9a and 9b).

Table 1. Comparison of dissociation constants and binding site sizes measured using BIND against reported values.

Binder	K_d / nM (this work)	Binding Site Size (this work)	Reported K_d / nM	Reported Binding Site Size
Actinomycin D	147.1	2.1	125.0[31]	2.5[32]
Echinomycin	246.5	5.6	322.0[33]	5.6[33]
Ellipticine	220.7	2.8	333.3[34]	4.4[35]
DAPP	N/A	N/A	~50000.0[36]	N/A
Quinacrine	0.4	4.8	0.5[37]	5.0[38]
DAPI	1.1	4.4	1.8[39]	4.0[40]
Pico Green	2.5	5.1	5.0[41]	3.8[41]
Netropsin	5.3	5.5	5.0[42]	5.9[43]
SG-I	7.1	2.6	3.1[44]	3.1[44]
Berenil	17.5	2.2	13.7[45]	1.7[45]
Doxorubicin	20.3	2.9	33.8[46]	3.0[47]
TO	25.6	3.5	66.6[48]	3.1[48]
Daunorubicin	27.0	3.3	86.2[46]	3.2[47]
Eva Green	56.4	3.2	344.8[49]	4.0[49]
Proflavine	31.6	2.2	66.7[50]	2.1[51]
EtBr	67.9	2.4	112.0[52]	2.2[53]
$RuPhen_3Cl_2$	N/A	N/A	113636.4[54]	3.0[54]
Crystal Violate	N/A	N/A	6666.7[55]	4.5[55]
Hoechst 33258	147.9	2.7	204.1[56]	3.0[57]

Thioflavin T	N/A	N/A	14000.0[58]	N/A

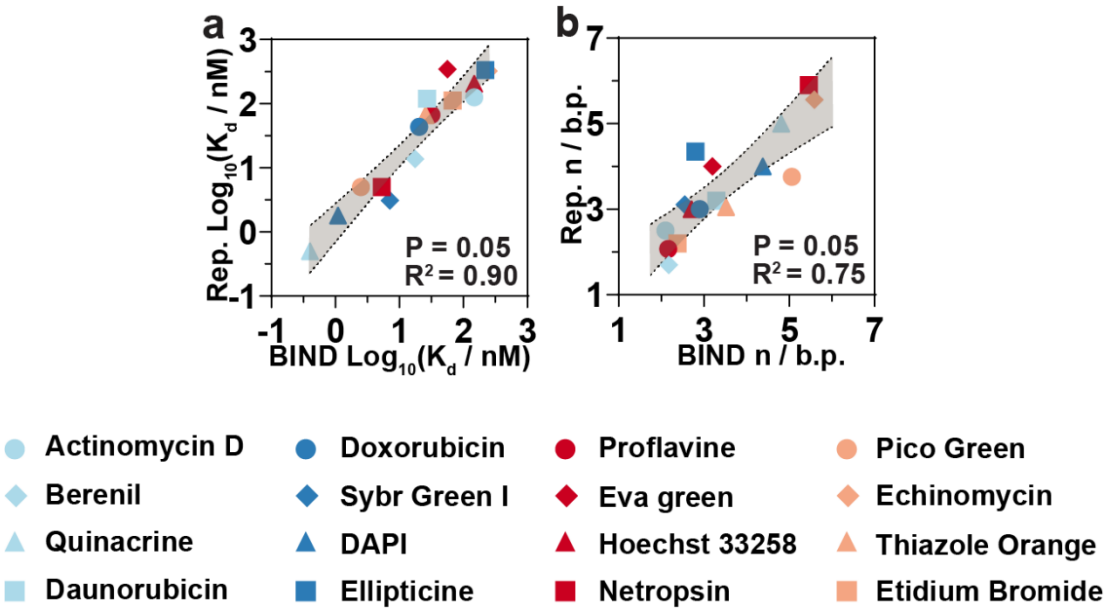

Fig. 9 | High consistencies between BIND and previous works reported binding affinity and binding site size. a. K_d values of 16 binders determined using BIND, which were then plotted against the reported values in the literatures. **b**. Binding site sizes of 16 binders determined using BIND, which were then plotted against the reported values in the literatures.

Besides Kd and n, binding cooperativity (ω) is another important parameter to characterize how the binding of one binder affects the binding of the next. A binder of positive cooperativity is likely to attract free binders to fulfill their empty neighbor slots on dsDNA, which is featured by a sharp binding curve with narrower dynamic range than that of a non-cooperative binder. Interestingly, when plotting CBC against K_d values of the 16 binders, all non-cooperative binders were lined up in Fig. 10a, which separated the quadrant into two parts. Binders distributed at the lower space indicated a shift of K_d to a greater numeric value and thus could be positively cooperative. To test this hypothesis, we measured ω for Pico Green and Eva Green, which were clearly distributed at the space of non-cooperative binders (on the line) and that of positively cooperative binders (at the lower space) in Fig. 10a, respectively. Despite of the same

CBC at 100 nM, the Kd of Eva Green was 25 times greater than that of Pico Green (Fig. 10b and 10c). I further fit the binding curve established using BIND against the mathematical model previously developed by McGhee and Hippel:[59].

$$^{v}/_{L} = \mathrm{K_a}(1-\mathrm{nv})[\frac{(2\omega-1)(1-\mathrm{nv})+\mathrm{v}-\mathrm{R}}{2(\omega-1)(1-\mathrm{nv})}]^{(n-1)}[\frac{1-(n+1)v+R}{2(1-nv)}]^{2}$$

where $\mathrm{R} = \sqrt{\{[1-(\mathrm{n}+1)\mathrm{v}]^2+4\omega\mathrm{v}(1-\mathrm{nv})\}}$, v stands for number of bound ligands per base pair, L stands for the concentration of unbound ligand in the solution, n stands for the binding site size. The cooperativity of Eva Green was determined to be 13.2, suggesting the binding of Eva Green was highly positively cooperative, which is consistent with previous study by Shoute and Loppnow ($\omega = 8.1$).[60]

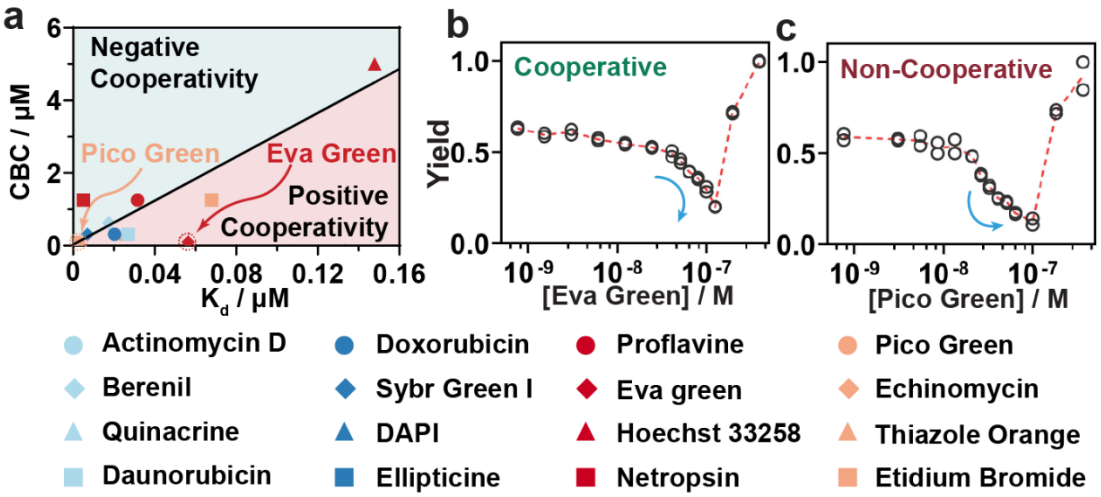

Fig. 10 | Profiling non-cooperative binders and a cooperative binder Eva Green (EG). a. Profiling the binding cooperativity of 16 binders by plotting their critical binder concentration (CBC) against the determined K_d values using BIND. **b.** BIND profile of a cooperative binder EG. **c.** BIND profile of a non-cooperative binder Pico Green (PG).

2.2.3 Profiling thermodynamic signatures of DNA-binder interactions using BIND

When employed for profiling the binding characteristics of DNA binders, BIND was found to be highly sensitive and reproducible, capable of accurately resolving

binding constants at temperature intervals less than 2 ºC. This feature allows us to gain critical thermodynamic parameters of DNA-binder interactions, including free energy (ΔG), enthalpy (ΔH), and entropy (ΔS), without the need for melting the DNA at wide temperature ranges. Instead, I measured K_a of 15 non-cooperative binders using BIND at 27 ºC, 30 ºC, 32 ºC, 35 ºC, and 37 ºC and fit the results using Van't Hoff's equation,

$$ln\ K_a = -\frac{\Delta H}{RT} + \frac{\Delta S}{R} \quad (9)$$

where K_a stands for the association constant, ΔH stands for enthalpy change, ΔS stands for entropy change, R is the gas constant and T is temperature in Kalvin (Fig. 11-25).

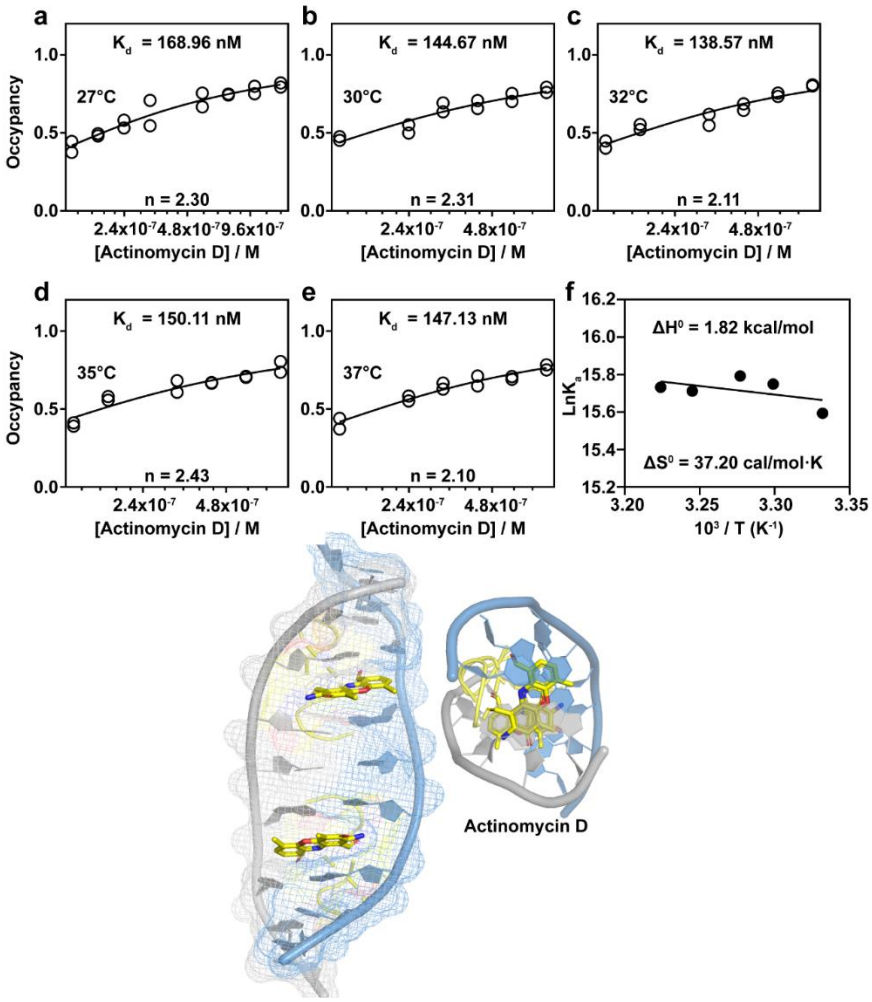

Fig. 11 | Profiling the binding thermodynamics of Actinomycin D using BIND. Binding curves established using the S_N1 region of BIND was used to determine the K_d

at varying temperatures. Van't Hoff plot was then established to determine the ΔHº and ΔSº. The binding mode was further visualized by molecular docking as outlined in the supplementary experimental section. The DNA 3D image was extracted from PDB file 1MNV.

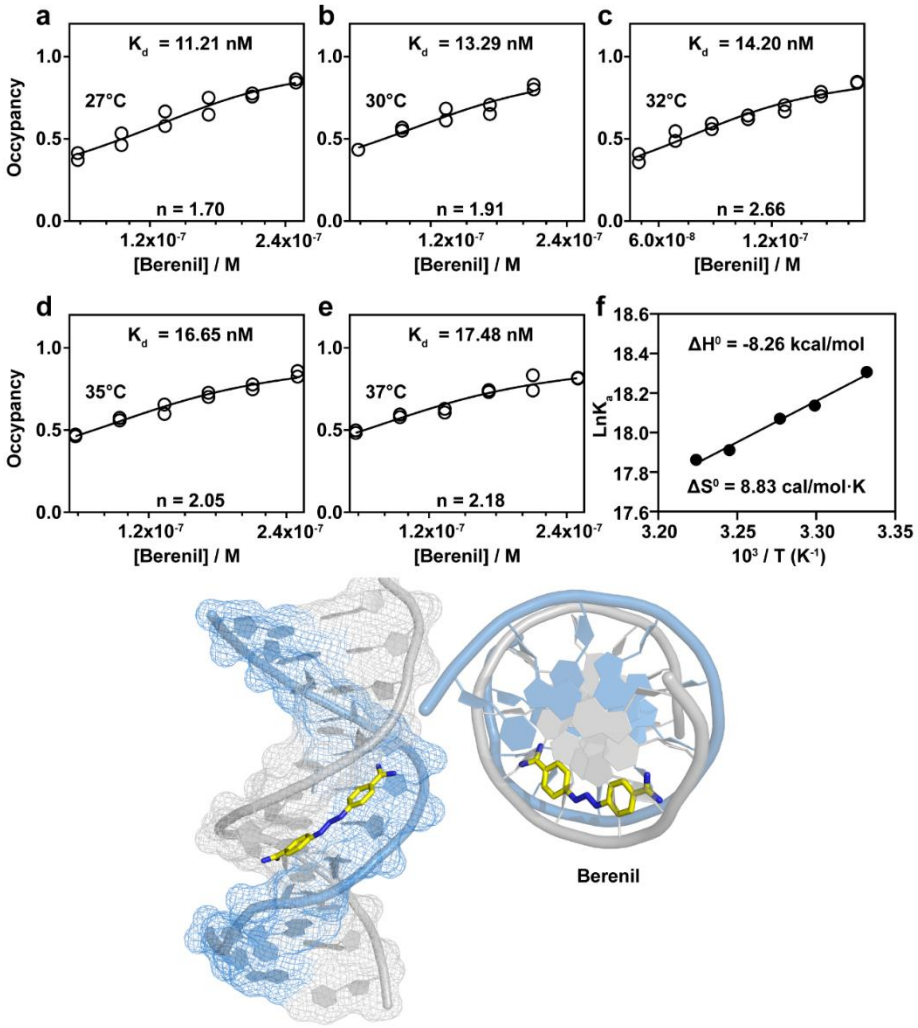

Fig. 12 | Profiling the binding thermodynamics of berenil using BIND. Binding curves established using the S_N1 region of BIND was used to determine the K_d at varying temperatures. Van't Hoff plot was then established to determine the ΔHº and ΔSº. The binding mode was further visualized by molecular docking as outlined in the supplementary experimental section. The DNA 3D image was extracted from PDB file 2GVR.

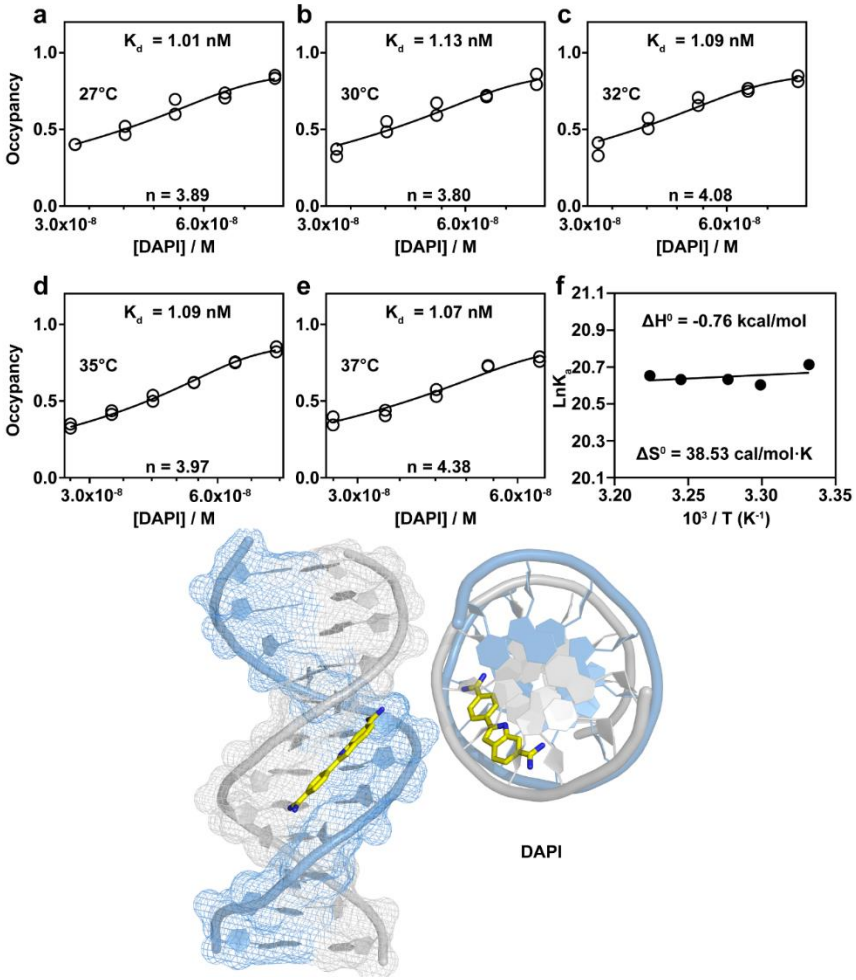

Fig. 13 | Profiling the binding thermodynamics of DAPI using BIND. Binding curves established using the S_N1 region of BIND was used to determine the K_d at varying temperatures. Van't Hoff plot was then established to determine the ΔHº and ΔSº. The binding mode was further visualized by molecular docking as outlined in the supplementary experimental section. The DNA 3D image was extracted from PDB file 1D30.

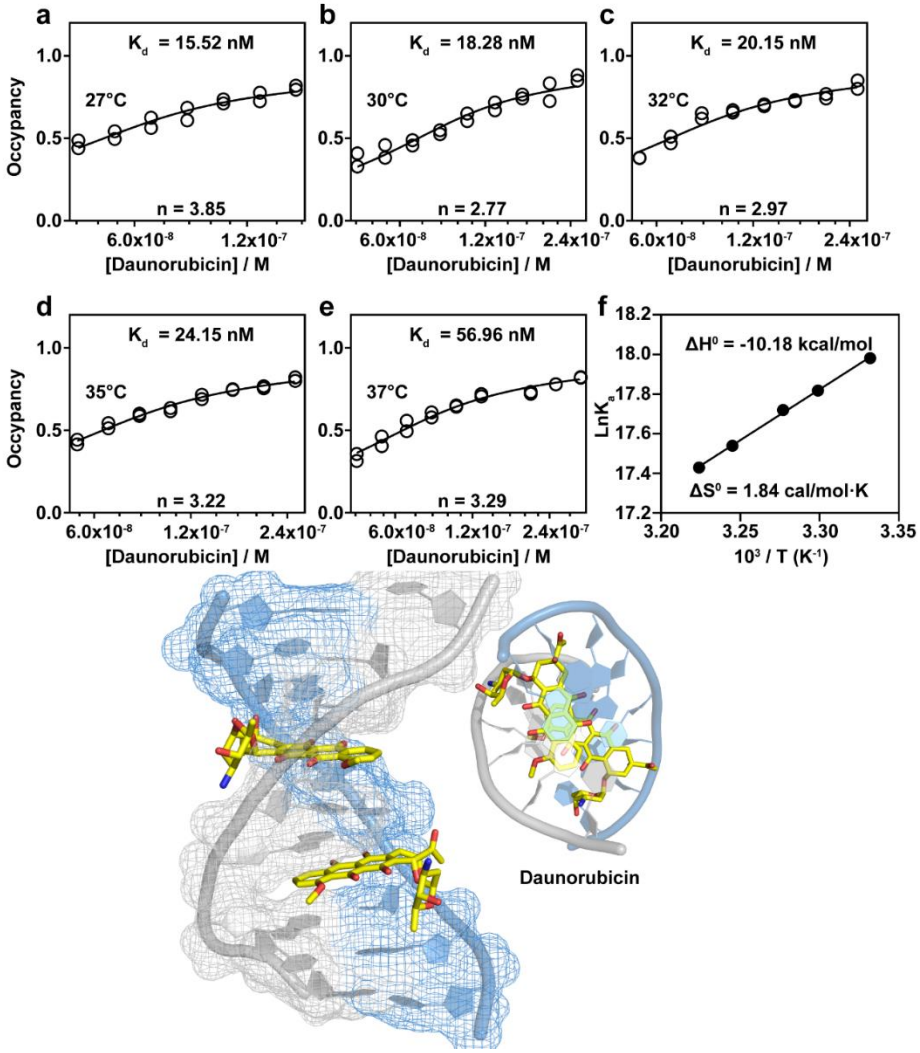

Fig. 14 | Profiling the binding thermodynamics of daunorubicin (Dau) using BIND. Binding curves established using the S_N1 region of BIND was used to determine the K_d at varying temperatures. Van't Hoff plot was then established to determine the ΔH^o and ΔS^o. The binding mode was further visualized by molecular docking as outlined in the supplementary experimental section. The DNA 3D image was extracted from PDB file 108D.

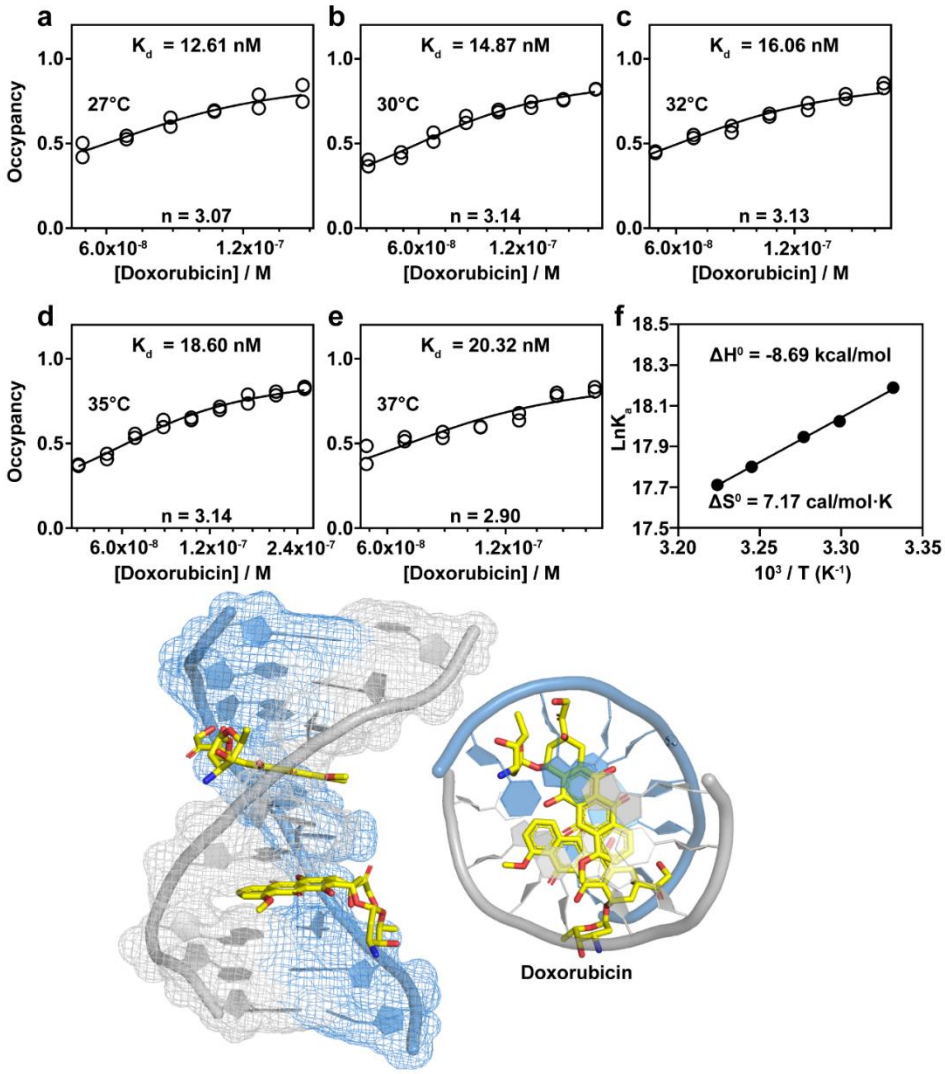

Fig. 15 | Profiling the binding thermodynamics of doxorubicin (Dox) using BIND. Binding curves established using the S_N1 region of BIND was used to determine the K_d at varying temperatures. Van't Hoff plot was then established to determine the ΔHº and ΔSº. The binding mode was further visualized by molecular docking as outlined in the supplementary experimental section. The DNA 3D image was extracted from PDB file 108D.

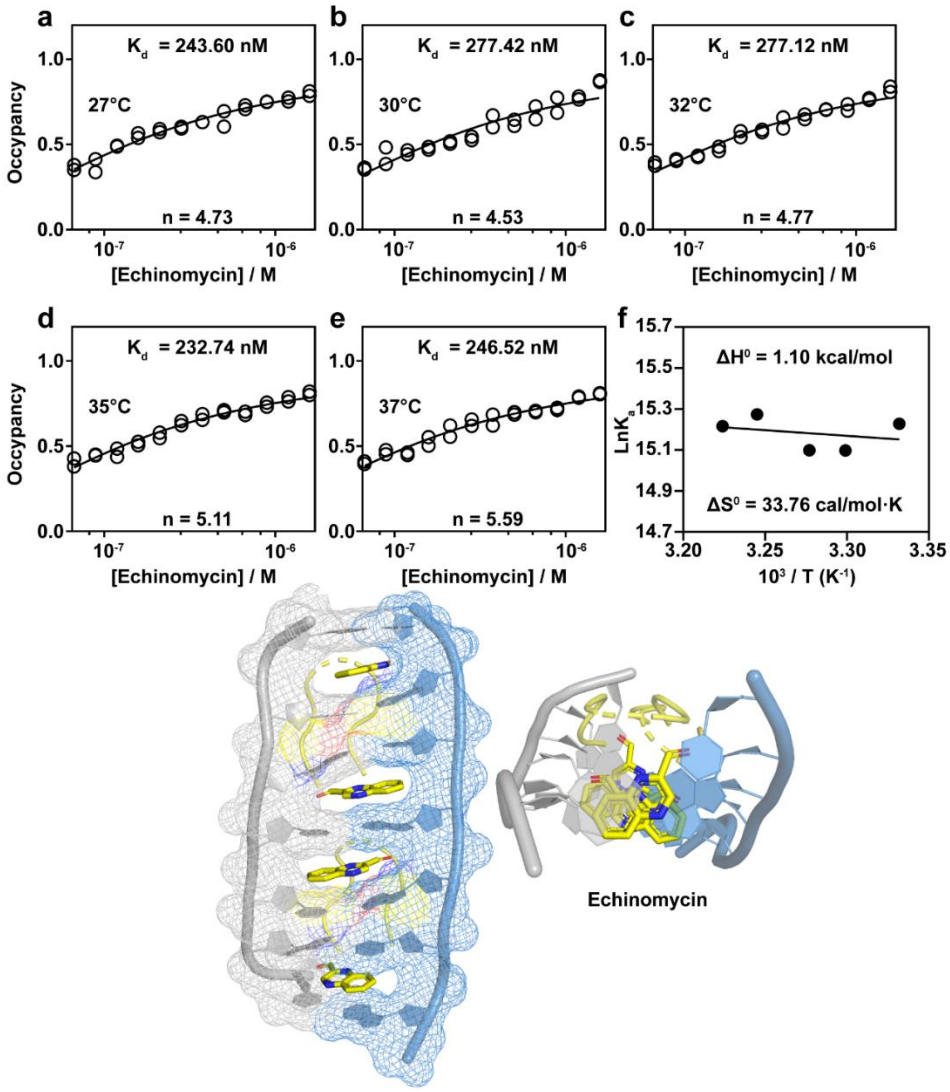

Fig. 16 | Profiling the binding thermodynamics of echinomycin using BIND. Binding curves established using the S_N1 region of BIND was used to determine the K_d at varying temperatures. Van't Hoff plot was then established to determine the ΔHº and ΔSº. The binding mode was further visualized by molecular docking as outlined in the supplementary experimental section. The DNA 3D image was extracted from PDB file 5YTY.

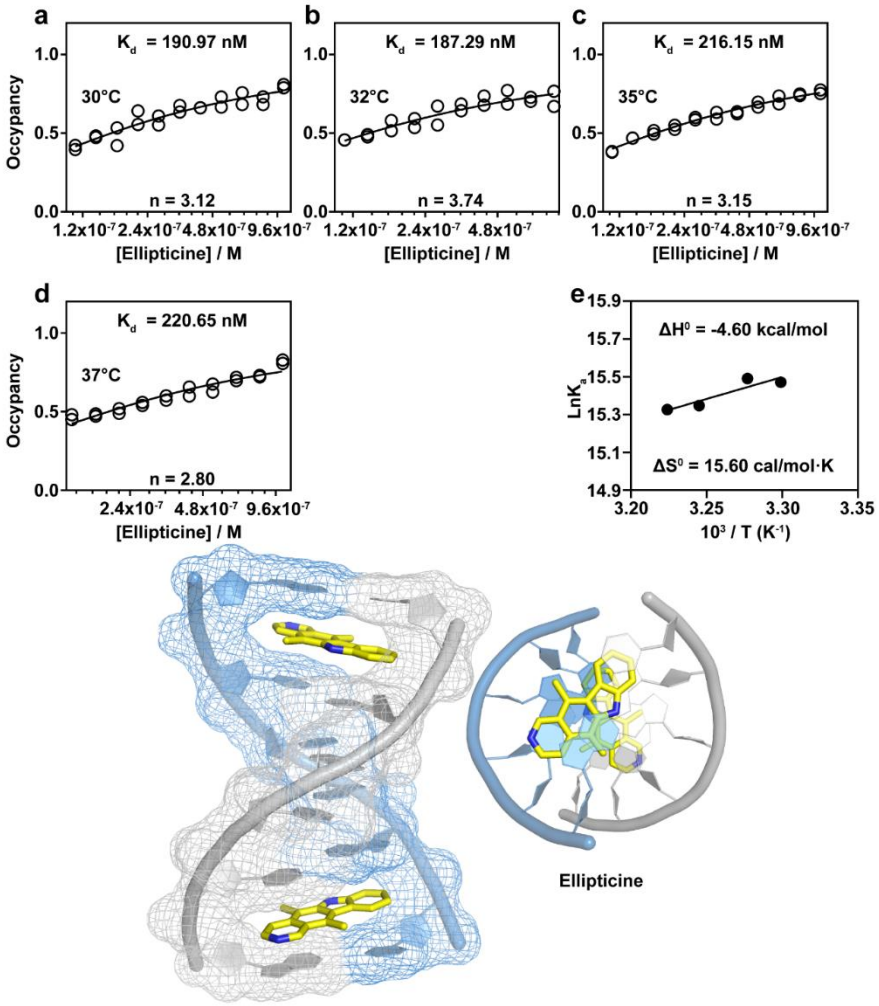

Fig. 17 | Profiling the binding thermodynamics of ellipticine using BIND. Binding curves established using the S_N1 region of BIND was used to determine the K_d at varying temperatures. Van't Hoff plot was then established to determine the ΔH^o and ΔS^o. The binding mode was further visualized by molecular docking as outlined in the supplementary experimental section. The DNA 3D image was extracted from PDB file 1Z3F.

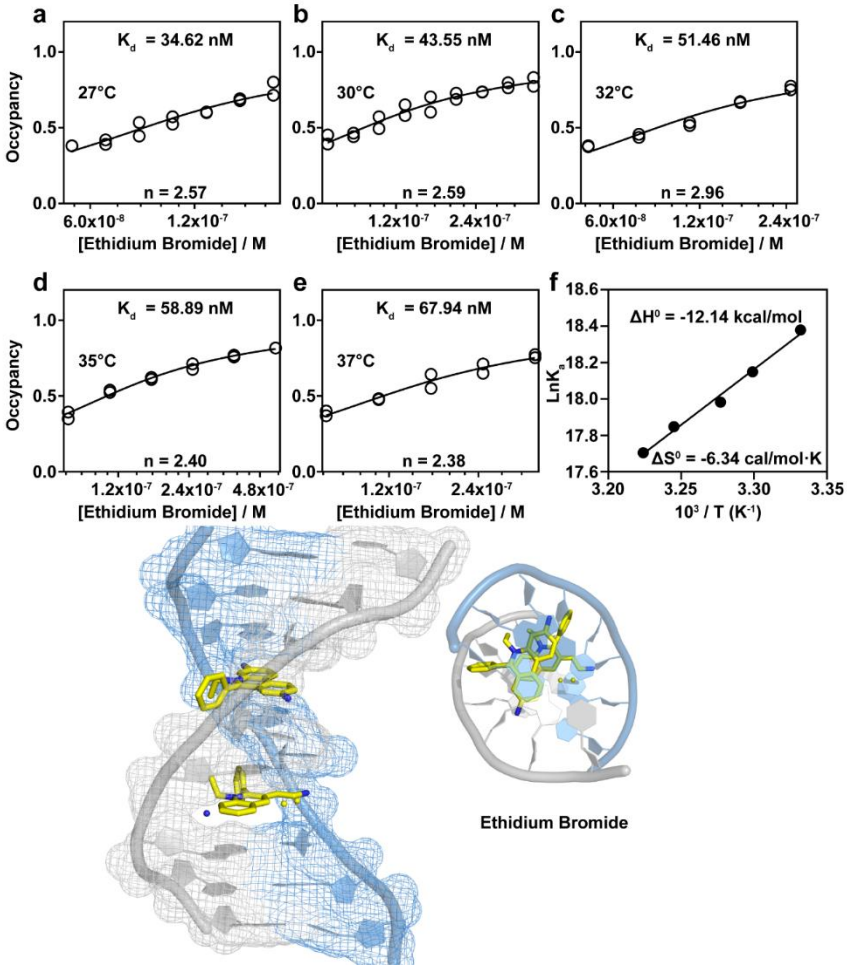

Fig. 18 | Profiling the binding thermodynamics of EB using BIND. Binding curves established using the S_N1 region of BIND was used to determine the K_d at varying temperatures. Van't Hoff plot was then established to determine the ΔH^o and ΔS^o. The binding mode was further visualized by molecular docking as outlined in the supplementary experimental section. The DNA 3D image was extracted from PDB file 108D.

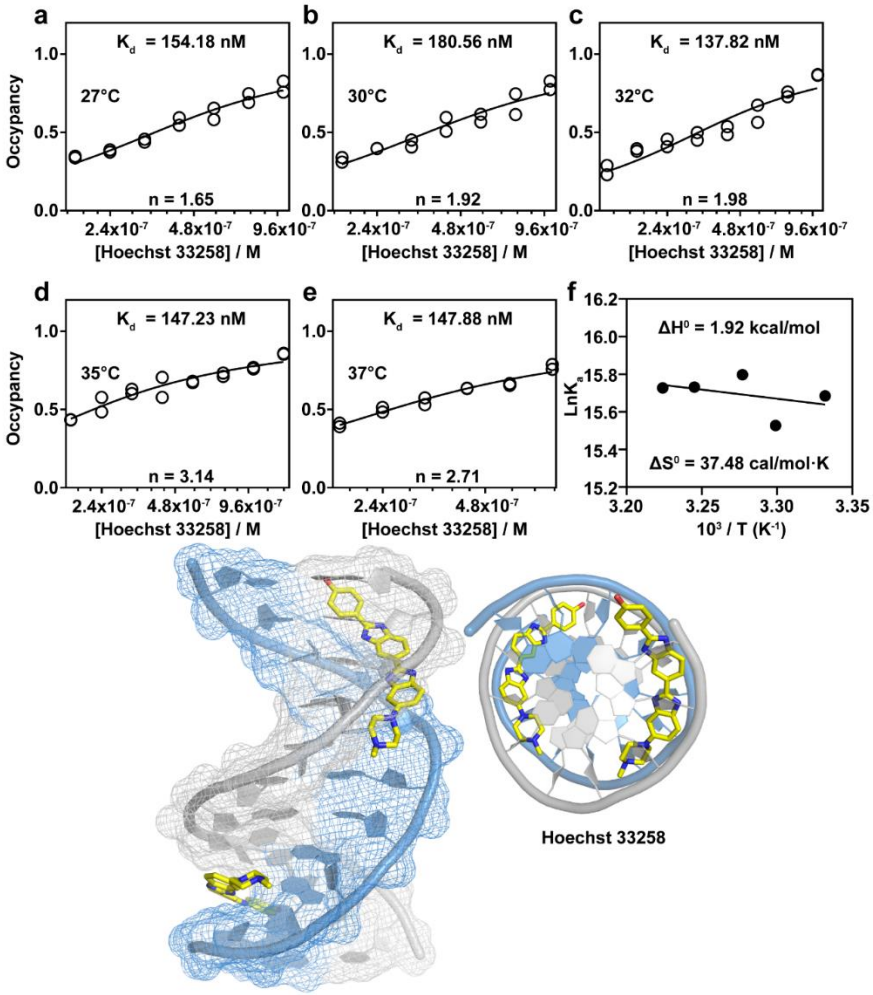

Fig. 19 | Profiling the binding thermodynamics of Hoechst 33258 using BIND. Binding curves established using the S_N1 region of BIND was used to determine the K_d at varying temperatures. Van't Hoff plot was then established to determine the ΔHº and ΔSº. The binding mode was further visualized by molecular docking as outlined in the supplementary experimental section. The DNA 3D image was extracted from PDB file 1QSX.

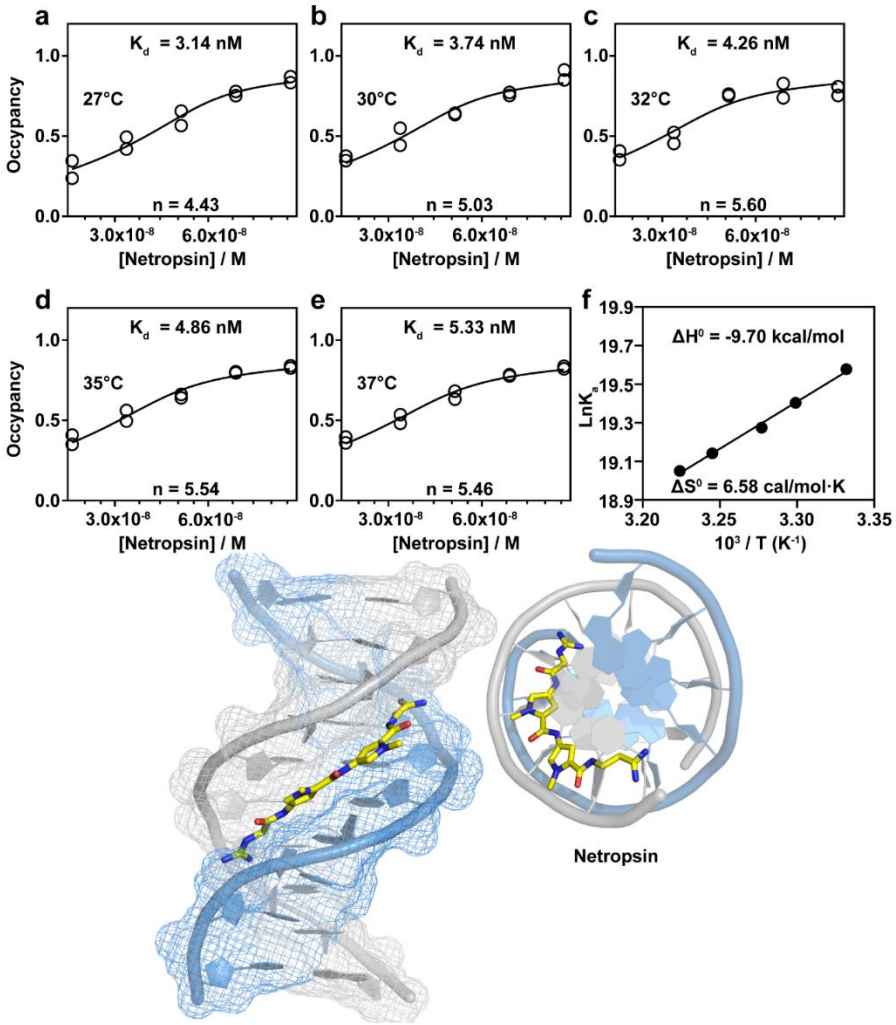

Fig. 20 | Profiling the binding thermodynamics of netropsin using BIND. Binding curves established using the S_N1 region of BIND was used to determine the K_d at varying temperatures. Van't Hoff plot was then established to determine the ΔHº and ΔSº. The binding mode was further visualized by molecular docking as outlined in the supplementary experimental section. The DNA 3D image was extracted from PDB file 2LWH.

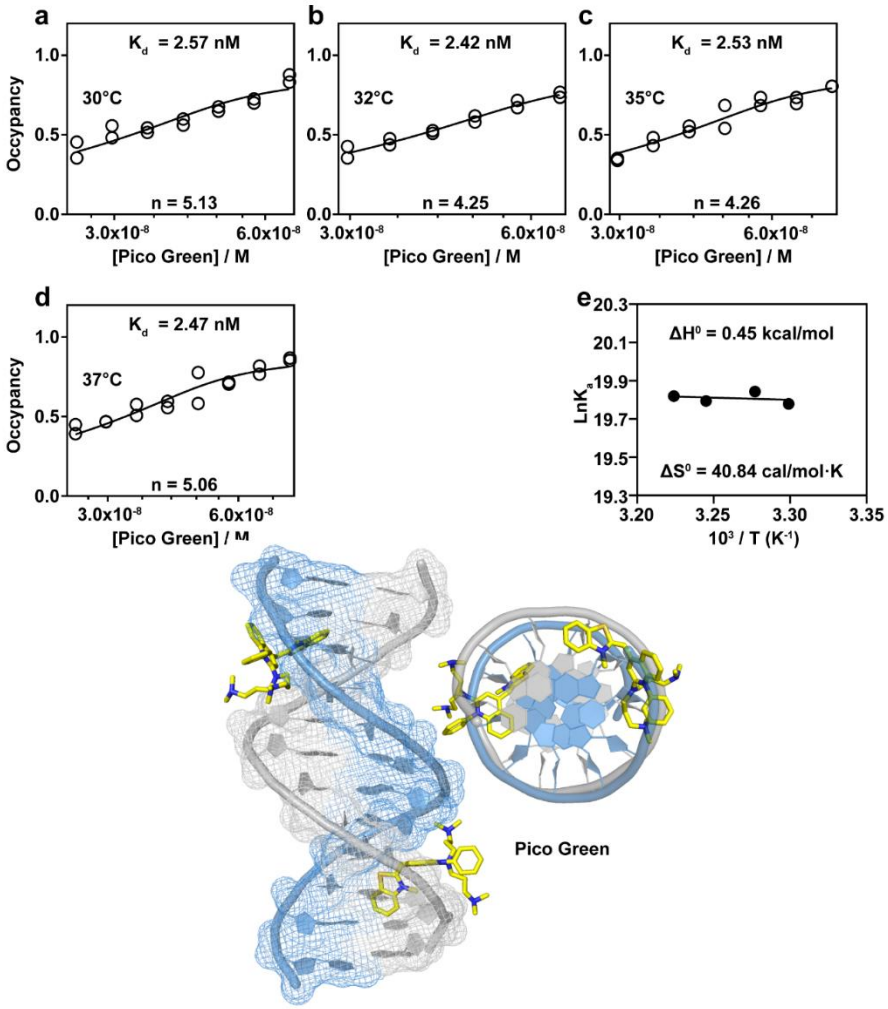

Fig. 21 | Profiling the binding thermodynamics of PG using BIND. Binding curves established using the S_N1 region of BIND was used to determine the K_d at varying temperatures. Van't Hoff plot was then established to determine the ΔHº and ΔSº. The binding mode was further visualized by molecular docking as outlined in the supplementary experimental section. The DNA 3D image was extracted from PDB file 1D30.

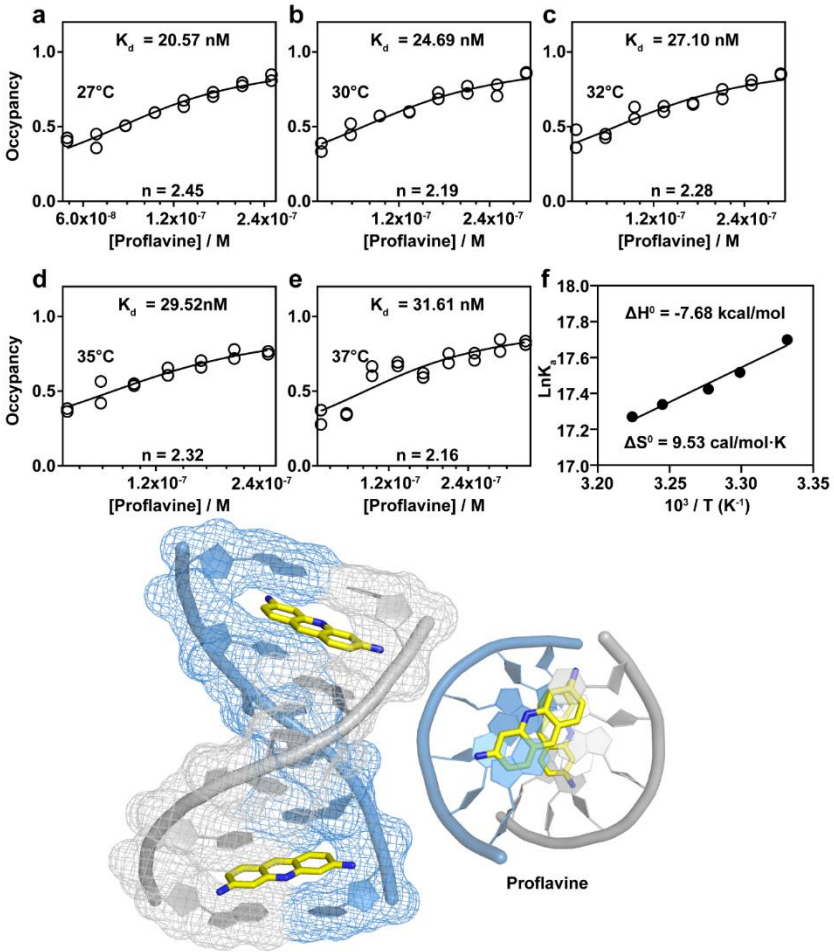

Fig. 22 | Profiling the binding thermodynamics of proflavine using BIND. Binding curves established using the S_N1 region of BIND was used to determine the K_d at varying temperatures. Van't Hoff plot was then established to determine the ΔHº and ΔSº. The binding mode was further visualized by molecular docking as outlined in the supplementary experimental section. The DNA 3D image was extracted from PDB file 3FT6.

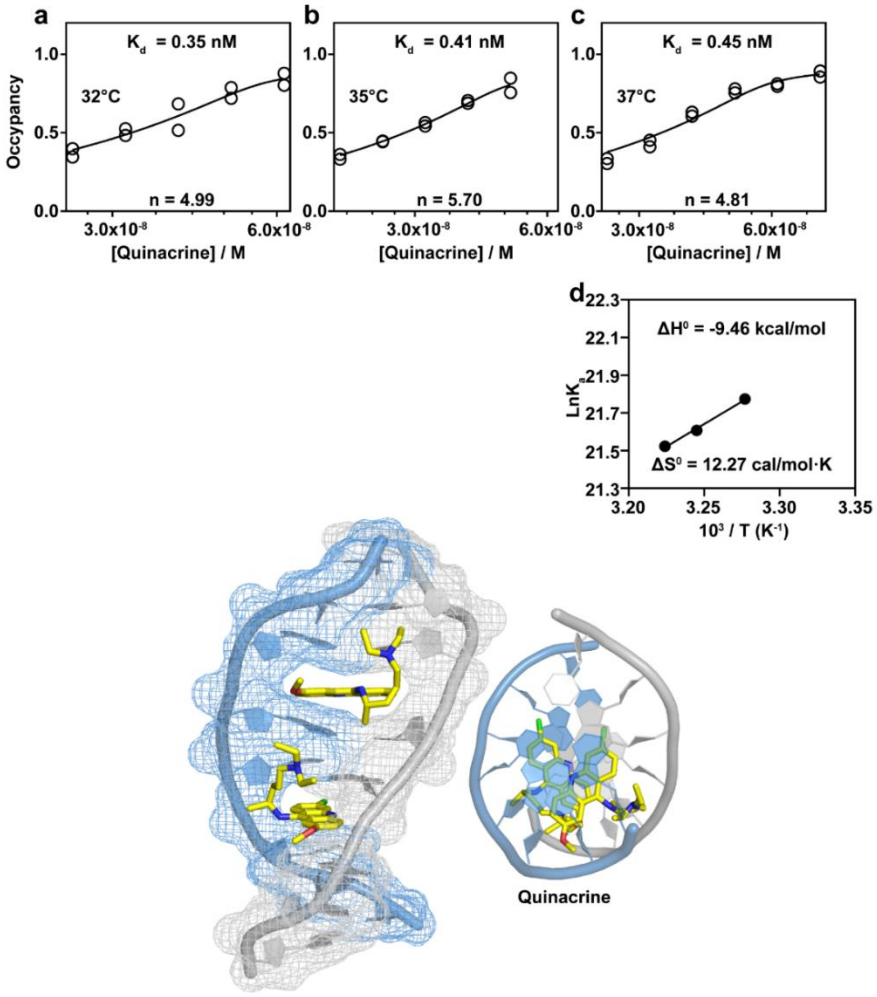

Fig. 23 | Profiling the binding thermodynamics of quinacrine using BIND. Binding curves established using the S_N1 region of BIND was used to determine the K_d at varying temperatures. Van't Hoff plot was then established to determine the ΔH^o and ΔS^o. The binding mode was further visualized by molecular docking as outlined in the supplementary experimental section. The DNA 3D image was extracted from PDB file 108D.

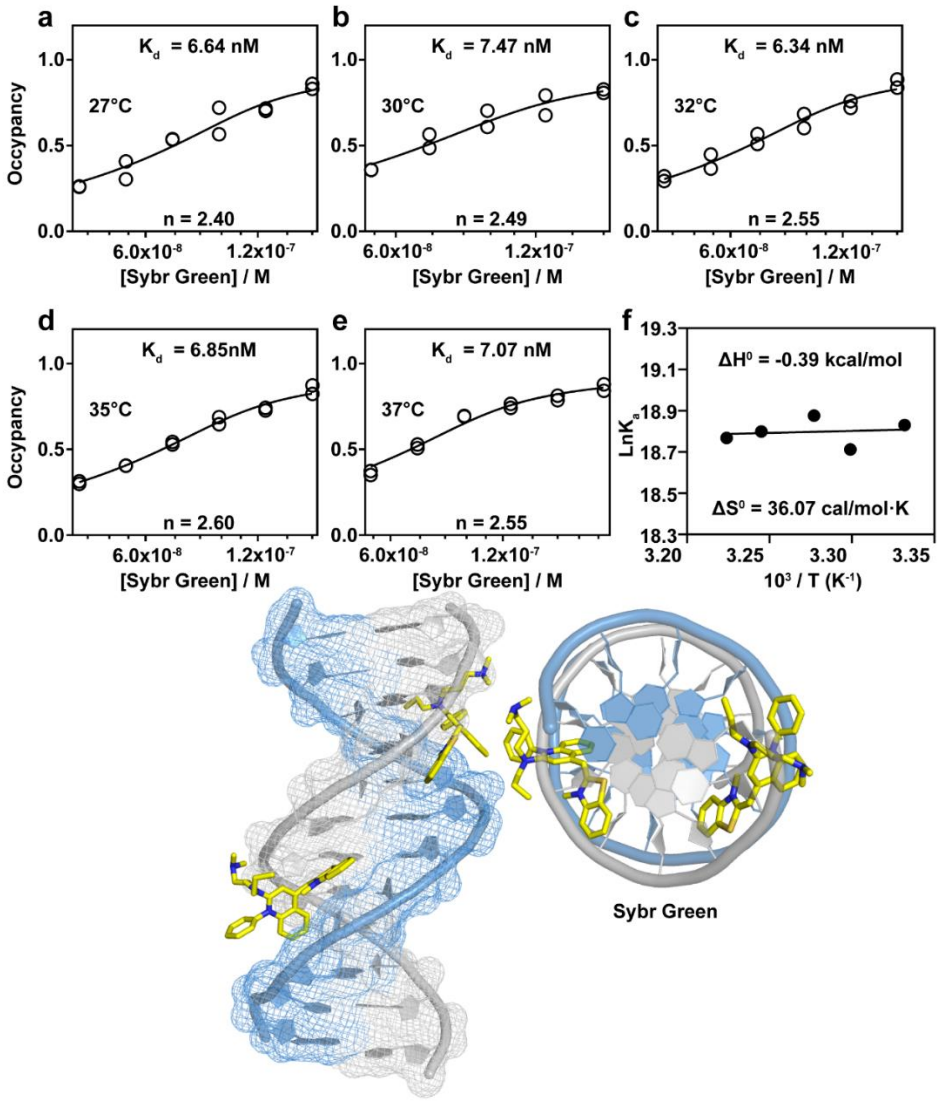

Fig. 24 | Profiling the binding thermodynamics of SG-I using BIND. Binding curves established using the S_N1 region of BIND was used to determine the K_d at varying temperatures. Van't Hoff plot was then established to determine the ΔH^o and ΔS^o. The binding mode was further visualized by molecular docking as outlined in the supplementary experimental section. The DNA 3D image was extracted from PDB file 108D.

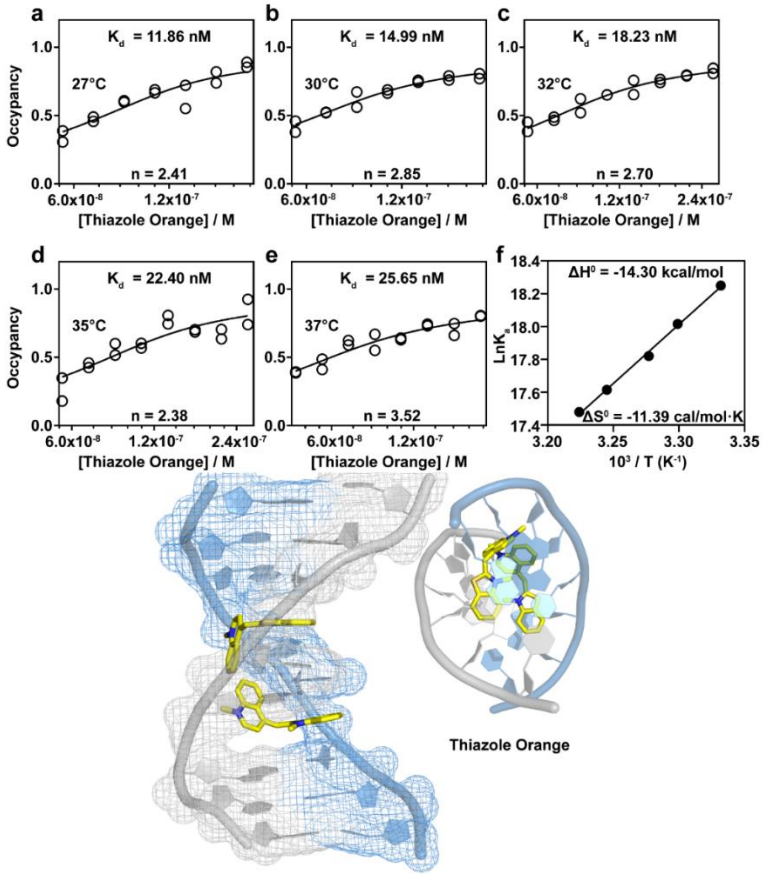

Fig. 25 | Profiling the binding thermodynamics of TO using BIND. Binding curves established using the S_N1 region of BIND was used to determine the K_d at varying temperatures. Van't Hoff plot was then established to determine the ΔHº and ΔSº. The binding mode was further visualized by molecular docking as outlined in the supplementary experimental section. The DNA 3D image was extracted from PDB file 108D.

I ranked 15 binders according to the measured Δ*S* values at 37 ºC in Fig. 26a, where ΔG ranges from -13.3 to -9.4 kcal/mol, ΔH ranges from -14.3 to +1.9 kcal/mol, and -TΔS ranges from -12.7 to +3.5 kcal/mol at 37ºC. I also calculated enthalpy contribution to the overall Gibbs free energy (ΔH/ΔG) for 12 binders with reported thermodynamic parameters, which ranges from -0.2 to +1.2 (Fig. 26b). The measured enthalpy contributions using BIND were highly consistent with reported values with a $R^2 = 0.94$ (Fig. 26b and Table 2).

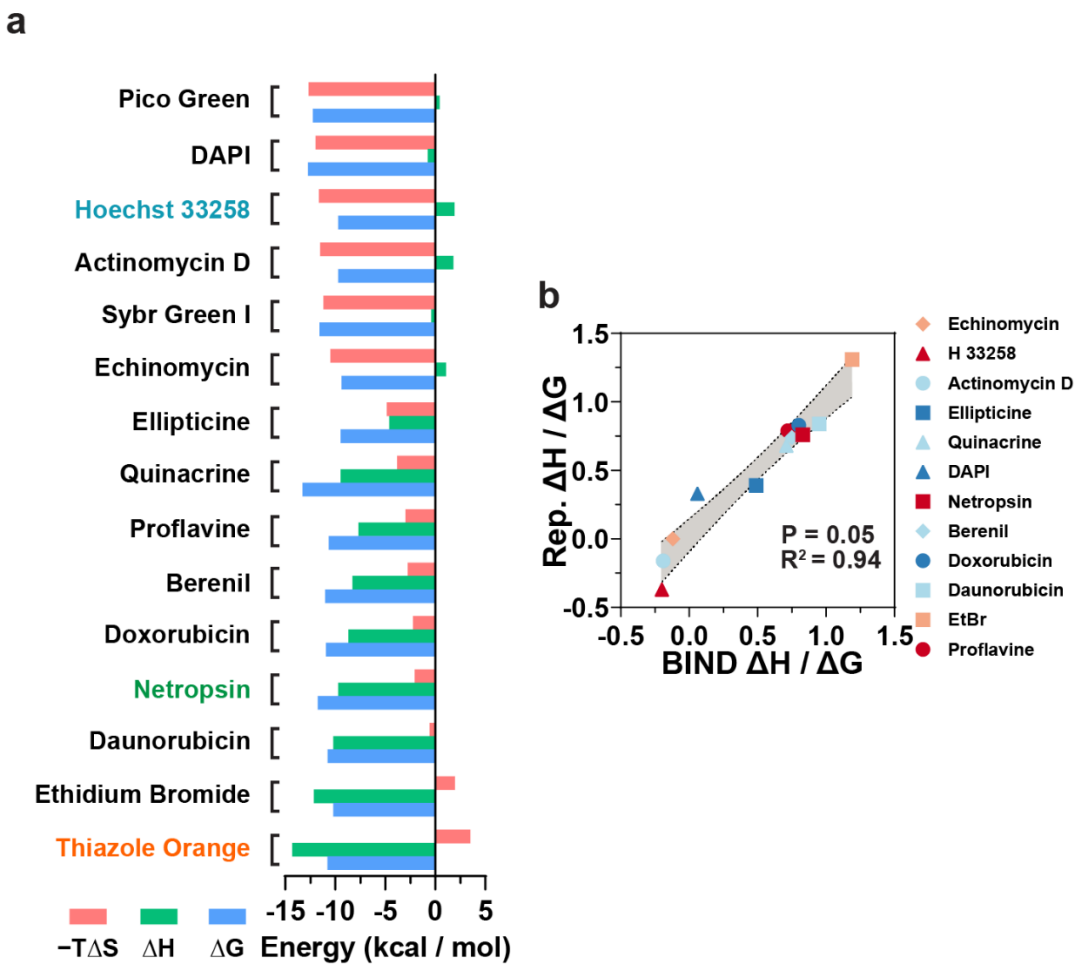

Fig. 26 | Summarizing thermodynamic signatures of 15 binders. a. Numerical values of ΔG, ΔH and -TΔS (T = 310.15K) for 15 DNA binders using BIND. These values were ranged against -TΔS. **b.** comparing values of enthalpy contribution obtained using BIND and literatures for 12 binders with reported thermodynamic parameters.

Table 2 Comparison of enthalpic and entropic contributions measured using BIND against reported values.

Binder	ΔH^0 / ΔG^0	$-T\Delta S^0$ / ΔG^0	ΔH^0 / ΔG^0 reported	$-T\Delta S^0$ / ΔG^0 reported
Actinomycin D	-19%	119%	-16%[61]	116%
Echinomycin	-12%	112%	0%[62]	100%
Ellipticine	49%	51%	39%[63]	61%
DAPP	N/A	N/A	N/A	N/A
Quinacrine	71%	29%	68%[64]	32%
DAPI	6%	94%	33%[65]	67%
Pico Green	-4%	114%	N/A	N/A
Netropsin	83%	17%	76%[43]	24%
SG-I	3%	97%	N/A	N/A
Berenil	75%	25%	74%[66]	26%
Doxorubicin	80%	20%	83%[67]	17%
TO	133%	-33%	N/A	N/A
Daunorubicin	95%	5%	84%[68]	16%
Eva Green	N/A	N/A	N/A	N/A
Proflavine	72%	28%	79%[69]	21%
EtBr	119%	-19%	131%[70]	-31%
$RuPhen_3Cl_2$	N/A	N/A	N/A	N/A
Crystal Violate	N/A	N/A	N/A	N/A
Hoechst 33258	-20%	120%	-37%[71]	137%
Thioflavin T	N/A	N/A	N/A	N/A

Analysis of the enthalpic and entropic contribution to the free energy of DNA binder interactions can reveal the molecular forces that drive the binding and thus shed light on the binding mode of each binder.[72, 73] For example, BIND reveals a favorable enthalpic contribution of -14.3 kcal/mol for a classic intercalator, thiazole orange, indicating that the main driving force for binding was the base stacking and the

formation of hydrogen bond (Fig. 27a). The entropic penalty of +3.5 kcal/mol also indicated the loss of rotational degrees of freedom, likely due to the constraint structure caused by the intercalation (Fig. 27b). While intercalation is mainly enthalpically driven, the driving force for the minor grooving binding can be highly diverse[73]. Using BIND, I demonstrated the binding of Hoechst 33258, a classic minor groove binder, was entropically driven *via* hydrophobic and electrostatic interactions, evidenced by a favorable entropy contribution (-TΔS) of -11.6 kcal/mol with a slight enthalpic penalty of +1.9 kcal/mol (Fig. 27c and 27d). By contrast, as an amide-linked minor groove binder, netropsin binding generated a favorable enthalpy contribution of -9.7 kcal/mol with a slight contribution from entropy (-2.0 kcal/mol), suggesting that the binding was driven by the hydrogen bonding and/or van der Waals interactions (Fig. 27e and 27f).[74]

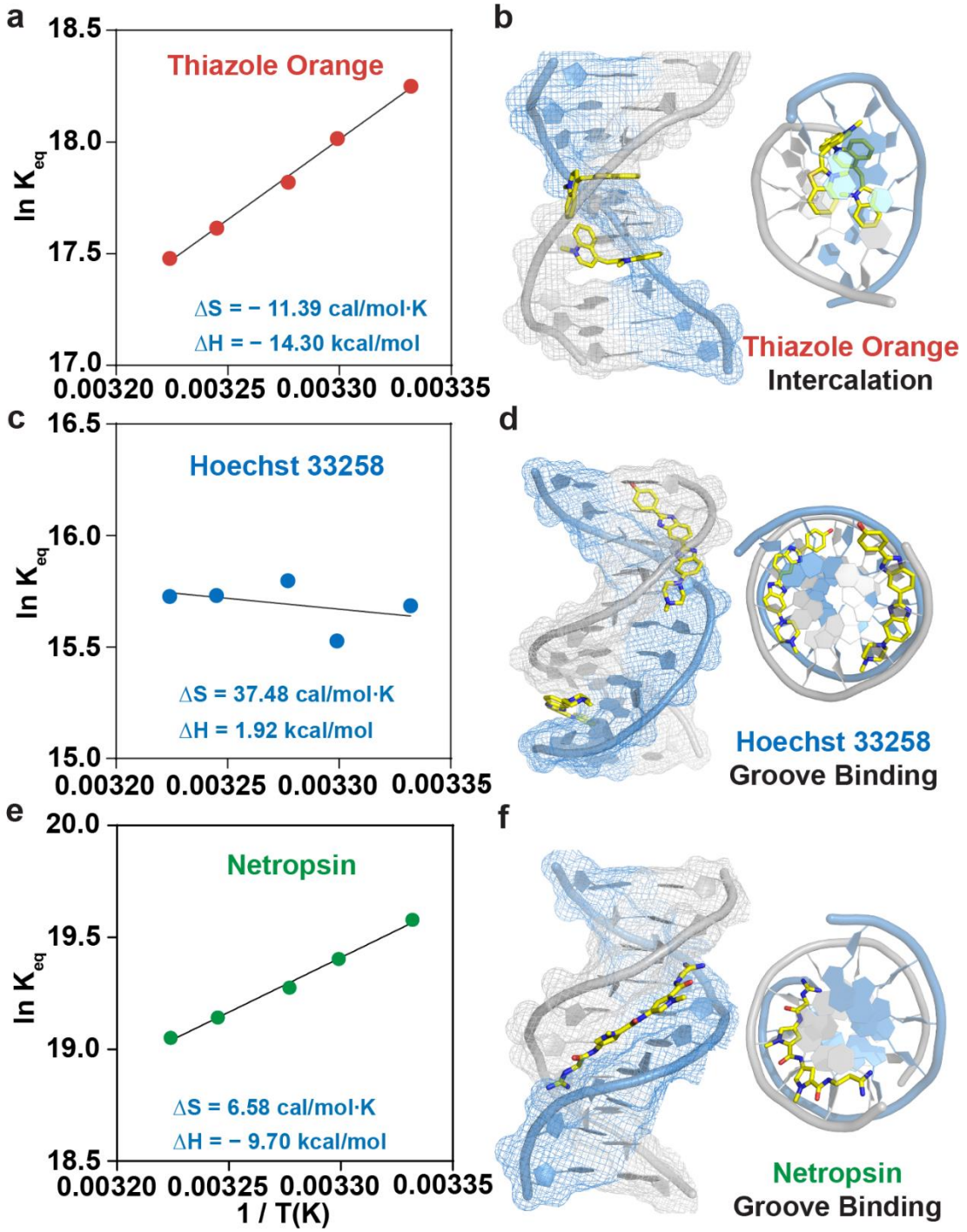

Fig. 27 | Indication of binding modes from thermodynamic signatures a. Determining ΔH and ΔS of a representative intercalator, TO, by plotting $\ln K_a$ against reaction temperature and fitting using Van't Hoff's equation. **b.** Predicted binding mode of Thiazole Orange using molecular docking. **c.** Determining ΔH and ΔS of a representative minor groove binder, Hoechst 33258, by plotting $\ln K_a$ against reaction temperature and fitting using Van't Hoff's equation. **d.** Predicted binding mode of Hoechst 33258 using molecular docking. **e.** Determining ΔH and ΔS of netropsin by plotting $\ln K_a$ against reaction temperature and fitting using Van't Hoff's equation. **f.** Predicted binding mode of netropsin using molecular docking.

2.2.4 Determining the sequence selectivity of DNA binders using BIND

DNA binders with high sequence selectivity may serve as antagonists of transcription factors or inhibitors of gene expression, and thus hold great therapeutic potential. Therefore, I next engineered BIND to evaluate the sequence selectivity of DNA binders. To achieve this goal, I designed a panel of stem-looped sink probes, each containing an 8 bp stem in the format of 5'-CGXXXXXC-3' and a 5-dA loop (Fig. 28a). DNA binders were incubated with a mixture of a sink probe containing a designated 5 bp sequence and BIND probes. The selective binding of binders to sink will reduce the effective concentration of binders to trigger the BIND reaction and thus cause a shift of BIND curve as well as CBC towards a higher concentration range (Fig. 28b). On the other hand, no shift will be observed if there is no favored binding to the sink (Fig. 28c).

I first verified the effectiveness of BIND for evaluating the sequence selectivity using 4',6'-Diamidine-2-phenylindole (DAPI) that binds selectivity to AT-rich sites in the minor groove (Fig. 28d). BIND curves of DAPI were found to keep shifting to higher concentration ranges when increasing the ratio between a 5'-TAAAT-3' sink and BIND (probe CP) from 0 to 100 (Fig. 28e). I then defined the concentration of DAPI at 50% yield of displacement at the S_N1 domain as a threshold concentration (C_T). A linear relationship was then established when plotting C_T against the ratios between sink and BIND probes (Fig. 28f). I defined the slope as a selectivity factor α, which is used to quantify the degree of sequence selectivity.

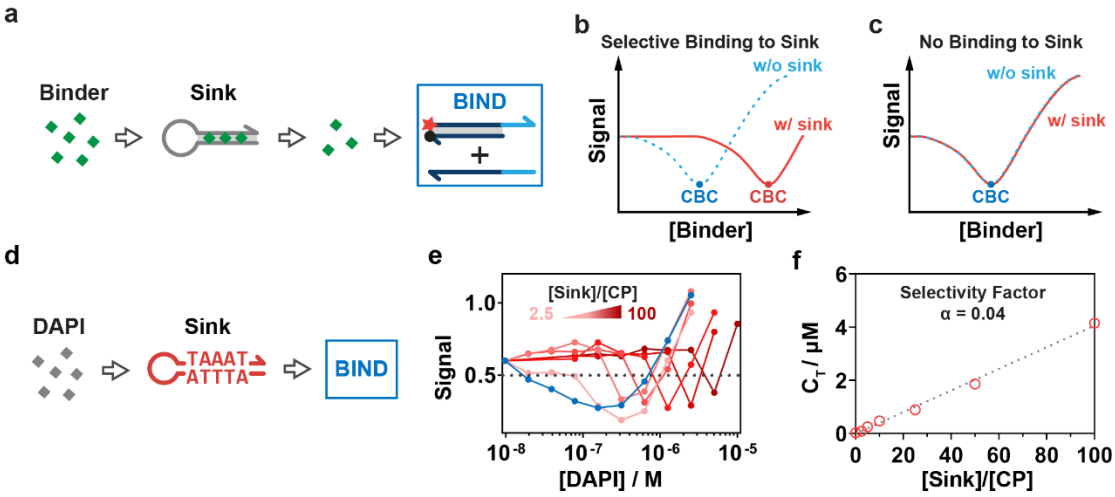

Fig. 28 | Illustration of parsing sequence selectivity using BIND. a. Schematic illustration of the competitive BIND reaction for determining the sequence selectivity of DNA binders. **b.** Schematic illustration of the expected shift of the BIND curve for a binder with favored binding to the sink probe. **c.** In the case that the binder has no sequence selectivity to the sink probe, no shift would be observed in the BIND curve. **d.** Schematic illustration of determining the sequence selectivity of DAPI to a sink probe containing 5'-TAAAT-3' stem domain using BIND. **e.** Experimentally observed shifts of BIND curves against increasing ratio of [sink]/[CP] from 0 to 100. **f.** Determining the selectivity factor of DAPI to the sink probe by plotting the critical concentration (C_T) of each BIND curve against the concentration ratio between sink and CP.

I measured and ranked α of DAPI against 8 sink probes containing representative combinations of base pairs. The observed preferences of DAPI for a five ≈ four > three > two bp AT binding site in sink probes were consistent with previous studies using NMR[75] and fluorescent intercalator displacement (FID) assays (Fig. 29).[48]

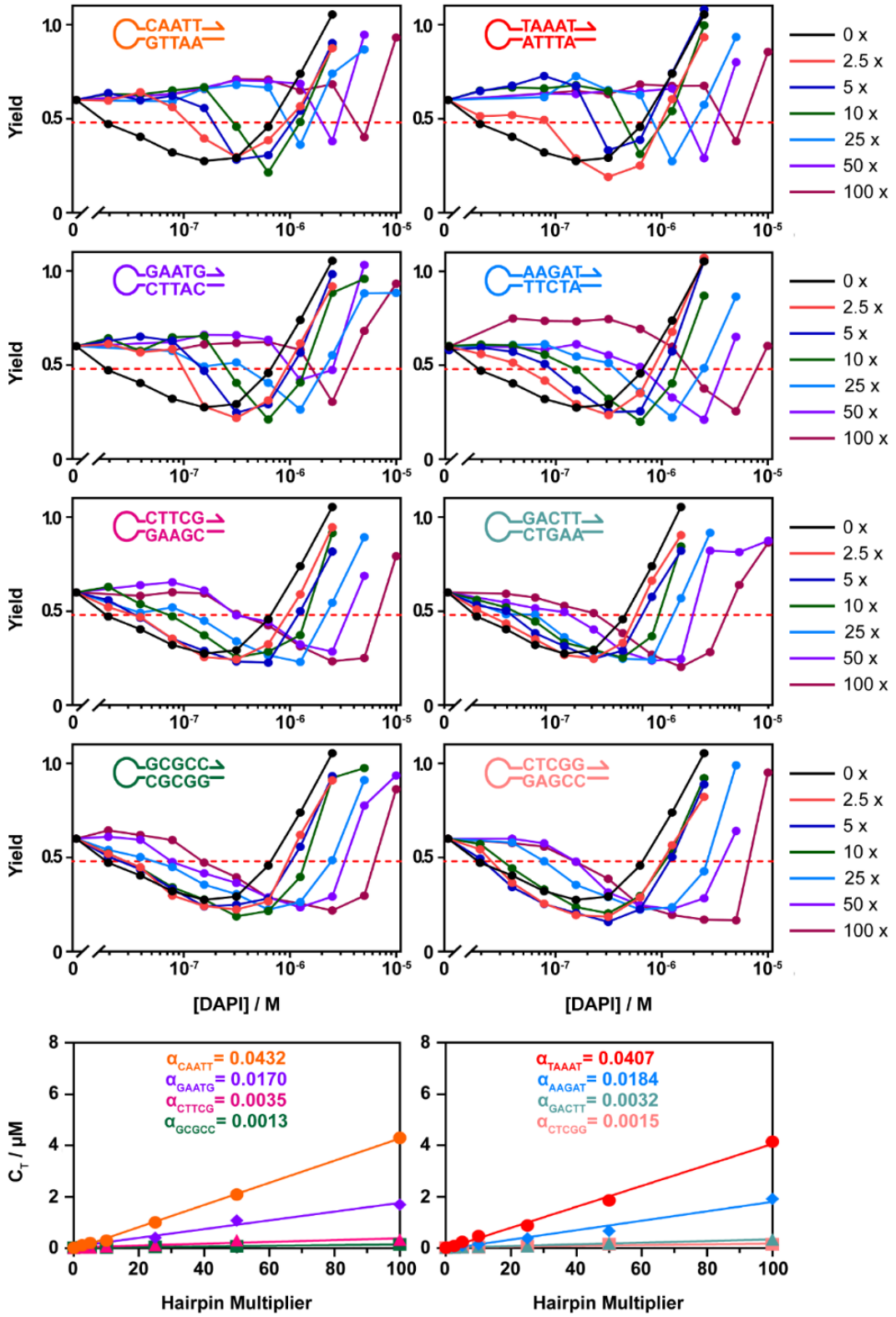

Fig. 29 | Determining sequence selectivity of DAPI. Eight types of sink probes containing different 5 bp stem sequences were used to interrogate the BIND reaction for DAPI. The shifts of BIND curves were quantitatively analyzed to obtain selectivity factor α. A general trend of sequence preference was determined to be five ≈ four > three > two bp AT binding site for DAPI.

Having confirmed the effectiveness of BIND to evaluate the sequence selectivity using DAPI, I surveyed the sequence selectivity of eight other binders using a pair of AT-rich (5'-TAAAT-3') and GC-rich (5'-GCGCC-3') sink probes (Fig. 30-37).

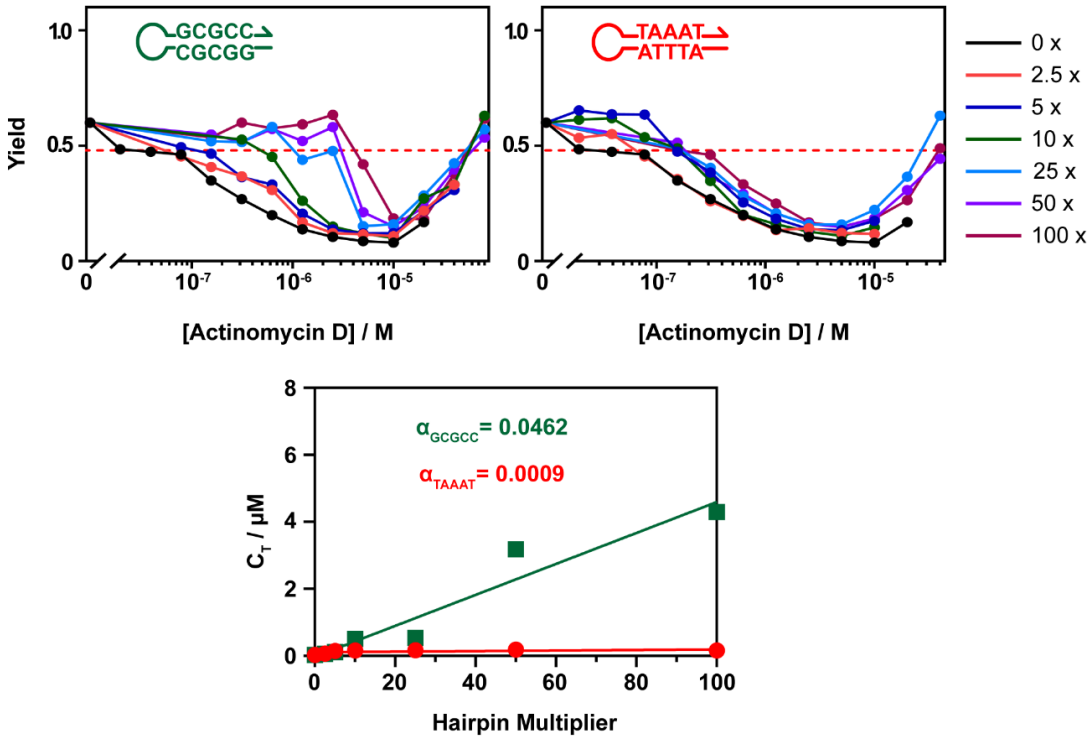

Fig. 30 | Determining sequence selectivity of Actinomycin D using GC and AT-rich sink probes.

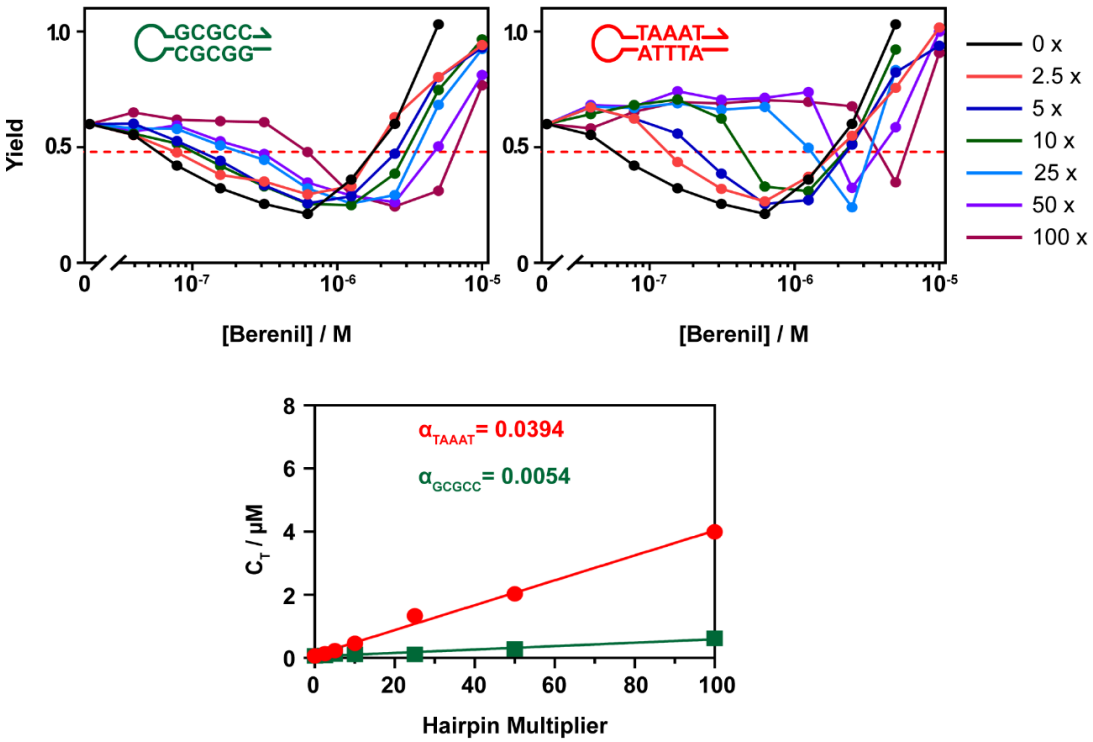

Fig. 31 | Determining sequence selectivity of berenil using GC and AT-rich sink probes.

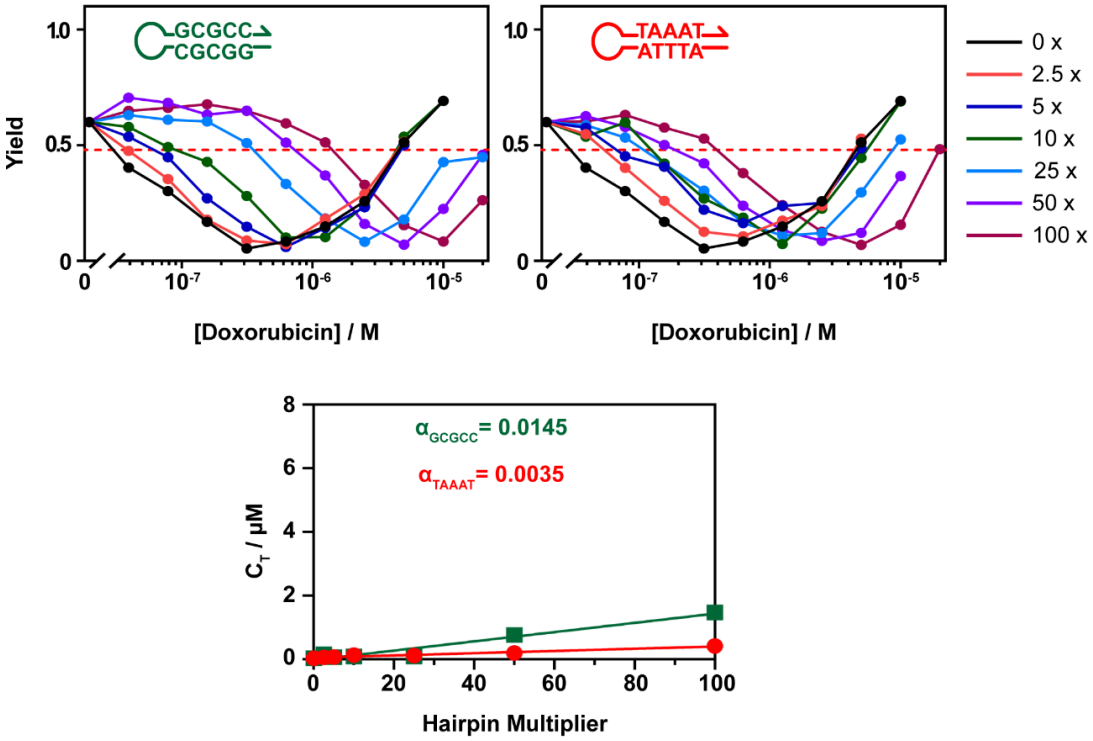

Fig. 32 | Determining sequence selectivity of Dox using GC and AT-rich sink probes.

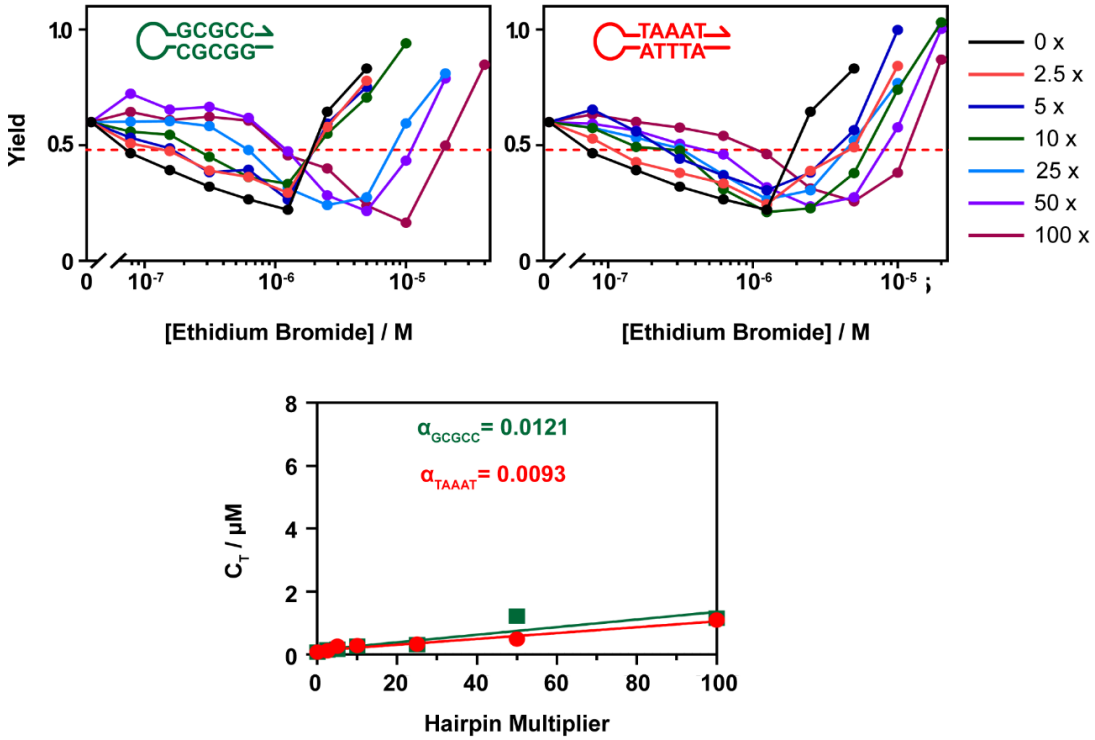

Fig. 33 | Determining sequence selectivity of EB using GC and AT-rich sink probes.

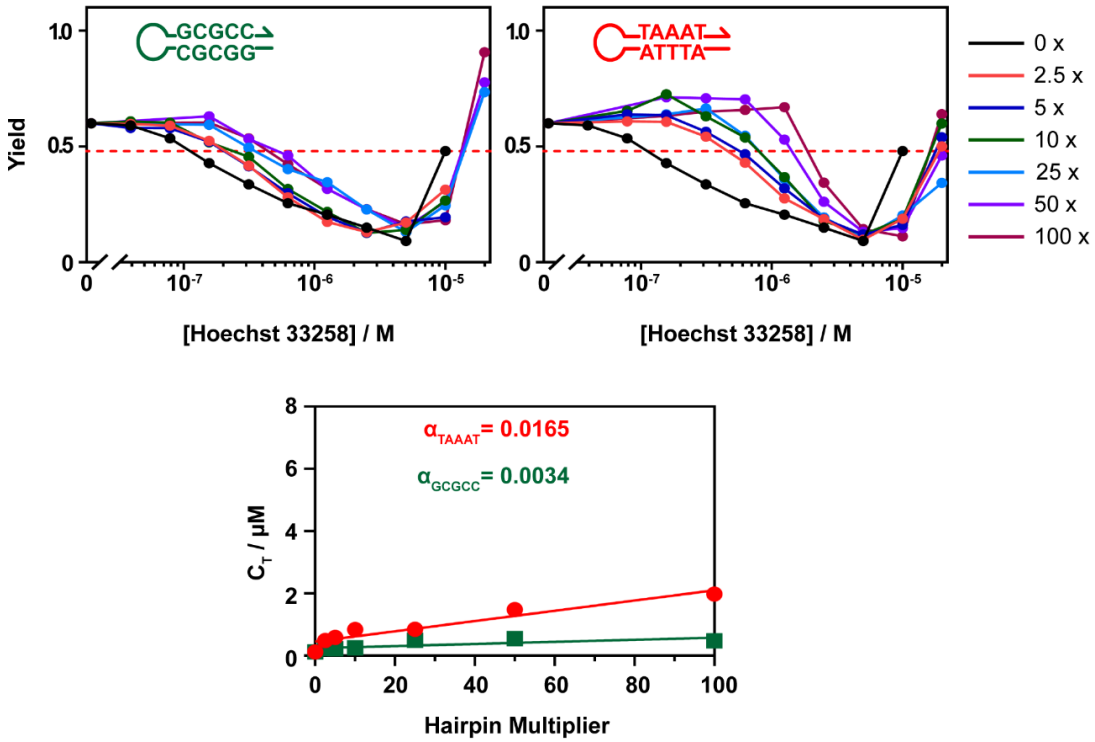

Fig. 34 | Determining sequence selectivity of Hoechst 33258 using GC and AT-rich sink probes.

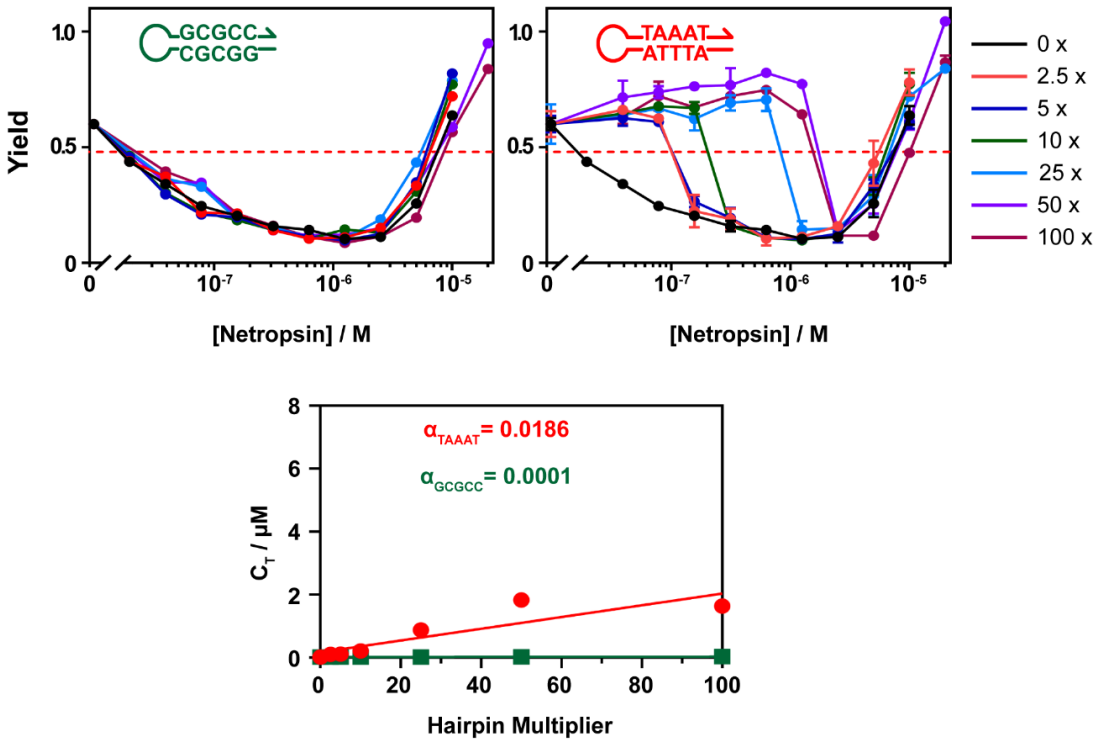

Fig. 35 | Determining sequence selectivity of netropsin using GC and AT-rich sink probes.

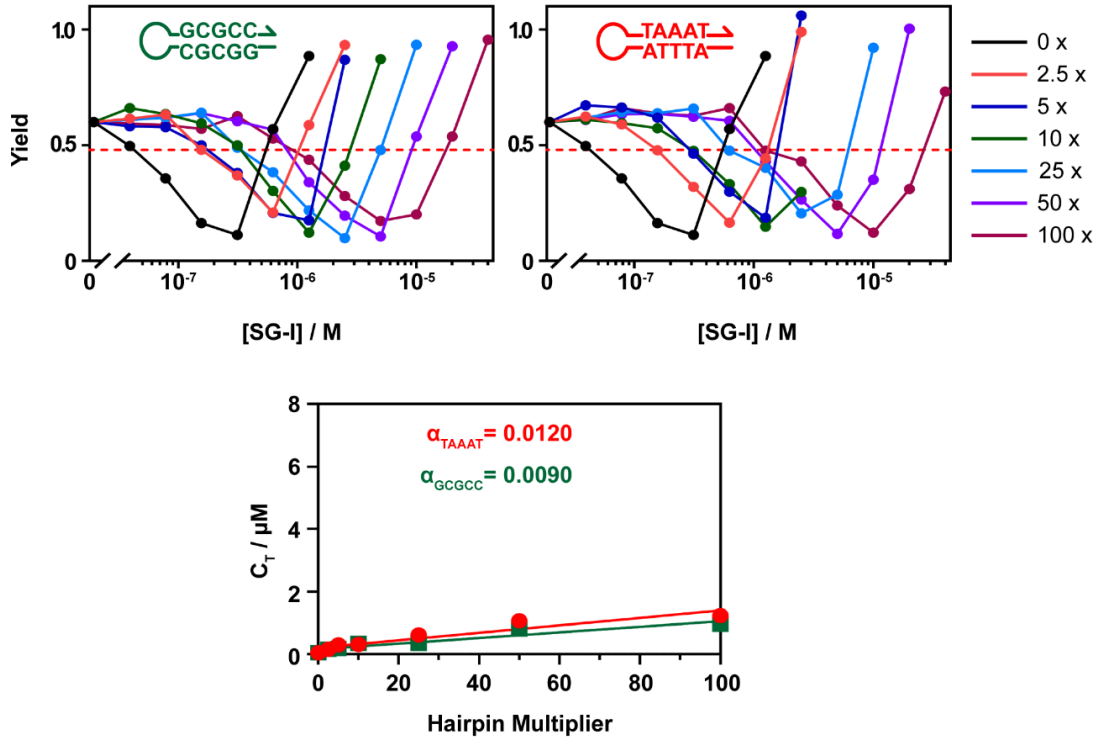

Fig. 36 | Determining sequence selectivity of SG-I using GC and AT-rich sink probes.

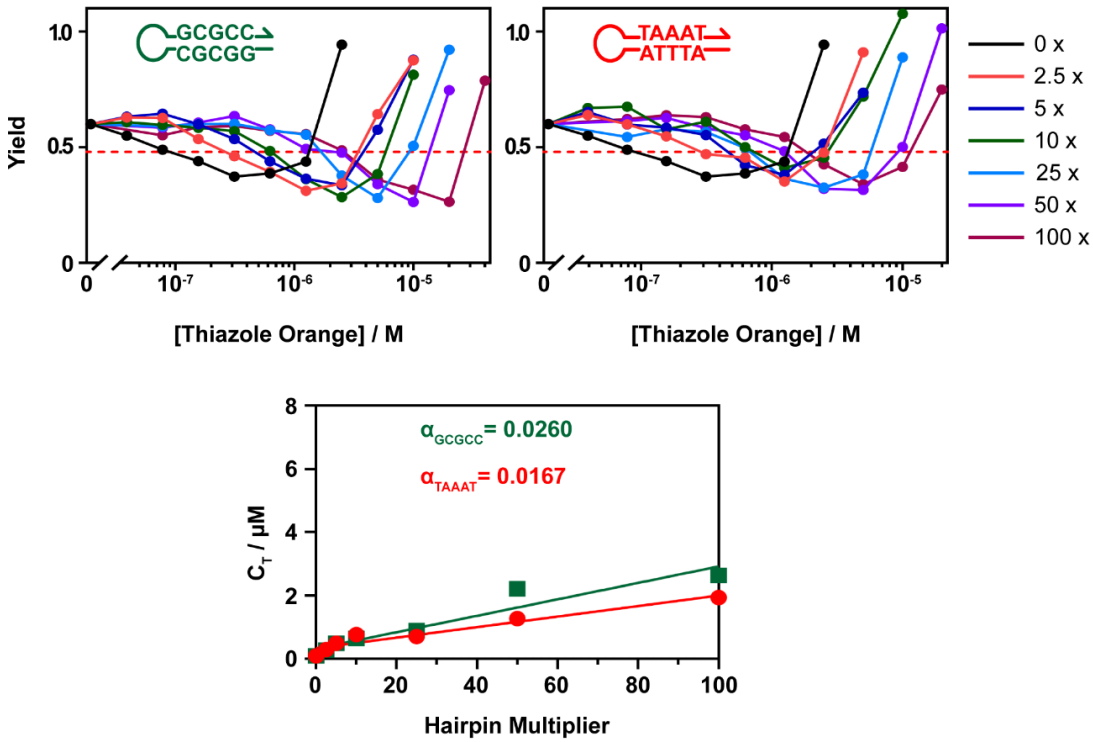

Fig. 37 | Determining sequence selectivity of TO using GC and AT-rich sink probes.

By calculating the ratio of the selectivity factors of the two probes (α_{AT}/α_{GC}), I was able to determine and rank the sequence selectivity of all nine binders (Fig. 38a). Four binders were found to be selective to AT-rich sequences ($\alpha_{AT}/\alpha_{GC} > 1$) with the rank of netropsin > DAPI > berenil > Hoechst 33258. Another four binders were found to be selective to GC-rich sequences ($\alpha_{AT}/\alpha_{GC} < 1$) with a rank of Actinomycin D > doxorubicin > thiazole orange > ethidium bromide. Remarkably, Netropsin was found to be highly selective to the AT-rich sink and showed no binding to the GC-rich sequence even when the sink was 100 times in excess (Fig. 38b and 38c), whereas Actinomycin D demonstrates a strong selectivity to the GC-rich sequence and shows no binding to the AT-rich sequence (Fig. 38d and 38e). BIND also reveals no sequence preference of SG-I towards either AT- or GC-rich sequences with α_{AT}/α_{GC} close to 1 (Fig. 38f and 38g).

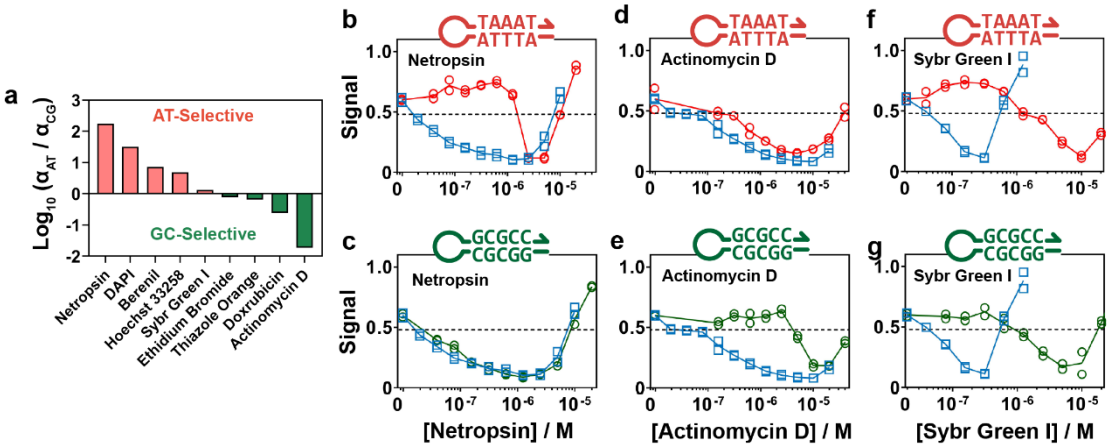

Fig. 38 | Summarizing 9 DNA binder sequence selectivity with comparison between one AT selective binder, one GC selective binder and one non-selective binder. a. Quantitatively profiling the sequence selectivity of 9 representative DNA binders against AT- and GC-rich sequences using BIND. Profiling the shifts in BIND curves against a AT- and GC-rich sink for netropsin (**b**, **c**), Actinomycin D (**d**, **e**), and SYBR Green I (**f**, **g**).

2.3 Conclusion

Since the introduction of TMSD in 2000, dynamic DNA nanotechnology has been pushed forward with each of the development of the new toehold designs, such as hidden toehold,[76] remote toehold[77], allosteric toehold[78], associative toehold[79], and cooperative hybridization[80], as well as new concepts strand displacement reactions, such as toehold exchange[81], hybridization chain reactions[82], and noncovalent DNA catalysis[83]. In this work, I introduced BIND as a new addition to the current toolbox of DNA strand displacement techniques, which established a new concept in regulating elementary DNA reactions using non-nucleic-acid molecules without the need for any functional motif, such as aptamers or DNAzymes. Our success in developing BIND also provides new mechanistic insights of DNA strand displacement reactions. Unlike existing strand displacement reactions that are dominated by the S_N2 reaction pathway, BIND possesses switchable reaction pathways from S_N1 to S_N2 in response to small

molecular DNA binders in a concentration dependent manner. Distinct BIND profiles have also been established in accordance with binder affinities and charge conditions.

BIND also provides a novel molecular platform for the comprehensive thermodynamic characterization of interactions between DNA and small molecules. Small molecules capable of binding to DNA either through intercalation or minor groove binding have long been an intensive focus of research because of their critical roles in therapeutics and biochemical research. Binding affinity, binding site size, sequence selectivity, enthalpy and entropy changes are critical thermodynamic determinants of binding behavior and functionality of DNA binders but remain difficult to be measured on a single analytical platform. Instrumental methods, such as SMFS, DSC, ITC, and thermal melting analysis, allows the accurate characterization of binding affinities but can seldomly provide information on sequence selectivity. Moreover, these techniques often require specialized equipment and procedures that are not widely available to many biochemical laboratories. Although FID is a simple assay that allows the determination of sequence selectivity of DNA binders, it relies heavily on the relative binding strength between a given binder and an indicator (e.g., EB) and thus may introduce significant measurement bias upon usage. For the first time, BIND enables a simple, unbiased assay that allows the comprehensive characterization of all critical thermodynamic properties of DNA binders on a single platform. Verified using 16 well-studied DNA binders, I demonstrated that BIND not only led to highly consistent numeric values of dissociation constant, binding site size, enthalpy contribution of each binder with previous studies using varied characterization

techniques, it also offers quantitative information on the binding cooperativity and sequence selectivity through unique BIND profiles.

To further expand the concept and strategies of BIND in DNA nanotechnology, the ongoing research focuses on two main challenges. First, BIND system requires a low ionic strength below 25 mM and the absence of Mg^{2+} (Fig. 39), which significantly limits its composability with existing strand displacement reactions often performed at a standard buffer containing 12.5 mM Mg^{2+}. A possible solution to this challenge is to finetune the length of DNA probes, so that BIND may work at standard buffer conditions. An alternative solution is to configurate DNA reaction networks at buffer conditions compatible with BIND.

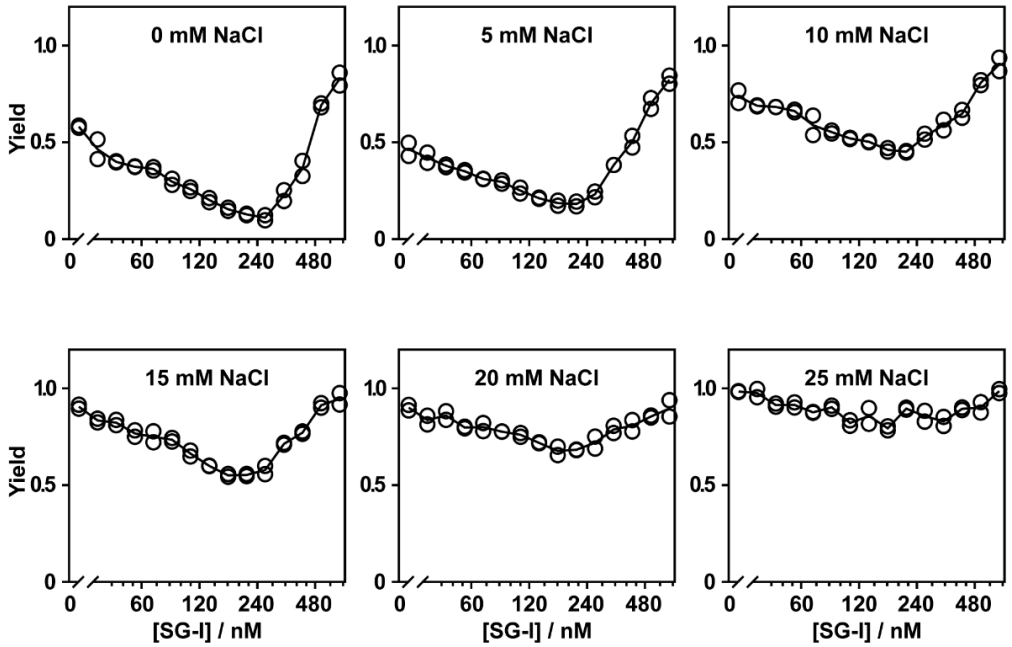

Fig. 39 | BIND profiles for SG-I in the absence of NaCl or the presence of varying concentrations of NaCl. BIND profiles were flattened by increasing concentrations of

NaCl and the attenuation region was disappeared when NaCl concentration was above 25 mM.

2.4 Experimental

Table 3. DNA sequences and modifications

DNA Names		Sequences
BIND probes	**C**	5'-Cy5-AGGTTGGTGAGTGATTGGAGGTT-3'
	P	5'-AATCACTCACCAACCT- Iowa Black FQ-3'
	I	5'-AACCT CCAATCACTCACCAA CCT-3'
Sink Probes	**5'-ATTTA-3'**	5'-CGATTTACAAAAAGTAAATCG-3'
	5'-AATTG-3'	5'-CGAATTGCAAAAAGCAATTCG-3'
	5'-CATTC-3'	5'-CGCATTCCAAAAAGGAATGCG-3'
	5'-ATCTT-3'	5'-CGATCTTCAAAAAG AAGATCG-3'
	5'-AAGTC-3'	5'-CGAAGTCCAAAAAGGACTTCG-3'
	5'-CGAAG-3'	5'-CGCGAAGCAAAAAGCTTCGCG-3'
	5'-CCGAG-3'	5'-CGCCGAGCAAAAAGCTCGGCG-3'
	5'-CGCGG-3'	5'-CGCGCGGCAAAAAGCCGCGCG-3'

2.4.2 Methods

Binder-induced nucleic acid strand displacement. The BIND probe CP was prepared by heating a reaction mixture containing 5 μM probe C, 7.5 μM probe P, 1 mM Mg^{2+} in 1 × TE buffer at 95 °C for 5 min and then gradually cooling to room temperature at a constant rate over a period of 40 min using a BioRad T100 thermocycler. The stock solution of CP at a final concentration of 5 μM was stored at 4 °C until use. For a typical BIND reaction, CP was diluted in 1 × TE buffer and then mixed with a given DNA binder at 37 °C for 5 min. To this mixture, the invader I was then added to initiate BIND reaction at 37 °C. The fluorescence of the reaction mixture containing 10 nM I, 20 nM

CP, a given concentration of DNA binder was measured in real-time using a BioTek Cytation 5 Multimode Microplate reader at a data acquisition rate of one data point per minute for a period of 1 hour. The excitation/emission wavelength was set at 640 nm/675 nm. All fluorescence signals were normalized against a reaction mixture containing 20 nM CP, 10 nM I, and 10 mM $MgCl_2$ in 1 x TE buffer as a positive control. 10 mM Mg^{2+} was added into the positive control to ensure a complete strand displacement. The solution containing 20 nM CP in 1 x TE buffer was also included as a negative control for fluorescence normalization.

Thermodynamic characterization of DNA-binder interactions using BIND. Endpoint fluorescence measurement was used to establish the BIND profile for measuring binding affinities and binding site sizes of DNA-binder interactions. Briefly, CP was diluted in 1 × TE buffer and then mixed with a given DNA binder at 37 °C for 5 min. To this mixture, the invader I was then added to initiate BIND reaction. The reaction mixture containing 10 nM I, 20 nM CP, a given concentration of DNA binder was incubated at 37 °C for 2 hours before an endpoint fluorescence measurement using a BioTek Cytation 5 Multimode Microplate reader by setting the excitation/emission wavelength at 640 nm/675 nm. The fluorescence signal was then normalized against the positive and negative controls as outlined above. The association binding constant Ka and binding site size n of each binder was then determined by fitting fractional occupancy of bound binders using the McGhee and Von Hippel's binding isotherm equation:

$$Y = \frac{n\cdot(C_{binder}-C_{DNA}\cdot\frac{Y}{n})\cdot K_a\cdot(1-Y)^n}{(1-Y+\frac{Y}{n})^{(n-1)}} \text{ (10)}$$

where Y is the fractional occupancy of the bound binder, C_{binder} is the total binder concentration at each sample, C_{DNA} is the concentration of base pairs in CP (e.g., 20 nM CP consists of 320 nM base pairs), K_a is the association constant and n was the binding site size. The value of Y was determined using the equation Y = 1 – [(F – F_{CBC}) / (F_0 – F_{CBC})], where F was the normalized fluorescence signal of a given sample, F_{CBC} was the normalized fluorescence when binder concentration equals to its CBC and F_0 was the normalized fluorescence signal when no binder was added to the strand displacement system. When taking cooperativity ω into consideration, the McGhee and Von Hippel's binding isotherm algorithm was transformed into:

$$Y = K_a(1-Y)\left(\frac{(2\cdot\omega-1)\cdot(1-\mathrm{Y})+\frac{Y}{n}-R}{2\cdot(\omega-1)\cdot(1-\mathrm{Y})}\right)^{n-1}\left(\frac{1-(n+1)\cdot\frac{Y}{n}+R}{2\cdot(1-Y)}\right)^2\left(C_{binder}-\frac{Y\cdot C_{DNA}}{n}\right)n \text{ (11)}$$

where $R = \sqrt{\{\left[1-(n+1)\frac{Y}{n}\right]^2 + 4\cdot\omega\cdot\frac{Y}{n}(1-Y)\}}$, and ω is the cooperativity. Binding enthalpy and binding entropy were determined by measuring Ka of a given biner using BIND reaction at 27 °C, 30 °C, 32 °C, 35 °C, 37 °C, respectively and then fit using Van't Hoff's equation.

$$ln\ K_a = -\frac{\Delta H}{RT} + \frac{\Delta S}{R} \text{ (12)}$$

where K_a is the association constant, ΔH is the binding enthalpy, R is the universal gas constant, T is temperature in Kelvin, and ΔS was the binding entropy.

Determine sequence selectivity of DNA binders using BIND. Sequence selectivity of DNA binders was determined using a competitive BIND reaction between CP and stem-looped sink probes. Each sink prob is designed to contain an 8 bp stem domain of

varying ATGC combination and a 5 nt polydA loop domain. For a typical competitive BIND reaction, a given DNA binder was pre-mixed a sink probe in 1 × TE buffer at 37 °C for 2 hours. This reaction mixture was subsequently mixed with CP and I to initiate BIND reaction using the protocol outlined above. The concentration ratios between the sink and CP probes were set to be 2.5, 5, 10, 25, 50, and 100 in the competitive bind reaction. The threshold concentrations (C_T) that were defined as the binder concentration at 50% displacement yield at the S_N1 domain were then plotted against the sink/CP ratios to determine the selectivity factor α that was defined as the slope of the fitted linear curve.

DNA oligonucleotides. All DNA oligonucleotides were purchased from Integrated DNA Technologies (IDT, Coralville, IA, United States) and were purified by IDT using high-performance liquid chromatography (HPLC). Sequences and modifications were listed in Table 3.

DNA Binders. Actinomycin D, Berenil, Daunorubicin, Doxorubicin, Echinomycin, Hoechst 33258, Ellipticine and Quinacrine were purchased from Cayman Chemical Company (Cayman Chemical, Ann Arbor, MI, United States). Crystal Violet,DAPI, DAPP, Ethidium Bromide (EtBr), Proflavine, $[Ru(phen)_3]Cl_2$, SYBR Green I (SG-I), Thiazole Orange and Thioflavin T were purchased from Sigma-Aldrich Chemical Company (Sigma-Aldrich, St. Louis, MO). Eva Green was purchased from Biotium, Inc (Biotium, Hayward, CA). Pico Green was purchased from Lumiprobe Corporation (Lumiprobe, Hunt Valley, MA). Netropsin was purchased from VWR International Company (VWR, Radnor, PA). Selleck's Express-Pick Library was provided by

Professor Weimin Li at the Department of Respiratory and Critical Care Medicine, Targeted Tracer Research and Development Laboratory, West China hospital of Sichuan University.

Buffer conditions. DNA oligonucleotides were re-suspended by dissolving in deionized water and then stored at -20 °C. Unless indicated otherwise, 1 x PBS buffer (pH 7.4, purchased as 10 × PBS stock from Sigma) containing 1 mM $MgCl_2$ and 0.1% (v/v) TWEEN 20 was used to prepare the CP duplex. 1 × Tris EDTA (10 mM Tris-HCl, pH 8.0, 1M EDTA, purchased from Sigma as 100 × stock) buffer containing 0.1% (v/v) TWEEN 20 (Sigma) was used as the BIND reaction buffer.

Molecular Docking. To visualize the binding mechanism between DNA and binders, specific binding models were obtained by downloading published crystal structures form Protein Data Band (https://www.rcsb.org/) or performing molecule docking. Specifically, the crystal structures of Actinomycin D, Berenil, DAPI, Echinomycin, Ellipticine, Hoechst 33258, Netropsin, Proflavine, and TOTO binding to DNA were downloaded from Protein Data Bank (https://www.rcsb.org/), and the binding modes were visualized by Pymol software. While binding modes of Daunorubicin, Doxorubicin, Pico Green, Quinacrine, SYBR Green I, Thiazole Orange were simulated by molecular docking software Autodock 4.2. In detail, the .mol files of binders were obtained through Chemdraw software, and .pdb files of DNA were obtained through PDB. In the preliminary preparations for the molecular docking, the binders were successively hydrogenated, detected root, chosen torsion and finally converted into PDBQT files, while DNAs were similarly hydrogenated, removed water molecules,

calculated gaseiger, assigned AD4 type, and finally converted to PDBQT files. The grid box was uniformly set to contain the entire DNA structure. During the docking process, the Lamarckian genetic algorithm was used for binder-DNA docking. Among them, the maximum number of energy evaluations was set to 2,500,000. The maximum number of generations was 27,000. The rate of gene mutation was 0.02. The rate of crossover was 0.8. Maximum number of top individuals that automatically survive was 1. Finally, we comprehensively evaluated and selected the optimal binding conformation of binder and DNA according to the stable binding energy, which were visualized with Pymol software.

Reference

1. Seeman, N.C. & Sleiman, H.F. DNA nanotechnology. *Nature Reviews Materials* **3** (2017).
2. Madsen, M. & Gothelf, K.V. Chemistries for DNA Nanotechnology. *Chem Rev* **119**, 6384-6458 (2019).
3. Seeman, N.C. Nucleic acid junctions and lattices. *J Theor Biol* **99**, 237-247 (1982).
4. Winfree, E., Liu, F., Wenzler, L.A. & Seeman, N.C. Design and self-assembly of two-dimensional DNA crystals. *Nature* **394**, 539-544 (1998).
5. Tikhomirov, G., Petersen, P. & Qian, L. Fractal assembly of micrometre-scale DNA origami arrays with arbitrary patterns. *Nature* **552**, 67-71 (2017).
6. Wei, B., Dai, M. & Yin, P. Complex shapes self-assembled from single-stranded DNA tiles. *Nature* **485**, 623-626 (2012).
7. Rothemund, P.W. Folding DNA to create nanoscale shapes and patterns. *Nature* **440**, 297-302 (2006).
8. Yao, G. et al. Meta-DNA structures. *Nat Chem* **12**, 1067-1075 (2020).
9. Ong, L.L. et al. Programmable self-assembly of three-dimensional nanostructures from 10,000 unique components. *Nature* **552**, 72-77 (2017).
10. Adleman, L.M. Molecular computation of solutions to combinatorial problems. *Science* **266**, 1021-1024 (1994).
11. Ball, P. Synthetic biology for nanotechnology. *Nanotechnology* **16**, R1-R8 (2005).
12. Hu, Q., Li, H., Wang, L., Gu, H. & Fan, C. DNA Nanotechnology-Enabled Drug Delivery Systems. *Chem Rev* **119**, 6459-6506 (2019).
13. Langer, R. New methods of drug delivery. *Science* **249**, 1527-1533 (1990).
14. Langer, R. Drug delivery and targeting. *Nature (London)* **392**, 5-10 (1998).
15. Zhang, F., Nangreave, J., Liu, Y. & Yan, H. Structural DNA nanotechnology: state of the art and future perspective. *J Am Chem Soc* **136**, 11198-11211 (2014).

16. Aldaye, F.A., Palmer, A.L. & Sleiman, H.F. Assembling materials with DNA as the guide. *Science* **321**, 1795-1799 (2008).
17. DeLuca, M., Shi, Z., Castro, C.E. & Arya, G. Dynamic DNA nanotechnology: toward functional nanoscale devices. *Nanoscale Horizons* **5**, 182-201 (2020).
18. Liu, X. et al. Complex silica composite nanomaterials templated with DNA origami. *Nature* **559**, 593-598 (2018).
19. Thubagere, A.J. et al. A cargo-sorting DNA robot. *Science* **357** (2017).
20. Ding, X., Lv, Z., Xu, N., Li, F. & Yang, D. Dynamic Transformation of DNA Nanostructures inside Living Cells. *Chempluschem* **87**, e202100519 (2022).
21. Ellington, A.D. & Szostak, J.W. In vitro selection of RNA molecules that bind specific ligands. *Nature* **346**, 818-822 (1990).
22. Tuerk, C. & Gold, L. Systematic evolution of ligands by exponential enrichment: RNA ligands to bacteriophage T4 DNA polymerase. *Science* **249**, 505-510 (1990).
23. Zhao, D., Kong, Y., Zhao, S. & Xing, H. Engineering Functional DNA-Protein Conjugates for Biosensing, Biomedical, and Nanoassembly Applications. *Top Curr Chem (Cham)* **378**, 41 (2020).
24. Stephanopoulos, N. Hybrid Nanostructures from the Self-Assembly of Proteins and DNA. *Chem* **6**, 364-405 (2020).
25. Breaker, R.R. & Joyce, G.F. A DNA enzyme that cleaves RNA. *Chemistry & Biology* **1**, 223-229 (1994).
26. Gehring, K., Leroy, J.L. & Gueron, M. A tetrameric DNA structure with protonated cytosine.cytosine base pairs. *Nature* **363**, 561-565 (1993).
27. Leroy, J.L., Gehring, K., Kettani, A. & Gueron, M. Acid multimers of oligodeoxycytidine strands: stoichiometry, base-pair characterization, and proton exchange properties. *Biochemistry* **32**, 6019-6031 (1993).
28. Yurke, B., Turberfield, A.J., Mills, A.P., Jr., Simmel, F.C. & Neumann, J.L. A DNA-fuelled molecular machine made of DNA. *Nature* **406**, 605-608 (2000).
29. Owczarzy, R., Moreira, B.G., You, Y., Behlke, M.A. & Walder, J.A. Predicting stability of DNA duplexes in solutions containing magnesium and monovalent cations. *Biochemistry* **47**, 5336-5353 (2008).
30. Reynaldo, L.P., Vologodskii, A.V., Neri, B.P. & Lyamichev, V.I. The kinetics of oligonucleotide replacements. *J Mol Biol* **297**, 511-520 (2000).
31. Chen, F.-M., Sha, F., Chin, K.-H. & Chou, S.-H. The nature of actinomycin D binding to d(AACCAXYG) sequence motifs. *Nucleic acids research* **32**, 271-277 (2004).
32. Lohani, N., Singh, H.N. & Rajeswari, M.R. Assessment of binding properties of Actinomycin-D to 21nt DNA segment of hmgb1 gene promoter using spectroscopic and calorimetric techniques. *Journal of biomolecular structure & dynamics* **36**, 504-511 (2018).
33. Wakelin, S.P. & Waring, M.J. The binding of echinomycin to deoxyribonucleic acid. *Biochemical journal* **157**, 721-740 (1976).
34. Ghosh, S., Kar, A., Chowdhury, S. & Dasgupta, D. Ellipticine Binds to a Human Telomere Sequence: An Additional Mode of Action as a Putative Anticancer Agent? *Biochemistry (Easton)* **52**, 4127-4137 (2013).
35. Dodin, G., Schwaller, M.A., Aubard, J. & Paoletti, C. Binding of ellipticine base and ellipticinium cation of calf-thymus DNA: a thermodynamic and kinetic study. *European*

journal of biochemistry **176**, 371-376 (1988).

36. Kubař, T., Hanus, M., Ryj áček, F. & Hobza, P. Binding of Cationic and Neutral Phenanthridine Intercalators to a DNA Oligomer Is Controlled by Dispersion Energy: Quantum Chemical Calculations and Molecular Mechanics Simulations. *Chemistry : a European journal* **12**, 280-290 (2005).
37. Wilson, W.D. & Lopp, I.G. Analysis of cooperativity and ion effects in the interaction of quinacrine with DNA. *Biopolymers* **18**, 3025-3041 (1979).
38. Sumner, A.T. Mechanisms of quinacrine binding and fluorescence in nuclei and chromosomes. *Histochemistry (Berlin)* **84**, 566-574 (1986).
39. Breusegem, S.Y., Clegg, R.M. & Loontiens, F.G. Base-sequence specificity of Hoechst 33258 and DAPI binding to five (A/T) 4 DNA sites with kinetic evidence for more than one high-affinity Hoechst 33258-AATT complex. *Journal of molecular biology* **315**, 1049-1061 (2002).
40. Trotta, E., Del Grosso, N., Erba, M. & Paci, M. The ATT strand of AAT.ATT trinucleotide repeats adopts stable hairpin structures induced by minor groove binding ligands. *Biochemistry (Easton)* **39**, 6799-6808 (2000).
41. Dragan, A.I. et al. Characterization of PicoGreen Interaction with dsDNA and the Origin of Its Fluorescence Enhancement upon Binding. *Biophysical journal* **99**, 3010-3019 (2010).
42. Premvardhan, L. & Maurizot, J.-C. Netropsin binding in five duplex-dimer DNA constructs as a function of size and distance between binding sites: circular dichroism and absorption spectroscopy. *European biophysics journal* **39**, 781-787 (2010).
43. Vardevanyan, P.O., Parsadanyan, M.A., Antonyan, A.P. & Sahakyan, V.G. Spectroscopic Study of the Binding of Netropsin and Hoechst 33258 to Nucleic Acids. *Journal of applied spectroscopy* **85**, 335-340 (2018).
44. Dragan, A.I. et al. SYBR Green I: Fluorescence Properties and Interaction with DNA. *Journal of fluorescence* **22**, 1189-1199 (2012).
45. Pilch, D.S., Kirolos, M.A., Liu, X., Plum, G.E. & Breslauer, K.J. Berenil [1,3-Bis(4'-amidinophenyl)triazene] Binding to DNA Duplexes and to a RNA Duplex: Evidence for Both Intercalative and Minor Groove Binding Properties. *Biochemistry (Easton)* **34**, 9962-9976 (1995).
46. Chaires, J.B. et al. Parsing the Free Energy of Anthracycline Antibiotic Binding to DNA. *Biochemistry (Easton)* **35**, 2047-2053 (1996).
47. Barcelo, F., Martorell, J., Gavilanes, F. & Gonzalez-Ros, J.M. Equilibrium binding of daunomycin and adriamycin to calf thymus DNA: Temperature and ionic strength dependence of thermodynamic parameters. *Biochemical pharmacology* **37**, 2133-2138 (1988).
48. Boger, D.L., Fink, B.E., Brunette, S.R., Tse, W.C. & Hedrick, M.P. A simple, high-resolution method for establishing DNA binding affinity and sequence selectivity. *J Am Chem Soc* **123**, 5878-5891 (2001).
49. Shoute, L.C.T. & Loppnow, G.R. Characterization of the binding interactions between EvaGreen dye and dsDNA. *Physical chemistry chemical physics : PCCP* **20**, 4772-4780 (2018).
50. MoradpourHafshejani, S., Hedley, J.H., Haigh, A.O., Pike, A.R. & Tuite, E.M. Synthesis and binding of proflavine diazides as functional intercalators for directed assembly on DNA.

RSC advances **3**, 18164 (2013).
51. Aslanoglu, M. Electrochemical and Spectroscopic Studies of the Interaction of Proflavine with DNA. *Analytical sciences* **22**, 439-443 (2006).
52. Hinton, D.M. & Bode, V.C. Ethidium binding affinity of circular lambda deoxyribonucleic acid determined fluorometrically. *The Journal of biological chemistry* **250**, 1061-1070 (1975).
53. Vardevanyan, P.O. et al. The influence of GC/AT composition on intercalating and semi-intercalating binding of ethidium bromide to DNA. *Journal of the Brazilian Chemical Society* **23**, 2016-2020 (2012).
54. Mihailovic, A. et al. Exploring the Interaction of Ruthenium(II) Polypyridyl Complexes with DNA Using Single-Molecule Techniques. *Langmuir* **22**, 4699-4709 (2006).
55. Wakelin, L.P.G., Adams, A., Hunter, C. & Waring, M.J. Interaction of crystal violet with nucleic acids. *Biochemistry (Easton)* **20**, 5779-5787 (1981).
56. Guan, Y., Shi, R., Li, X., Zhao, M. & Li, Y. Multiple Binding Modes for Dicationic Hoechst 33258 to DNA. *The journal of physical chemistry. B* **111**, 7336-7344 (2007).
57. Vardevanyan, P.O. et al. Influence of Ionic Strength on Hoechst 33258 Binding with DNA. *Journal of biomolecular structure & dynamics* **25**, 641-646 (2008).
58. Liu, S., Peng, P., Wang, H., Shi, L. & Li, T. Thioflavin T binds dimeric parallel-stranded GA-containing non-G-quadruplex DNAs: a general approach to lighting up double-stranded scaffolds. *Nucleic acids research* **45**, 12080-12089 (2017).
59. McGhee, J.D. & von Hippel, P.H. Theoretical aspects of DNA-protein interactions: co-operative and non-co-operative binding of large ligands to a one-dimensional homogeneous lattice. *J Mol Biol* **86**, 469-489 (1974).
60. Shoute, L.C.T. & Loppnow, G.R. Characterization of the binding interactions between EvaGreen dye and dsDNA. *Phys Chem Chem Phys* **20**, 4772-4780 (2018).
61. Galo, A.L. et al. The Influence of Solutes on the Enthalpy/Entropy Change of the Actinomycin D Binding to DNA: Hydration, Energy Compensation and Long-Range Deformation on DNA. *The journal of physical chemistry. B* **115**, 8883-8890 (2011).
62. L. P. G, W. & M. J, W. The Unwinding of Circular Deoxyribonucleic Acid by Phenanthridinium Drugs: Structure-Activity Relations for the Intercalation Reaction. *Molecular pharmacology* **10**, 544-561 (1974).
63. Schwaller, M.A., Dodin, G. & Aubard, J. Thermodynamics of drug–DNA interactions: Entropy-driven intercalation and enthalpy-driven outside binding in the ellipticine series. *Biopolymers* **31**, 519-527 (1991).
64. Hossain, M., Giri, P. & Kumar, G.S. DNA intercalation by quinacrine and methylene blue: a comparative binding and thermodynamic characterization study. *DNA and cell biology* **27**, 81-90 (2008).
65. Daniel, S.P. et al. A Terbenzimidazole that Preferentially Binds and Conformationally Alters Structurally Distinct DNA Duplex Domains: A Potential Mechanism for Topoisomerase I Poisoning. *Proceedings of the National Academy of Sciences - PNAS* **94**, 13565-13570 (1997).
66. Schmitz, H.U. & Hübner, W. A thermodynamic and spectroscopic study on the binding of berenil to poly d(AT) and to poly (dA) · poly (dT). *Biophysical chemistry* **48**, 61-74 (1993).
67. Schneider, Y.J., Baurain, R., Zenebergh, A. & Trouet, A. DNA-binding parameters of

daunorubicin and doxorubicin in the conditions used for studying the interaction of anthracycline-DNA complexes with cells in vitro. *Cancer chemotherapy and pharmacology* **2**, 7-10 (1979).

68. Remeta, D.P., Mudd, C.P., Berger, R.L. & Breslauer, K.J. Thermodynamic characterization of daunomycin-DNA interactions: microcalorimetric measurements of daunomycin-DNA binding enthalpies. *Biochemistry (Easton)* **30**, 9799-9809 (1991).
69. Quadrifoglio, F., Crescenzi, V. & Giancotti, V. Calorimetry of DNA-dye interactions in aqueous solution: I. Proflavine and ethidium bromide. *Biophysical chemistry* **1**, 319-324 (1974).
70. Chou, W.Y., Marky, L.A., Zaunczkowski, D. & Breslauer, K.J. The Thermodynamics of Drug-DNA Interactions: Ethidium Bromide and Propidium Iodide. *Journal of biomolecular structure & dynamics* **5**, 345-359 (1987).
71. Haq, I., Ladbury, J.E., Chowdhry, B.Z., Jenkins, T.C. & Chaires, J.B. Specific binding of hoechst 33258 to the d(CGCAAATTTGCG) 2 duplex: calorimetric and spectroscopic studies. *Journal of molecular biology* **271**, 244-257 (1997).
72. Chaires, J.B. A thermodynamic signature for drug-DNA binding mode. *Arch Biochem Biophys* **453**, 26-31 (2006).
73. Alniss, H.Y. Thermodynamics of DNA Minor Groove Binders. *J Med Chem* **62**, 385-402 (2019).
74. Marky, L.A. & Breslauer, K.J. Origins of netropsin binding affinity and specificity: correlations of thermodynamic and structural data. *Proc Natl Acad Sci U S A* **84**, 4359-4363 (1987).
75. Trotta, E. et al. 1H NMR study of [d(GCGATCGC)]2 and its interaction with minor groove binding 4',6-diamidino-2-phenylindole. *Journal of Biological Chemistry* **268**, 3944-3951 (1993).
76. Xing, Y., Yang, Z. & Liu, D. A responsive hidden toehold to enable controllable DNA strand displacement reactions. *Angew Chem Int Ed Engl* **50**, 11934-11936 (2011).
77. Genot, A.J., Zhang, D.Y., Bath, J. & Turberfield, A.J. Remote toehold: a mechanism for flexible control of DNA hybridization kinetics. *J Am Chem Soc* **133**, 2177-2182 (2011).
78. Yang, X., Tang, Y., Traynor, S.M. & Li, F. Regulation of DNA Strand Displacement Using an Allosteric DNA Toehold. *J Am Chem Soc* **138**, 14076-14082 (2016).
79. Chen, X. Expanding the rule set of DNA circuitry with associative toehold activation. *J Am Chem Soc* **134**, 263-271 (2012).
80. Zhang, D.Y. Cooperative hybridization of oligonucleotides. *J Am Chem Soc* **133**, 1077-1086 (2011).
81. Zhang, D.Y. & Winfree, E. Control of DNA strand displacement kinetics using toehold exchange. *J Am Chem Soc* **131**, 17303-17314 (2009).
82. Dirks, R.M. & Pierce, N.A. Triggered amplification by hybridization chain reaction. *Proc Natl Acad Sci U S A* **101**, 15275-15278 (2004).
83. Zhang, D.Y. & Winfree, E. Dynamic allosteric control of noncovalent DNA catalysis reactions. *J Am Chem Soc* **130**, 13921-13926 (2008).

Chapter 3

A high-throughput screening (HTS) assay identifying small molecules that interact with duplexed DNA based on BIND

Contribution statement

I performed all the work for this section.

3.1 Introduction

Small molecular drugs or chemical drugs (New Molecular Entities, NMEs) have heralded the age of medicinal chemistry since the first synthesis of Aspirin in 1853, a compound that has been applied to fight against pain, fever and inflammation for almost 170 years.[1] Currently, the introduction of NMEs is still the dominant therapeutic method, tracing back 25 years in new Food & Drug Administration (FDA)-approved drugs. More than 80% of novel drugs fall into this category, but less than one-fifth of biologics license applications (BLAs) are obtained for biopharmaceuticals, based on U.S. FDA released data.[2] Compared with BLAs, NMEs are more structurally stable and require less intracellular delivery assistance as well as better persistence and expansion among live cells. Additionally, the paratheatrical cure of any central nervous system (CNS) disease relies only on small molecule blood-brain barrier (BBB) penetrants as current drug delivery vectors cannot transport any BLAs through the BBB distally. Finally, the difference in cost to treat a specific disease by applying NEMs or BLAs is usually well above 100 times.[3]

Targeting the DNA duplexed region continues to be vital for small molecular drug

design and research with potential antineoplastic and antimicrobial functions.[4] Many sound names, including cisplatin, doxorubicin, epirubicin, actinomycin D and N-[2-(dimethylamino)-ethyl]-acridine-4-carboxamide (DACA) are DNA intercalators that are still the foremost treatment against cancer today. More dominantly, when dealing with nonlife-threatening diseases, such as infections, almost all treatments rely on small molecular drugs such as quinacrine for malaria[5] and quercetin for scalp infection.[6] In animal husbandry, fishery and veterinary science, small DNA binders are the most essential drugs for curing and preventing diseases due to their broad-spectrum anticancer and antibacterial effects and low cost. Berenil, an AT preferred minor groove binder (MGB) is usually administered to livestock suffering from a contagious infection caused by trypansomals. Research has revealed that this small molecule usually binds to the parasite's kinetoplast DNA (kDNA), in which a large piece of the AT-rich region is found, resulting in complete loss of superhelical kDNA in Typpanosoma equiperdum (parasite offspring) due to inhibition of kDNA duplication.[7]

The field of DNA chemistry lacks an applicable and reliable approach to identify small DNA binders and satisfies HTS criteria simultaneously: on the one hand, none of the binding affinity characterization methods are suitable for HTS design. On the other hand, FID is the only HTS assay for DNA binder HTS but this assay is subject to low screening efficiency and high screening bias.[8]

Using the tandem BIND assay allowed us to apply the second approach of HTS in discovering small DNA binders with less screening bias and an increased screening window.

A total of 8 possible charged binders were identified form the pool of 700 different chemical structures. The interaction between dsDNA and the strongest positively charged hit was thoroughly characterized by BIND. Furthermore, the drug activity of this hit against six different cell lines was also researched. This candidate was determined to show a broad-spectrum inhibitory effect on cell growth via the MTT assay.

3.2 Results

3.2.1 High-throughput screening of small molecular DNA binders using BIND.

Having examined the comprehensive characterization of existing DNA binders using BIND, I aim to further engineer BIND as an HTS platform for discovering new DNA binders. To do so, I designed a tandem BIND assay in which S_N1 and S_N2 reaction pathways were programmed by adding two binders in tandem (Fig. 1a). Specifically, BIND was first induced by SG-I at a final concentration equal to its CBC, so minimal strand displacement occured between CP and I (Fig. 1a and 1b). A secondary binder was then added to promote strand displacement via the S_N2 reaction pathway (Fig. 1a and 1b). The possibility of programming strand displacement reaction pathways using two tandem binders was successfully demonstrated using both SG-I/netropsin and SG-I/$Ru(Phen)_3Cl_2$ (Fig. 1c). More importantly, fluorescence signals were found to be specific to DNA binders and increased monotonically as a function of both binder affinity and concentration at the S_N2 domain, confirming that the tandem BIND assay is an ideal HTS platform for discovering new binders.

I then employed the tandem BIND assay for HTS of DNA binders. Netropsin and 1-BQC were used as positive controls (P. C.) and negative controls (N. C.), respectively. Using these two controls with each repeatedly tested 10 times, a Z' factor of 0.64 was determined, suggesting that the tandem BIND was an excellent potential assay for HTS (Fig. 1d).[9]

Z' was calculated with the following equation:

$$Z' = 1 - \frac{3(\sigma_{P.C.}+\sigma_{N.C.})}{|\mu_{P.C.}-\mu_{N.C.}|} \quad (1)$$

where $\sigma_{P.C.}$ and $\sigma_{N.C.}$ stand for the standard deviations of the P.C. and the N.C., respectively, and $\mu_{P.C.}$ and $\mu_{N.C.}$ stand for means of the P.C. and the N.C., respectively.

This was further confirmed upon validation against 15 existing DNA binders, in which 12 hits were determined by BIND and 3 misses (Fig. 2a). The 3 misses include two neutral binders (Actinomycin D and Echinomycin) and Hoechst 33258 due to the strong inner filter effect at the assay concentration (30 μM).[10] As a comparison, the Z' factor was determined to be only 0.39 for the classic FID screening assay using EB as the prebound binder (Fig. 3). As a result of the narrow screening window or the severe spectral overlap, only 6 out of 15 existing binders were determined to be positive hits using the FID screening assay (Fig. 2b).

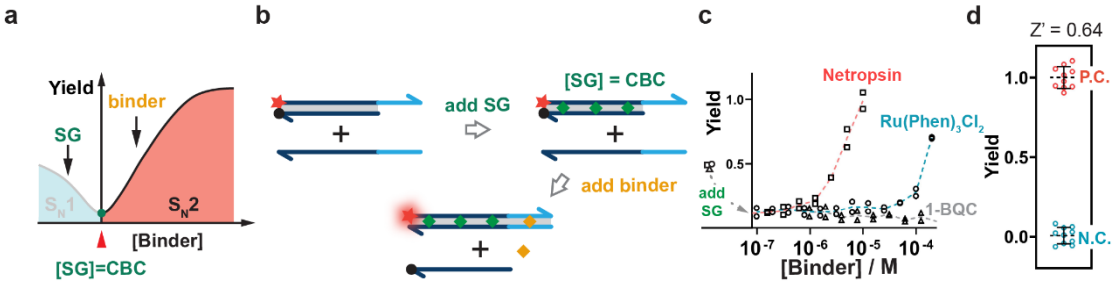

Fig. 1 | The algorithm of HTS using bind and validation. a. Design principle of the tandem BIND reaction as an HTS assay for new DNA binders. **b.** Schematic illustration of the workflow for tandem BIND. **c.** Validation of the tandem BIND reaction against representative strong (Netropsin), weak ($Ru(Phen)_3Cl_2$), and nonbinder (1-BQC). **d.** Determination of the Z' factor of the tandem BIND assay using netropsin as a positive control and 1-BQC as a negative control.

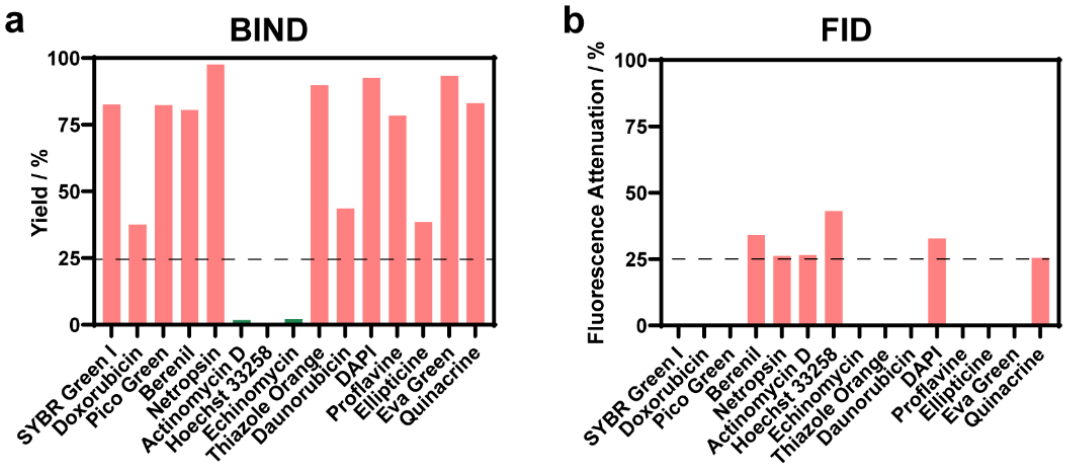

Fig. 2 | Comparing BIND and FID HTS results for 15 known DNA binders. A total of 15 successfully characterized small DNA binders (except for EtBr) were rescreened by both BIND (**a**) and FID (**b**) HTS assays.

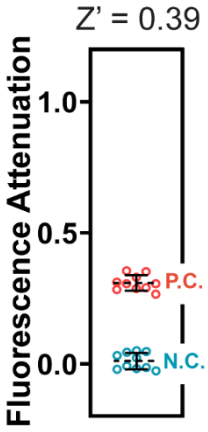

Fig. 3 | Determination of the Z' factor of the conventional FID HTS assay. The Z' factor of conventional FID HTS was determined using netropsin as a positive control and 1-BQC as a negative control.

I finally employed the tandem BIND assay to discover new binders by screening against a pool containing 700 compounds collected from Selleck's express pick library L3600 (Fig. 4a). This sublibrary is part of a collection of 4208 chemical compounds provided by Pfizer that featuring with different pathway inhibitors with high structural diversities. Screening DNA binders from these pathway inhibitors will expand our knowledge of their mechanism of action and reveal possible drug leads with antineoplastic and/or anti-infectious activities. A wide screening window was achieved between the sample and P. C. with a Z-factor of 0.54 (Fig. 4b).

Z was calculated with the following equation:

$$Z = 1 - \frac{3(\sigma_{Sample} + \sigma_{P.C.})}{|\mu_{Sample} - \mu_{P.C.}|} \quad (2)$$

where σ_{Sample} and $\sigma_{P.C.}$ represent the standard deviations of all drug candidates and the P.C., respectively and μ_{Sample} and $\mu_{P.C.}$ represent the means of all drug candidates and the N.C., respectively.

The close numerical values between the Z and Z' factors suggest negligible effect of the compound library on the tandem BIND assay. A threshold of 0.25 ($\mu_S + 3\ \sigma_S$) was set and 8 hits were successfully returned (Fig. 2b & 4d) with decreasing affinity to duplexed DNA listed in Fig. 4c-4j (S20 > J15 > H27 > A33 > L17 > L7 > D19 > Q6).

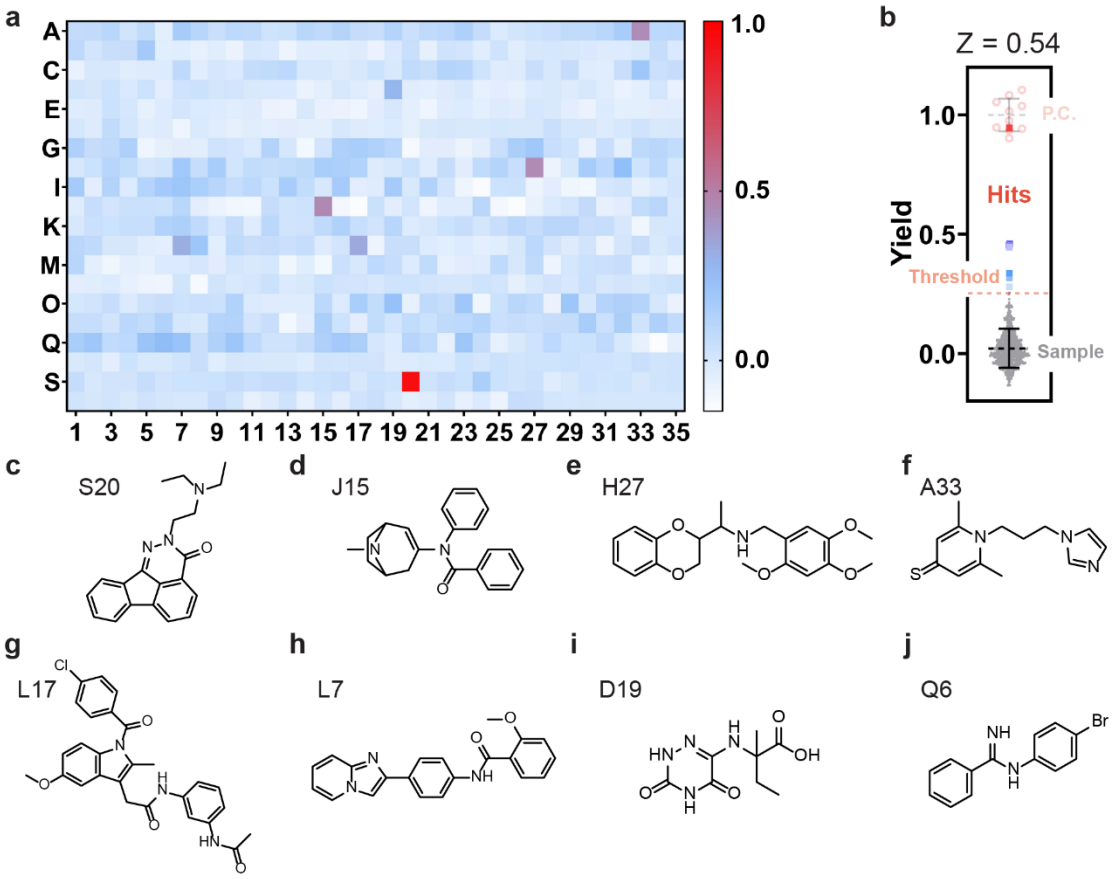

Fig. 4 | BIND HTS results. a. Results of the HTS BIND assay for a pool of 700 compounds. **b.** Determining Z factor that reflects the influence of sample to the HTS. **c-j.** A list of eight hits obtained from the tandem BIND assay with decreasing affinity to duplexed DNA.

Of the 8 hits, S20 **(**2-(2-(diethylamino)ethyl)indeno[1,2,3-de]phthalazine-3(2H)-one) demonstrated strongest activity in the tandem BIND assay. By comprehensively profiling this compound using BIND, a K_d of 212 nM and a binding site size of 1.3 were otbained (Fig. 5a). The strong binding between S20 and dsDNA was further confirmed using classic melting analysis (Fig. 5b).

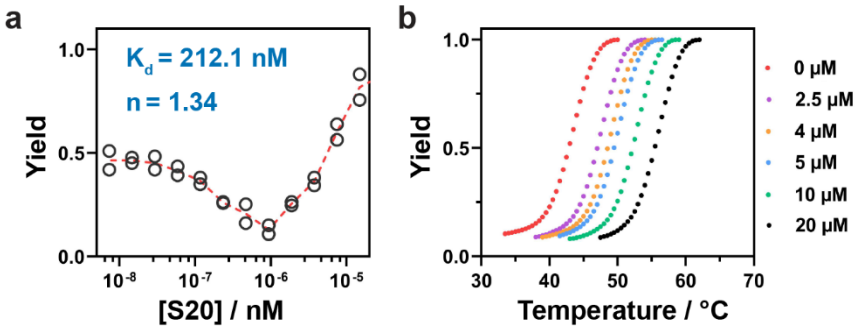

Fig. 5 | Parsing charged binder S20 with BIND. a. Determining the binding affinity and binding site size of S20 using BIND. **b.** Melting curves for dsDNA in the presence of varying concentrations of S20.

I also determined the sequence selectivity of S20 using the competitive BIND assay, which shows no sequence preference with an α_{AT}/α_{GC} value close to 1 (Fig. 6). Thermodynamic analysis of S20 using BIND revealed a strong enthalpic contribution with $\Delta H°$ of -9.72 kcal/mol and a weak entropic contribution with a $T\Delta S°$ of -0.22 kcal/mol (Fig. 7a-7e). The high enthalpic contribution suggests that S20 is likely an intercalator, which was supported by molecular docking with a dsDNA model extracted from PDB file 108D.

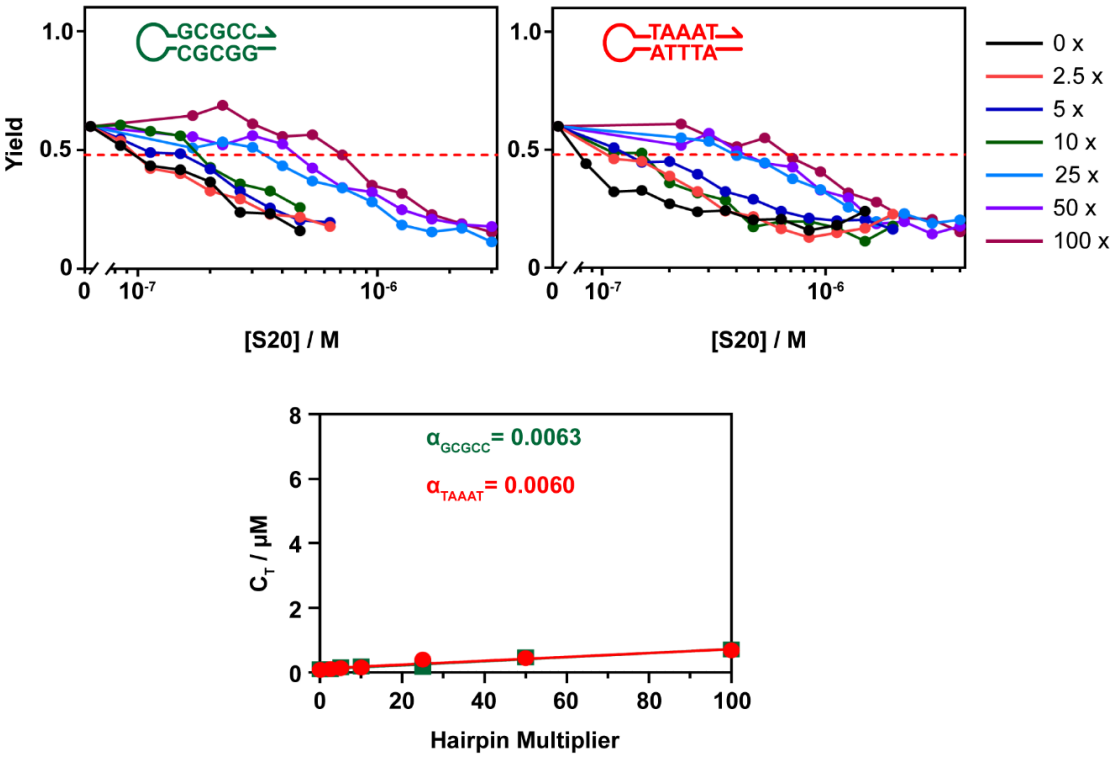

Fig. 6 | Determining sequence selectivity of the newly discovered DNA binder S20 using GC and AT-rich sink probes.

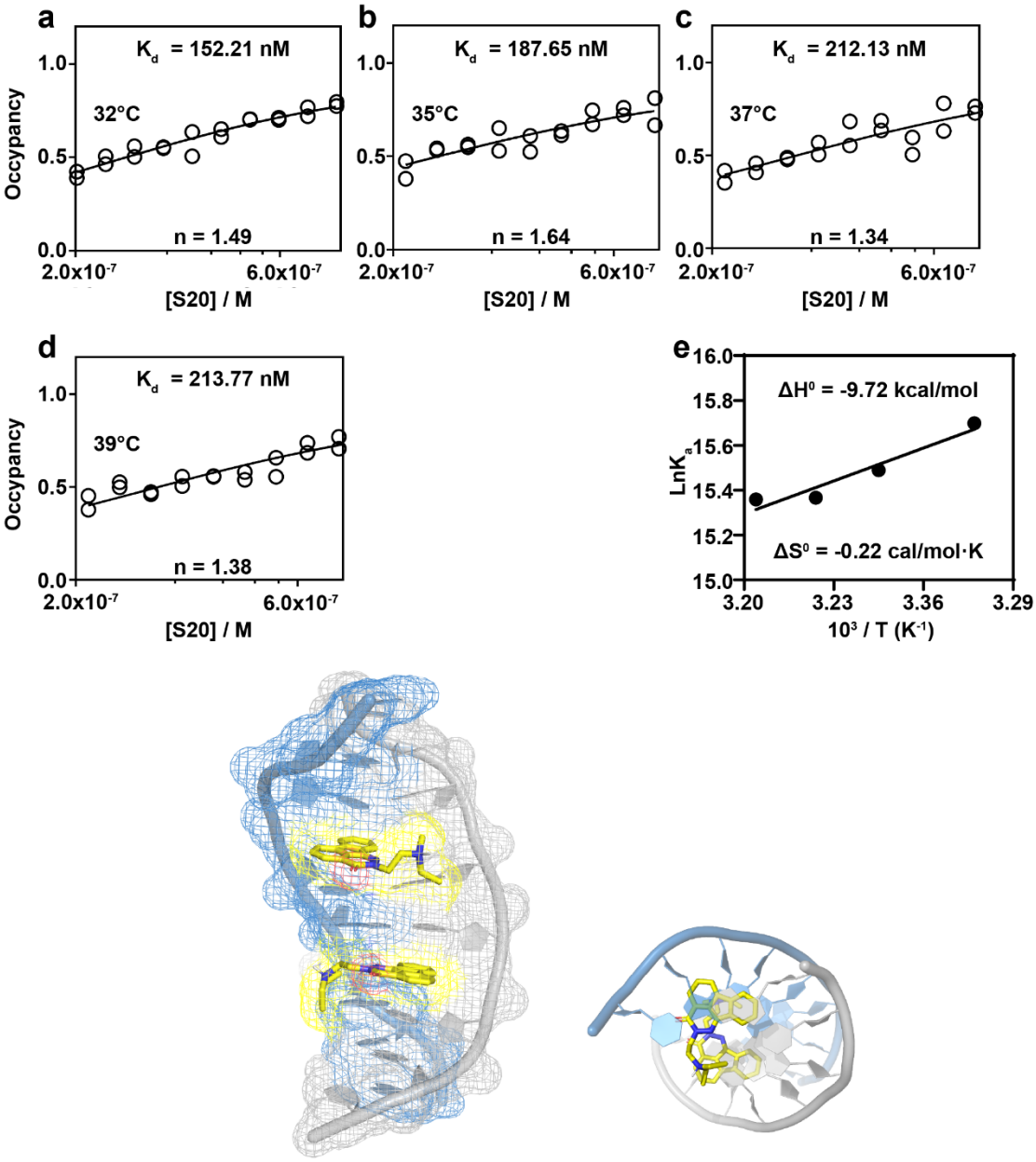

Fig. 7 | Profiling the binding thermodynamics of S20 using BIND. Binding curves established using the S_N1 region of BIND were used to determine the K_d at varying temperatures. A Van't Hoff plot was then established to determine ΔHº and ΔSº. The binding mode was further visualized by molecular docking. The DNA 3D image was extracted from PDB file 108D.

A cytotoxicity study revealed that S20 had broad-spectrum growth inhibitory activities against normal and cancer cells, with healthy cell inhibitory concentrations (IC 50) of 11.47 μM, 7.70 μM and 1.87 μM for NIH/3T3, HEK293T and RAW264.7

cells, respectively and with neoplastic cell IC 50 values of 13.07 μM, 18.26 μM and 94.68 μM for HeLa, HepG2 and A549 cells, respectively (Fig. 8).

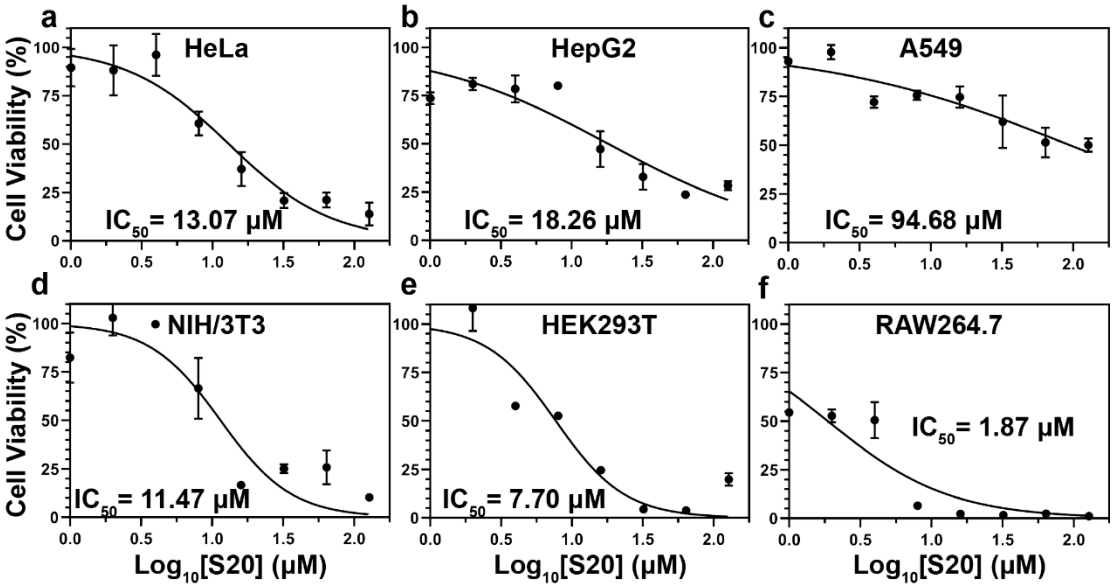

Fig. 8 | Cytotoxicity study (MTT assay) of S20 with three healthy cell lines and three neoplastic cell lines. Growth inhibition was researched for S20 against normal and cancerous cell lines, and significant growth inhibition was observed among all six lines of cells (**a-f**). The 50% inhibition concentration (IC_{50}) was 11.47 μM, 7.70 μM and 1.87 μM for NIH/3T3, HEK293T and RAW264.7 cells, respectively (healthy cell lines) and 13.07 μM, 18.26 μM and 94.68 μM for HeLa, HepG2 and A549 cells, respectively (neoplastic cell lines).

3.3 Discussion

For the first time, BIND enabled us to use HTS for small DNA binders that change the process of competitive binding against preintercalated ligands into collaboratively S_N2 promoted DNA strand displacement. To identify a novel small molecule with weak interaction with duplexed DNA, forceful removal of prebound EB/TO is no longer needed, as long as the EB/TO can occupy the empty and newly formed toehold region to facilitate an S_N2 DNA strand displacement reaction. The monitored channel can also be readily switched because it depended on the chemically modified fluorophore rather than monitoring the fixed wavelength of the EB or the TO channel, avoiding

fluorescence overlapping. DNA intercalators and groove binders shared quite a few structural similarities such as tricyclic/tetracyclic rings for DNA base stacking and heterocyclic and/or aromatic rings with an overall crescent shape (not perturbing the duplexed structure) for minor groove binding. Fluorescence excitation and emission peaks of duplexed DNA interacting small molecules are usually poorly spaced within the 300-550 nm range due to these structural similarities. Inevitably, the fluorescence of many new DNA binders overlapped with their competitor EB/TO and resulted in false-negative signals in FID HTS. Moreover, because BIND is practically simple to use with no need for specialized equipment or procedures, I anticipate that BIND will be widely adopted as a one-stop HTS and comprehensive characterization platform to accelerate the discovery of new DNA binders and DNA binding drugs.

As BIND is also a powerful characterization platform, I was able to further establish a comprehensive thermodynamic profile of the strongest hit, S20, in terms of its binding affinity, sequence selectivity, and enthalpy/entropy contributions to the binding thermodynamics. S20 was patented in 2012 as an interferon-inducting compound. Despite the low interferon induction activity, S20 showed relatively high cytotoxicity to MDCK cells (IC_{50} = 6.6 μM) compared to that of its derivative.[11] Our finding that S20 is also a strong DNA binder may also contribute to its high cytotoxicity.

However, using the tandem BIND assay excluded the possibility of finding neutral DNA binders and a positive formal charge was mandatory to facilitate an S_N2 strand displacement reaction. A possible solution to this flaw was to design and merge BIND with FID to develop an orthogonal HTS method since the FID HTS assay did not

discriminate binder charging status in small DNA binder identification.

3.4 Experimental

Table 1. DNA sequences and modifications

DNA Names		Sequences
BIND probes	**C**	5'-Cy5-AGGTTGGTGAGTGATTGGAGGTT-3'
	P	5'-AATCACTCACCAACCT- Iowa Black FQ-3'
	I	5'-AACCT CCAATCACTCACCAA CCT-3'
Sink Probes	**5'-ATTTA-3'**	5'-CGATTTACAAAAAGTAAATCG-3'
	5'-AATTG-3'	5'-CGAATTGCAAAAAGCAATTCG-3'
	5'-CATTC-3'	5'-CGCATTCCAAAAAGGAATGCG-3'
	5'-ATCTT-3'	5'-CGATCTTCAAAAAG AAGATCG-3'
	5'-AAGTC-3'	5'-CGAAGTCCAAAAAGGACTTCG-3'
	5'-CGAAG-3'	5'-CGCGAAGCAAAAAGCTTCGCG-3'
	5'-CCGAG-3'	5'-CGCCGAGCAAAAAGCTCGGCG-3'
	5'-CGCGG-3'	5'-CGCGCGGCAAAAAGCCGCGCG-3'

3.4.1 Methods

High-throughput screening of small-molecule DNA binders using BIND. Tandem BIND reactions performed in parallel in 96-well microplates were used to establish the HTS assay for discovering new DNA binders from a pool of 700 compounds collected from Selleck's express pick library. Briefly, the fluorescence signal of each BIND reaction mixture containing 20 nM CP and 10 nM I in 1 × TE buffer was suppressed by adding SG-I at a final concentration equal to its CBC (250 nM) and incubated at 37 °C for 10 min. To this reaction mixture, a candidate compound at a final concentration of 30 μM was added. After another incubation at 37 °C for 2 hours, endpoint fluorescence was measured using a BioTek Cytation 5 Multimode Microplate reader at excitation/emission wavelengths of 640 nm/675 nm. The fluorescence signal in each

well was normalized using the positive and negative controls as outlined above. Compounds with numeric values above the threshold (0.25) were considered positive hits and selected hits were subjected to subsequent thermodynamic characterization using BIND and thermal melting analysis.

Thermodynamic characterization of DNA-binder interactions using BIND. Endpoint fluorescence measurement was used to establish the BIND profile for measuring binding affinities and binding site sizes of DNA-binder interactions. Briefly, CP was diluted in 1 × TE buffer and then mixed with a given DNA binder at 37 °C for 5 min. Invader I was then added to this mixture to initiate the BIND reaction. The reaction mixture containing 10 nM I, 20 nM CP, and a given concentration of DNA binder was incubated at 37 °C for 2 hours before endpoint fluorescence measurement using a BioTek Cytation 5 Multimode Microplate reader by setting the excitation/emission wavelength at 640 nm/675 nm. The fluorescence signal was then normalized against the positive and negative controls as outlined above. The association binding constant Ka and binding site size n of each binder were then determined by fitting the fractional occupancy of bound binders using McGhee and Von Hippel's binding isotherm equation as follows:

$$Y = \frac{n\cdot(C_{binder}-C_{DNA}\cdot\frac{Y}{n})\cdot K_a\cdot(1-Y)^n}{(1-Y+\frac{Y}{n})^{(n-1)}} \quad (3)$$

where Y is the fractional occupancy of the bound binder, C_{binder} is the total binder concentration at each sample, C_{DNA} is the concentration of base pairs in CP (e.g., 20 nM CP consists of 320 nM base pairs), K_a is the association constant and n is the

binding site size. The value of Y was determined using the equation $Y = 1 – [(F – F_{CBC}) / (F_0 – F_{CBC})]$, where F is the normalized fluorescence signal of a given sample, F_{CBC} is the normalized fluorescence when the binder concentration equals its CBC and F_0 is the normalized fluorescence signal when no binder is added to the strand displacement system.

Binding enthalpy and binding entropy were determined by measuring Ka of a given biner using the BIND reaction at 27 °C, 30 °C, 32 °C, 35 °C, and 37 °C and then fit using Van't Hoff's equation as follows:

$$ln\ K_a = -\frac{\Delta H}{RT} + \frac{\Delta S}{R} \quad (4)$$

where K_a is the association constant, ΔH is the binding enthalpy, R is the universal gas constant, T is the temperature in Kelvin, and ΔS is the binding entropy.

Determining the sequence selectivity of DNA binders using BIND. The sequence selectivity of DNA binders was determined using a competitive BIND reaction between CP and stem-looped sink probes. Each sink prob was designed to contain an 8 bp stem domain of varying ATGC combinations and a 5 nt polydA loop domain. For a typical competitive BIND reaction, a given DNA binder was premixed with a sink probe in 1 × TE buffer at 37 °C for 2 hours. This reaction mixture was subsequently mixed with CP and I to initiate the BIND reaction using the protocol outlined above. The concentration ratios between the sink and CP probes were set to 2.5, 5, 10, 25, 50, and 100 in the competitive binding reaction. The threshold concentrations (C_T) that were defined as the binder concentration at 50% displacement yield at the S_N1 domain were then plotted against the sink/CP ratios to determine the selectivity factor α that was

defined as the slope of the fitted linear curve.

DNA oligonucleotides. All DNA oligonucleotides were purchased from Integrated DNA Technologies (IDT, Coralville, IA, United States) and were purified by IDT using high-performance liquid chromatography (HPLC). Sequences and modifications are listed in Table 1.

Selleck's express pick library L3600. The selected 700 compounds from Selleck's express pick library L3600 were generally provided by Dr. Deng, Department of Respiratory and Critical Care Medicine, Targeted Tracer Research and Development Laboratory, West China Hospital, Sichuan University, Chengdu, Sichuan, P.R. China, 610064.

Molecular Docking. To visualize the binding mechanism between DNA and binders, specific binding models were obtained by performing molecule docking. Specifically, the binding modes were visualized by PyMOL software. The binding modes of S20 were simulated by the molecular docking software Autodock 4.2. In detail, the .mol files of binders were obtained through Chemdraw software, and .pdb files of DNA were obtained through PDB ID 108D. In the preliminary preparations for the molecular docking, the binders were successively hydrogenated, detected root, chosen torsion and finally converted into PDBQT files, while DNAs were similarly hydrogenated, removed water molecules, calculated gaseiger, assigned AD4 type, and finally converted to PDBQT files. The grid box was uniformly set to contain the entire DNA structure. During the docking process, the Lamarckian genetic algorithm was used for binder-DNA docking. Among them, the maximum number of energy evaluations was

set to 2,500,000. The maximum number of generations was 27,000. The rate of gene mutation was 0.02. The rate of crossover was 0.8. The maximum number of top individuals that automatically survive was 1. Finally, I comprehensively evaluated and selected the optimal binding conformation of the binder and DNA according to the stable binding energy, which was visualized with PyMOL software.

Melting analysis of S20. Briefly, a mixture containing 200 nM CP and S20 in 1x TE buffer containing 20 mM NaCl was used at a final volume of 50 μL. The solution was then analyzed using an Analytik Jena qTOWER3G quantitative PCR system by a temperature program including an initial incubation at 20 °C for 15 min and then increasing the temperature at a rate of 0.5 °C per minute until 90 °C. The fluorescence signal was recorded at a data acquisition rate of 1 data point per minute. Fluorescence excitation and emission wavelengths were set at 640 nm/675 nm.

Cytotoxicity study (MTT assay) of S20 with three healthy and three neoplastic cell lines. Cells were seeded into 96-well plates (BIOFIL, catalog number TCP-011-096) at 1×10^4 cells per well and incubated for 12 h at 37 °C in 5% CO_2 to facilitate attachment. Cells were treated with different concentrations of compounds in DMEM with 10% FBS and then incubated for 24 h. Cells with no compounds added served as controls. After incubation, the old medium was removed, and the cells were washed with PBS once before the cell medium was replaced with 120 μL of fresh medium with MTT (0.5 mg/mL). The cells were incubated for another 1.5 h at 37 °C in 5% CO_2. Next, the medium was replaced with 100 μL of DMSO and cell viability was determined by measuring the absorbance at 595 nm. The cell viability values were expressed as

percentages and calculated as follows: Viability % = [Abs595 nm of treated sample) / [Abs595 nm of control] × 100%.

Reference

1. Desborough, M.J.R. & Keeling, D.M. The aspirin story - from willow to wonder drug. *Br J Haematol* **177**, 674-683 (2017).
2. Robert, A., Benoit-Vical, F., Liu, Y. & Meunier, B. in Essential Metals in Medicine: Therapeutic Use and Toxicity of Metal Ions in the Clinic 17-48 (2019).
3. Makurvet, F.D. Biologics vs. small molecules: Drug costs and patient access. *Medicine in Drug Discovery* **9** (2021).
4. Wang, M., Yu, Y., Liang, C., Lu, A. & Zhang, G. Recent Advances in Developing Small Molecules Targeting Nucleic Acid. *Int J Mol Sci* **17** (2016).
5. Sumner, A.T. Mechanisms of quinacrine binding and fluorescence in nuclei and chromosomes. *Histochemistry* **84**, 566-574 (1986).
6. Srivastava, S. et al. Quercetin, a Natural Flavonoid Interacts with DNA, Arrests Cell Cycle and Causes Tumor Regression by Activating Mitochondrial Pathway of Apoptosis. *Sci Rep* **6**, 24049 (2016).
7. Kuriakose, S. et al. Diminazene aceturate (Berenil) modulates the host cellular and inflammatory responses to Trypanosoma congolense infection. *PLoS One* **7**, e48696 (2012).
8. Glass, L.S., Bapat, A., Kelley, M.R., Georgiadis, M.M. & Long, E.C. Semi-automated high-throughput fluorescent intercalator displacement-based discovery of cytotoxic DNA binding agents from a large compound library. *Bioorg Med Chem Lett* **20**, 1685-1688 (2010).
9. Zhang, J.H., Chung, T.D. & Oldenburg, K.R. A Simple Statistical Parameter for Use in Evaluation and Validation of High Throughput Screening Assays. *J Biomol Screen* **4**, 67-73 (1999).
10. Busto, N. et al. Aggregation Features and Fluorescence of Hoechst 33258. *The Journal of Physical Chemistry B* **119**, 4575-4581 (2015).
11. Shaw, M., Ortigoza, M., Garcia-Sastre, A. & Palese, P. Interferon-Inducing Compounds and Uses Thereof. *US 0,308,608 A1* (2012).

Chapter 4

High-fidelity screening of small-molecule DNA binders using a single assay with dual orthogonal sensing mechanisms

Contribution statement

I performed all the work in this section.

4.1 Introduction

Duplexed DNA interacting with small molecules has been an intensive research focus over several decades, and the application of small DNA binders can be roughly divided into the following aspects: DNA sensing such as applying SYBR Green I for DNA tracing purposes;[1] disease treatment, such as prescribing doxorubicin as a chemotherapy agent for cancer bearing patients[2-4], and other chemical applications such as intercalating dsDNA with coralyne to make this nanostructure the smallest diode in the world.[5] I have also developed an HTS method based on BIND with much less screening bias compared with that of the FID method for charged binder discovery (Chapter 3). However, I must admit that BIND HTS could not identify any neutral binders which significantly hindered its ability to find noncharged small molecule binder drug leads or DNA tracing agents through this approach alone. Herein I designed and reported an orthogonal HTS method merging BIND with FID and successfully achieved a higher fidelity in screening duplexed DNA interacting small molecules without missing any neutral binder hits.

The introduction of applications of small binders especially for positively charged

ones has been thoroughly discussed within Chapters 1 & 3, therefore, the introduction within this chapter will mainly focus on uncharged small molecule binders binding with dsDNA.

Small neutral binder-DNA interactions are primarily directed by hydrophobic interactions, and quite a few interactions also benefit from coin-pile base stacking and hydrogen bonding. Compared with the three abovementioned driving forces, electrostatic interaction contributed the least among these four kinds of binding contributions.[6]

Almost all neutral binders to DNA contain a hydrophobic interacting core is usually buried between DNA grooves. Expanding our knowledge base on hydrophobic interactions could have at least four benefits in DNA nanotechnology. 1) As a major driving force in stabilizing the DNA duplexed structure, increasing hydrophobic interactions could increase DNA nanostructure biostability. 2) Hydrophobic interaction could facilitate DNA interactions with other bioconjugated structures, such as synthetic and biological membranes, drug delivery vectors and peptide-based cargos. 3) The hydrophobic interaction is highly tunable and adjustable. 4) Structural DNA nanotechnology would also be beneficial since hydrophobic interactions usually directed higher-order self-assembled DNA nanostructures.[7] As a result, extending our structural understanding in directing DNA self-assembly with hydrophobic interactions is in high demand. Exploring novel small molecules that could offer intense hydrophobic interactions to duplexed DNA structures could increase our structural knowledge within this field and might further enable us to couple noncharged binders

with DNA strands to fulfill complex biological tasks. A notable example was provided by Jones et al., who covalently linked duplexed DNA nanostructures with hydrophobic tags such as DNA binding cholesterol. These tags are small neutral hydrophobes that could stabilize the DNA duplexed structure in a buffer and more excitingly, when these DNA strands interacted with biological membranes, these small molecule tags helped the DNA nanostructure by increasing the lipophilicity. By changing the position of DNA linking and the hydrophobe structure, researchers could control the distribution of these DNA strands either clumped onto the surface of the cell membrane or penetrated through the double-lipid layer of the cell membrane.[8]

In this small neutral and charged binder-DNA interaction discovery HTS work, I applied EB as the new S_N1 pathway inhibiting agent and not only rescreened the 700 compounds examined previously by BIND (SG-I HTS) alone. I further screened additional 470 structures, making the total of tested compound number 1170 via this FID merged orthogonal BIND HTS method. The EB fluorescence channel and Cy5 fluorescence channel were monitored simultaneously to avoid missing any possible hits. As BIND predicted, when EB was at its CBC concentration and the CP-I triplex was at the most S_N1 inhibitory status, the introduction of a nonbinder neither promote the S_N2 pathway (Cy5 fluorescence held) nor displaces prebound EB (EB fluorescence held); the introduction of a positively charged binder would both facilitate S_N2 pathway displacement (Cy5 fluorescence increase) and prebound EB displacement (EB fluorescence decrease). For a neutral binder, as previously confirmed, the S_N2 promotion process required both specific binding and the protonated structure of the

small DNA binder, so that the S_N2 promotive activity was hindered (Cy5 fluorescence held), but the presence of the overwhelming amount of neutral DNA binder still bound into the duplexed region of CP, resulting in EB fluorescence attenuation. Based on this knowledge, this FID-incorporated HTS method can be used to screen neutral and charged binders, and to predict the binding small molecule's charging status simultaneously.

The orthogonal BIND HTS method is highly consistent with previous BIND HTS work as 7 of 8 previously found charged binders from Chapter 3 (700 pool) were found to be positive in S_N2 promotion in this orthogonal BIND HTS. In addition, there were no more charged hits identified within this pool of 700, rather, I discovered 2 possible neutral hits via EB fluorescence attenuation from this range of compounds. In addition to the 470 compounds added later, I identified 9 possible charged binders. One of the strongest hits among the newly identified charged binders was thoroughly parsed by BIND. The two potential novel neutral binders were subjected to DNA melting analysis and absorbance, one of them was confirmed and the other was denied as a neutral binder. I also performed a MTT assay on the thoroughly parsed charged hit and the one confirmed neutral hit for cell toxicity characterization.

4.2 Results

4.2.1 High-throughput screening of small molecular DNA binders using orthogonal BIND.

Knowing the mechanics behind BIND and successfully performing a HTS using SG-I introduced BIND, I aim to further develop an orthogonal BIND merging FID with

BIND together to discover new DNA binders in which neutral binders are no longer false-negative reported. The reason I applied EB instead of SG-I to suppress S_N1 displacement is that the EB FID for duplexed DNA interacting small molecule identification has already been well established and its parameters were optimized by previous work.[9] Additionally, similar to SG-I, EB could inhibit and promote strand displacement via the S_N1 and S_N2 pathways with the same algorithm as that of BIND. Therefore, this orthogonal BIND assay was designed and validated by programming S_N1 and S_N2 reaction pathways by adding two binders in sequence (EB and netropsin). Specifically, BIND was first induced by EB at a final concentration equal to its CBC (1 μM), and a secondary binder (netropsin) was then added to promote strand displacement via the S_N2 pathway. The cy5 fluorescence yield was found to increase monotonically as a function of binder concentration at the S_N2 region, rendering a potent assay for screening novel binders, additionally, the EB fluorescence was decreased with increasing concentrations of netropsin due to the FID effect. Since this assay monitored the double channel, there were a total of four combinations regarding positive/negative from each monitored fluorescence wavelength; thus, I specifically picked the following molecules for elucidation: charged binder berenil, charged binder thiazole orange, neutral binder actinomycin D and nonbinder 1-BQC. Both charged binders successfully promoted strand displacement in a S_N2 manner and both reflected with a positive reading through the cy5 channel. However, since the thiazole orange fluorescence partially overlapped with EB, I did not observe fluorescence attenuation of the EB channel after adding excessive amounts of thiazole orange into this reacting

mixture, which was opposite to the berenil result. The neutral binder actinomycin D failed to facilitate strand displacement via the S_N2 pathway, as BIND mechanics predicted, as a result, its cy5 channel showed a negative reading. This valuable chemotherapy agent lead would have been missed if I performed the BIND HTS alone, however, if I apply the orthogonal BIND HTS monitoring double channels, a positive reading would be returned from the EB FID channel indicated its interaction with dsDNA. Finally, with a DNA nonbinder, both channels showed negative data. To prove its potency in finding DNA binders, I rescreened 15 existing binders with this orthogonal HTS and analyzed each channel individually while assuming no prior knowledge. I found that the cy5 channel yielded identical results between SG-I (Fig. 2 from Chapter 3) and EB HTS in determining hit/miss within these 15 binders. Additionally, when EB FID results were added for consideration, a higher true positive screening rate was achieved (BIND displacement 80%, EB FID 60% and orthogonal: 93%) (Fig. 1).

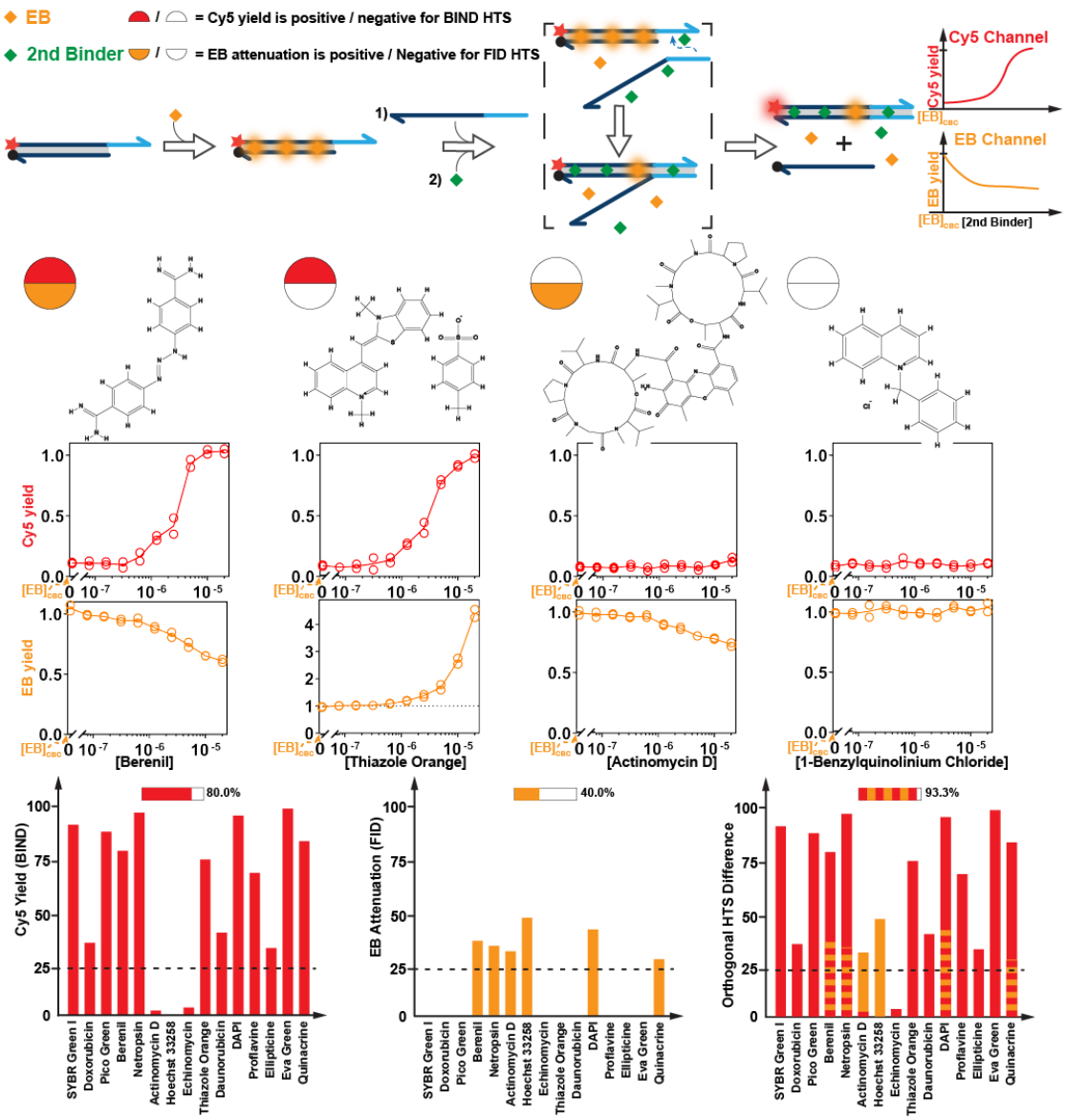

Fig. 1 | Algorithm of high-fidelity HTS with reduced false-negative rate. This orthogonal HTS identifying small DNA binders was achieved by monitoring the DNA displacement channel (cy5) and FID channel (EB) simultaneously. A total of four possible results with each of their typical molecules (charged binder without fluorescence overlapping, charged binding with fluorescence overlapping, neutral binder without fluorescence overlapping and charged nonbinder) were listed. Combining the results from these two channels in screening 15 known binders assuming no prior knowledge increased the true positive rate (combined 93% vs BIND displacement 80% and EB FID 40% respectively).

I then applied this orthogonal BIND assay for HTS of DNA binders, and netropsin and 1-BQC were used as P.C. and N.C., respectively. Using these two controls with each repeatedly tested 10 times produces Z' values to judge whether the difference in

response in this HTS assay is large enough to warrant further concerns. A Z' factor of 0.61 was determined when the BIND displacement (cy5) channel was monitored, in which fluorophores are covalently linked to one end of the DNA strand and a Z' factor of 0.31 was achieved when the intercalated EB channel was monitored at an assay concentration of 30 μM controls (Fig. 2).

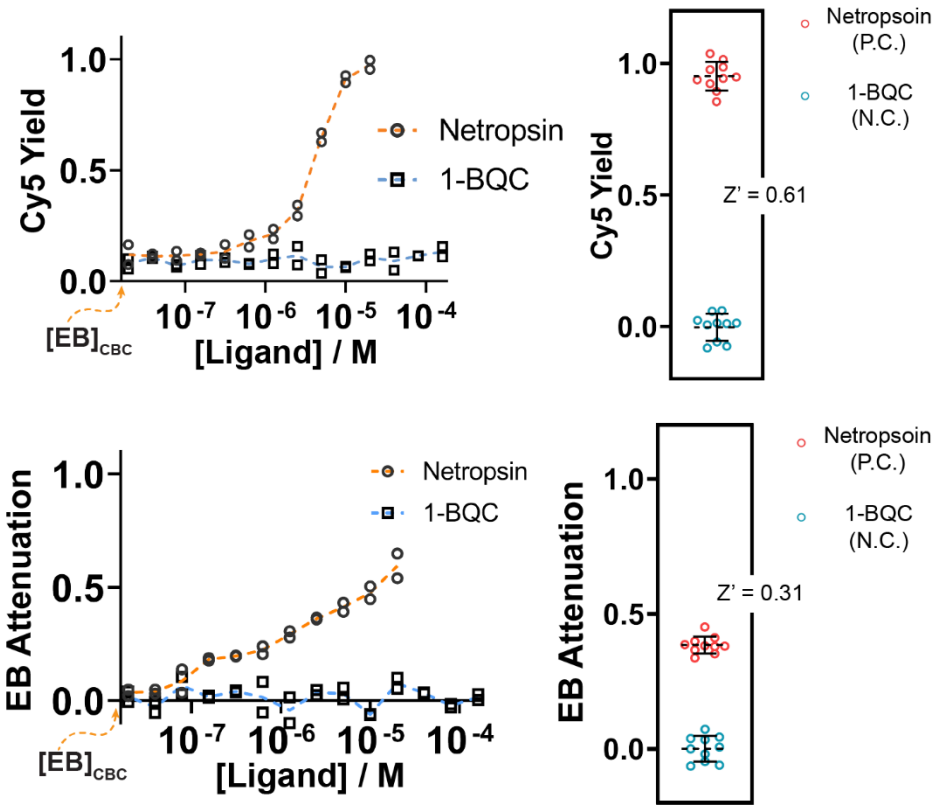

Fig. 2 | High-fidelity HTS validation via the Z' factor. Applying netropsin and 1-BQC as P.C. and N.C. with 10 repeated tests, a Z' factor of 0.61 was achieved for the strand displacement channel (cy5) indicating an excellent assay (top), a Z' factor of 0.31 was achieved for the FID channel (EB), indicating a marginal assay (bottom).

I finally applied the orthogonal BIND assay to discover new binders by screening against a pool containing 1170 compounds including 700 rescreened from the SG-I BIND HTS and 470 additional compounds collected from Selleck's express pick library L3600. This sublibrary was part of a collection of 4208 chemical compounds provided by Pfizer that featured with different pathway inhibitors and exhibited high structural

diversities. Identifying novel DNA binders will expand our knowledge of their mechanism of action on a structural basis, which provides further benefits for rationally designing duplexed DNA targeting small molecules. On the other hand, the discovered small DNA binding molecules might also provide good drug leads for anticancer and/or antimicrobial purposes. The threshold for the cy5 channel was optimized and set to 0.25, as Chapter 3 described, and the threshold for the EB channel was 0.25, in accordance with previous work.[9] Rescreening the pool of 700 plus screening the additional pool of 470 gives a total of 17 hits from the EB-introduced S_N2 strand displacement channel (Fig. 3).

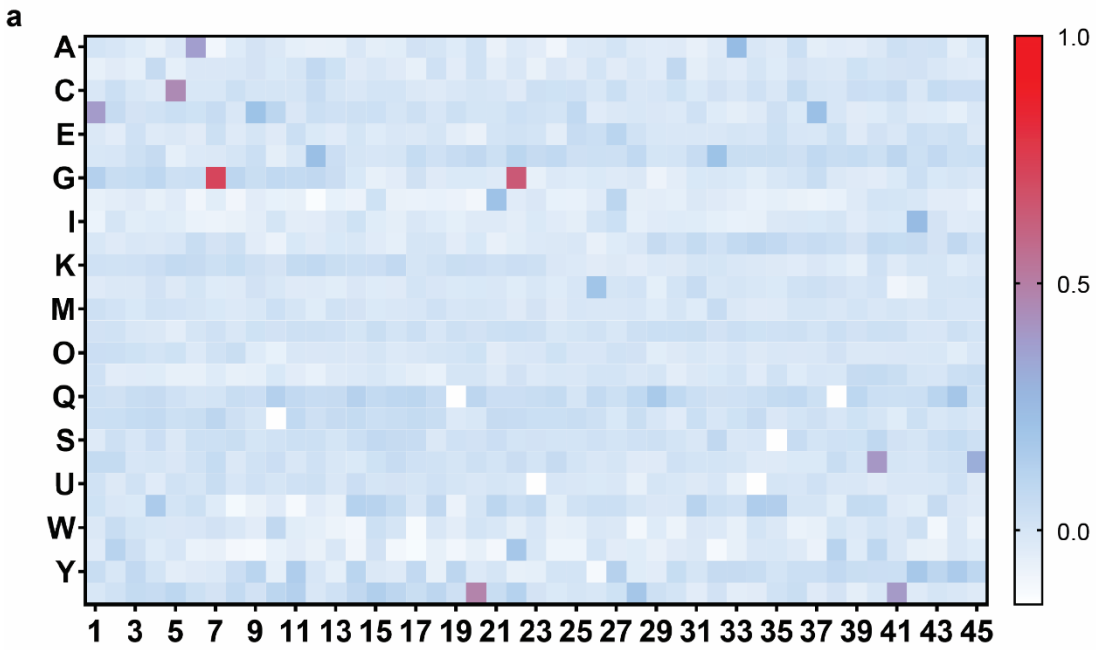

Fig. 3 | Heatmap of strand displacement channel (cy5) screening a total of 1170 compounds. A total of 17 hits (>25% S_N2 promotion) were identified using EB BIND HTS assay.

For the rescreened 700 small molecules, 7 of 8 identified charged binders from SG-I BIND HTS were returned as positive through BIND displacement yield initially suppressed by EB (Fig. 4). The only inconsistency, D6 (Q6 in SG-I BIND HTS, Chapter

3), was due to its weak or inexistant interaction with the duplexed DNA strand. In the SG-I HTS assay, this compound generated a value of 0.26 which was just above the cutoff (0.25) between hit and miss. Additionally, no more charged hits were found, rendering an overall accuracy rate of 99.9% (699/700) within these 700 structures, rendering high consistency between SG-I and EB BIND HTS (Fig. 4).

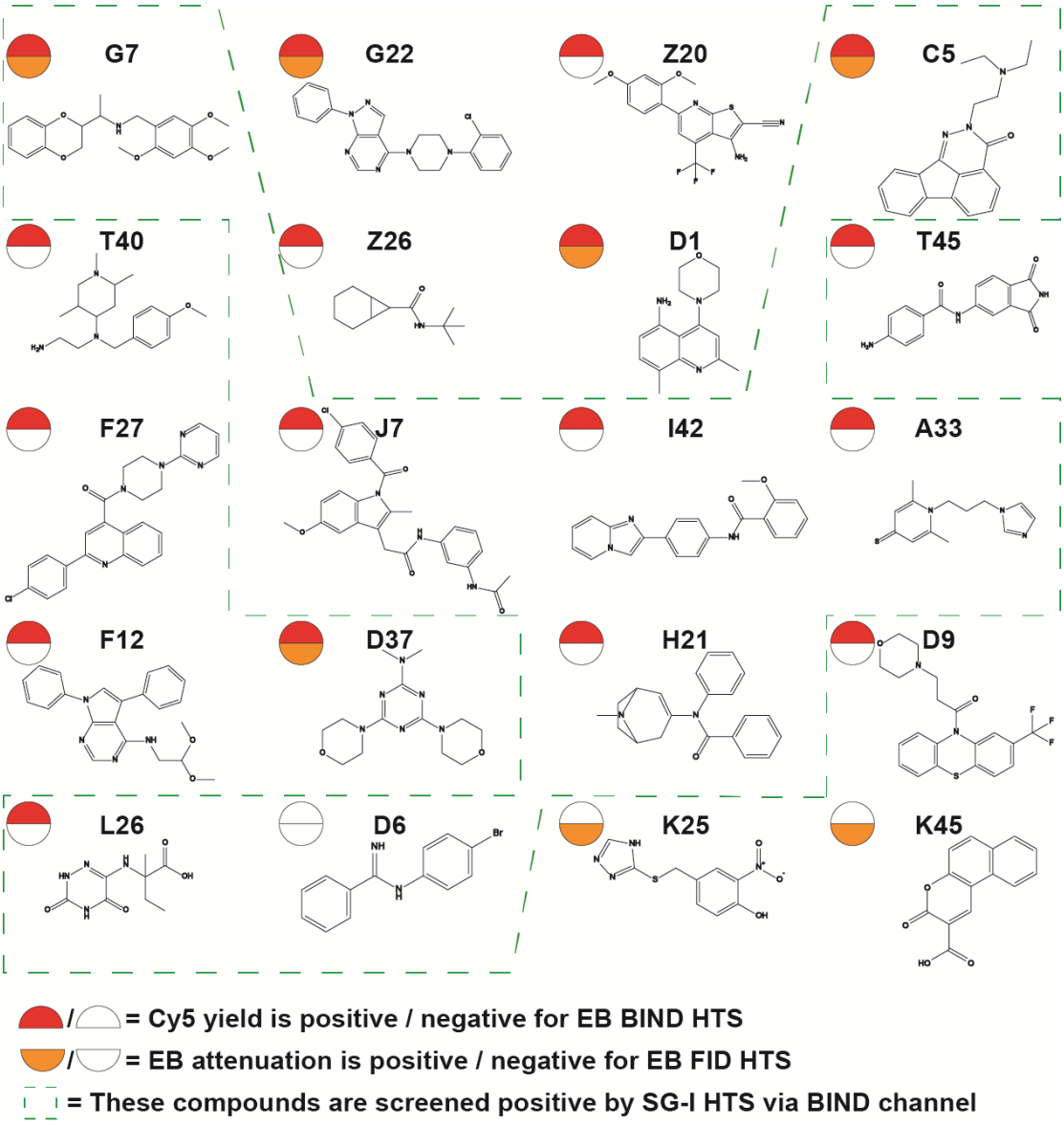

Fig. 4 | All possible binders identified by the EB orthogonal HTS and SG-I BIND HTS combined. K25 and K45 were also screened by SG-I HTS but due to the assay limitations, SG-I HTS could not recognize these two compounds as possible DNA binders. Binders were ranked by decreasing S_N2 promotion ability.

When analyzing the EB fluorescence results, it was not a surprise that only 5 of 17 EB BIND S_N2 strand displacement hits were positive in the intercalated EB channel, which was consistent with the knowledge that the EB FID suffered from significant screening bias, as concluded in Chapter 3 (Fig. 5). In addition, I identified two possible neutral hits (K25 and K45) with significant intercalated EB fluorescence attenuation without obvious cy5 fluorescence promotion (Figs. 4 and 5).

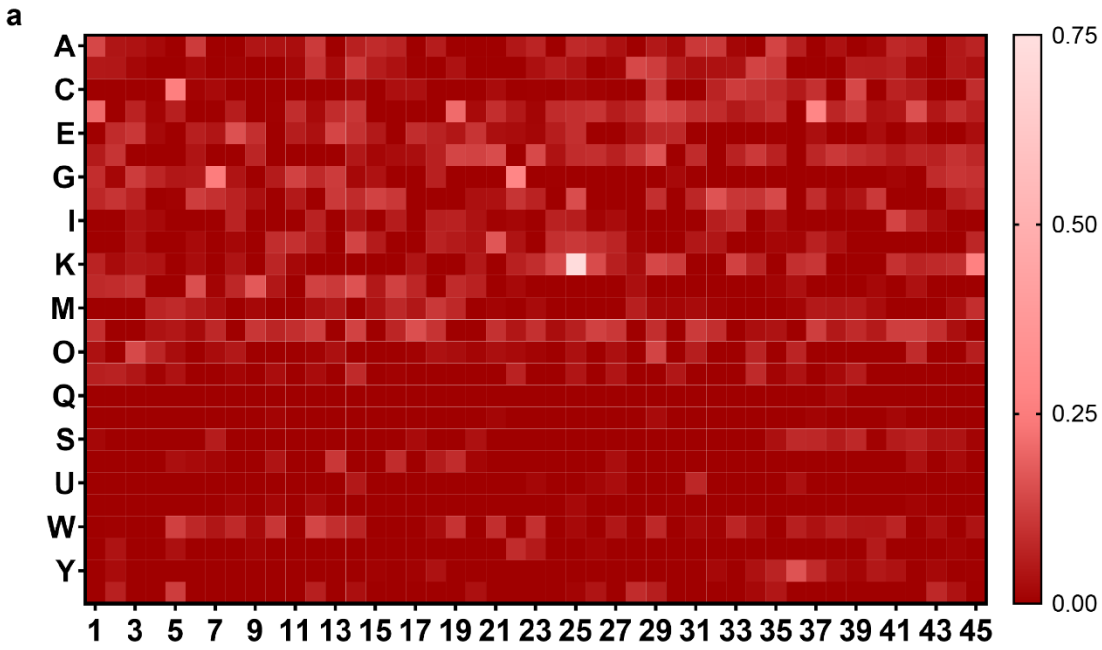

Fig. 5 | Heatmap of FID channel (EB) screening a total of 1170 compounds. A total of 7 possible hits were discovered by the FID channel (EB) individually: G7, G22, C5, D1 and D37 were found to be positive in the FID (EB) channel among the 17 positive results via the strand displacement channel (cy5). K25 and K45 possess near zero formal charge status so that they could not be identified via the BIND channel but were witnessed with significant EB fluorescence attenuation in the FID channel.

4.2.2 BIND curves and DNA melting analysis of one possible charged binder G22 and two possible neutral binders K25 and K45

G22, K25 and K45 were specifically picked for parsing by BIND and traditional parsing methods, and only G22 showed an inhibition-promotion fashion within its BIND curve. Additionally, G22 was confirmed by conventional DNA denaturation

research with its duplexed DNA binding ability (ΔT_m > 15 ºC at 20 μM), while neither of the two discovered possible neutral binders K25 and K45 could produce a ΔT_m greater than 1 ºC at 20 μM which means the traditional DNA denaturation research could not confirm that they exhibited DNA binding activity (Fig. 6).

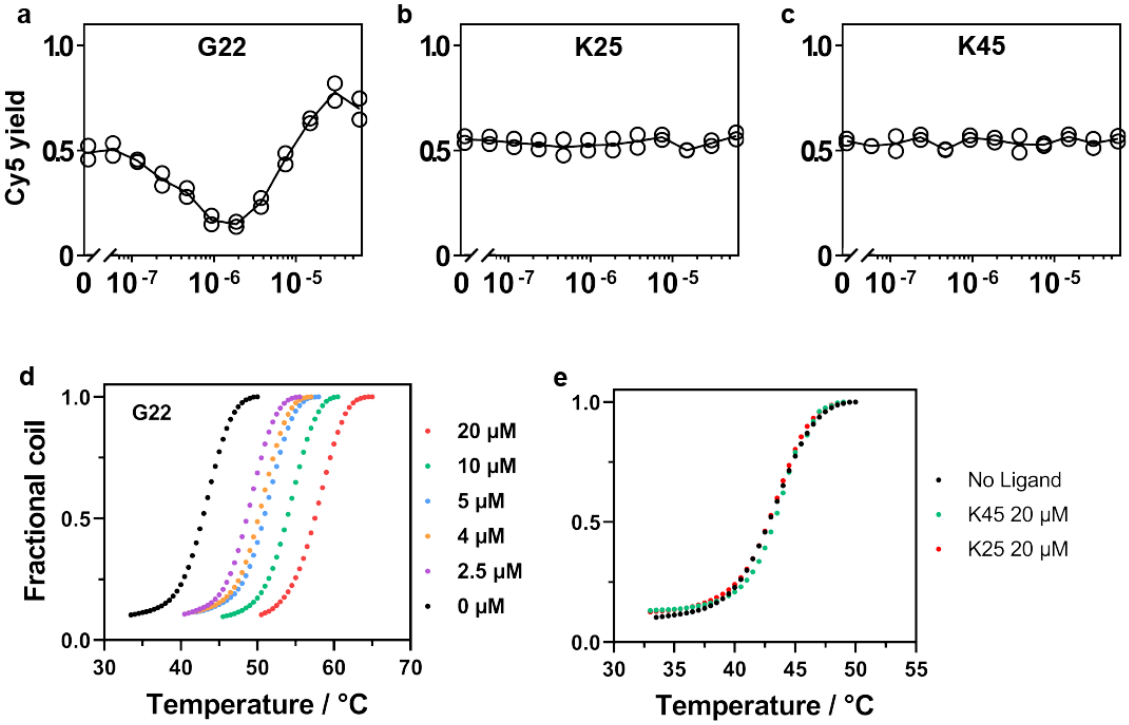

Fig. 6 | BIND curves and DNA denaturation research performed with bare DNA strands and DNA strands bound by 3 different binders. Only the BIND curve of G22 was witnessed with an S_N1 inhibition and S_N2 promotion region among three drug candidates (a-c). For the possible charged binder G22, the melting shift was increased with increased ligand concentration (d). For the possible neutral binders, both K25 and K45 failed to introduce a significant melting shift at 20 μM (ΔT_m > 1 ºC) (e).

Technically, a comparatively weak interaction between the binding ligand and dsDNA could not be proven by DNA denaturation research. Based on the theoretical calculations of the helix-coil transition of DNA reported by Dr. Mcghee, at the assay concentration (30 μM), to introduce a melting shift of 1 ºC, the target drug must have a binding dissociation constant value smaller than 10 μM, assuming its binding site size equals 2.[10]

4.2.3 Thermodynamic signature of charged binder G22 with dsDNA.

The confirmed charged binder G22 was thoroughly characterized by BIND as developed in Chapter 2. Parsing of this compound via BIND produced a K_d of 260 nM and a binding site size of 1.4. The BIND-characterized thermodynamic signature revealed that the binding of G22 to ds-DNA was enthalpically driven, the contribution of ΔH° was -8.06 kcal/mol and the contribution of -TΔS° was -1.22 kcal/mol. The high enthalpic contribution suggests that G22 is likely an intercalator, which was supported by molecular docking with a dsDNA model extracted from PDB file 108D (Fig. 7).

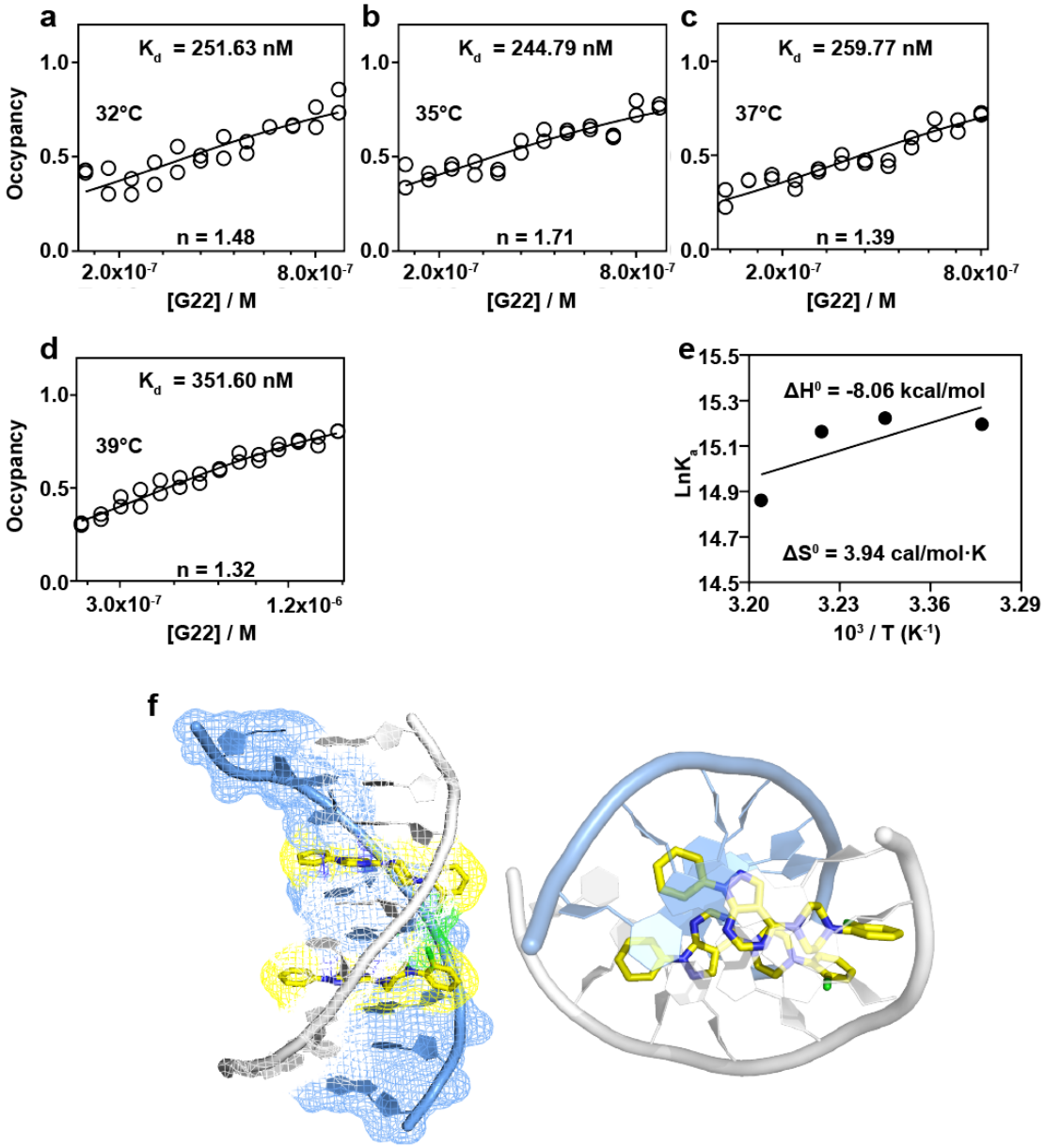

Fig. 7 | Profiling the binding thermodynamics of G22 using BIND. Binding curves established using the S_N1 region of BIND were used to determine the K_d at varying temperatures. A Van't Hoff plot was then established to determine ΔHº and ΔSº. The binding mode was further visualized by molecular docking as outlined in the experimental section. The DNA 3D image was extracted from PDB file 108D.

4.2.4 UV-vis absorption characterization of possible neutral binders K25 and K45 with dsDNA

UV-vis absorption spectroscopy identified extremely weak interactions between bound small molecules and dsDNA. In this section, increasing amounts of ds-DNA

were titrated against fixed amounts of binding ligand. A decrease in the binding molecule characteristic peak usually indicates binding activity.

The absorbance spectrum of K25 showed a characteristic peak at apporximately 430 nm, and I did not observe an absorbance peak decrease at a dye-to- base pair ratio of approximately 0.2. When the ratio of unpccupied NDA base paris to the unbound ligands was 5, absorption attenuation was absent, confirming that K25 did not interact with bare dsDNA (Fig. 8).[11] On the opposite side, two characteristic absorbance peaks were observed for compound K45 at 330 nm and 360 nm, and both peaks decreased monotonically with increasing amounts of titrated DNA base pairs (Fig. 9). Analyzing the absorbance peak with the Wolfe-Shimmer equation could reveal the binding affinity between the binder and target DNA.[12] The dissociation constant K_d was returned as 49.3 μM using the K45 absorption peak at 360 nm (Fig. 10). This further confirmed that a DNA binder with this weak interaction between dsDNA and the ligand itself (K_d > 10 μM) could not be recognized by DNA denaturation research at ligand concentration of 30 μM.

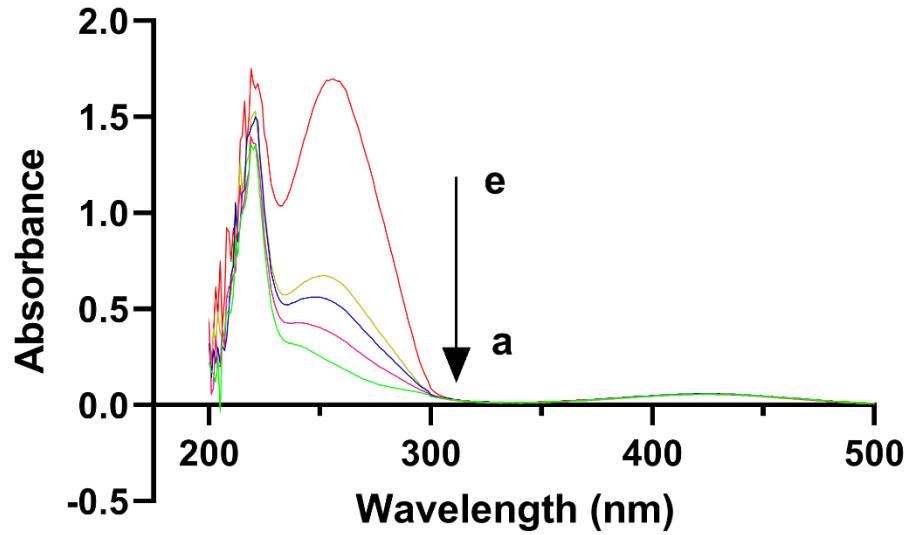

Fig. 8 | Absorption spectra of 20 µM K25 in the presence of dsDNA at different concentrations. A fixed concentration of possible neutral binder K25 was titrated with increasing concentrations of dsDNA base pairs (a: 0 µM, b: 10.4 µM, c: 20.8 µM, d: 31.2 µM and e: 104 µM), and a decrease in the characteristic absorption peak was not observed.

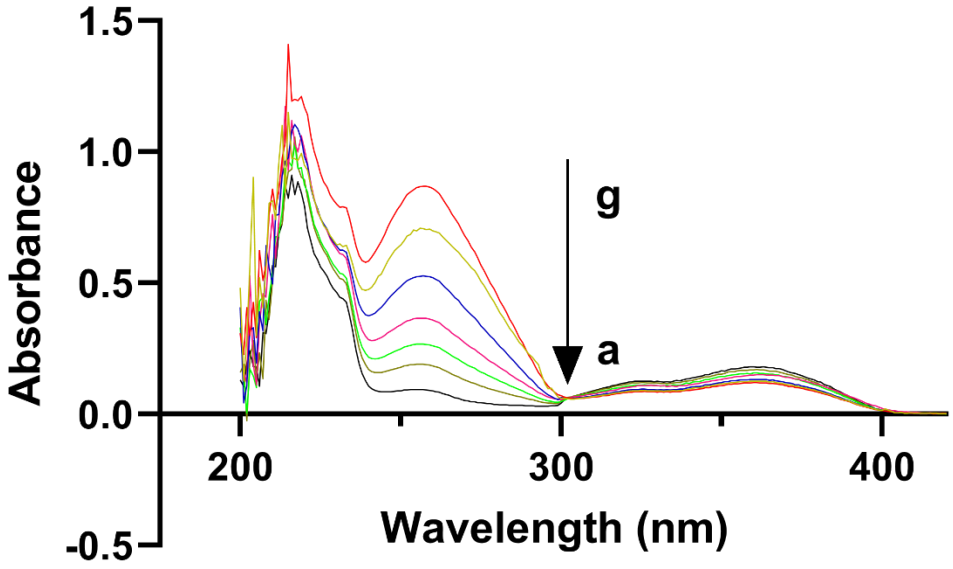

Fig. 9 | Absorption spectra of 10 µM K45 in the presence of dsDNA at different concentrations. A fixed concentration of possible neutral binder K45 was titrated with increasing concentrations of dsDNA base pairs (a: 0 µM, b: 5.2 µM, c: 10.4 µM, d: 15.6 µM, e: 31.2 µM, f: 41.6.2 µM and g: 52 µM), and both characteristic peaks at 330 and 360 nm were witnessed with decreasing absorption trend.

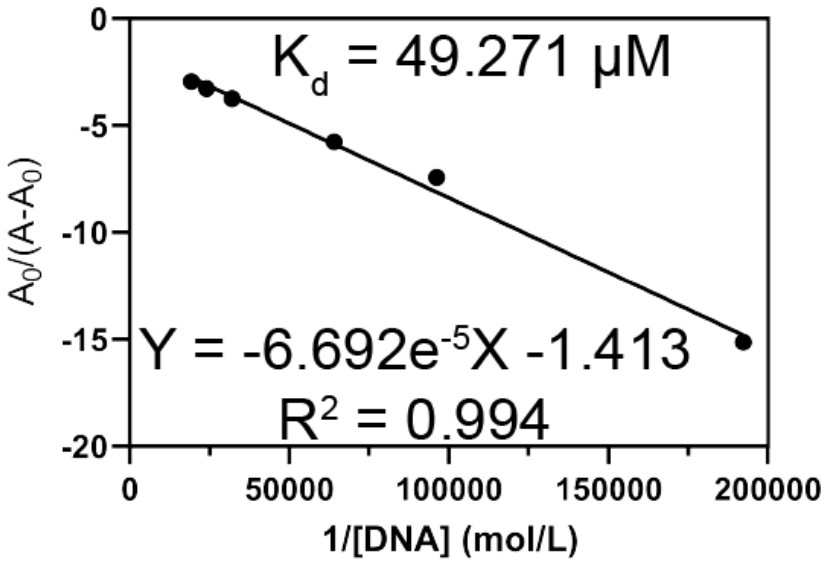

Fig. 10 | Analyzing K45 binding affinity to dsDNA with the Wolfe-Shimmer equation. A binding dissociation constant of 49.3 μM was returned when these data were linearly fitted with the Wolfe-Shimmer equation.

4.2.5 Sequence selectivity of G22 characterized by BIND

Positively charged binder G22 was characterized by BIND with its sequence selectivity. BIND revealed no sequence specificity of this binder toward either AT- or GC-rich sequences with αAT/αGC close to 1 (Fig. 11). Both neutral binders K25 and K45 were not characterized by BIND with sequence selectivity since neither of them was able to generate an S_N1 inhibition region on their BIND curves (Fig. 6).

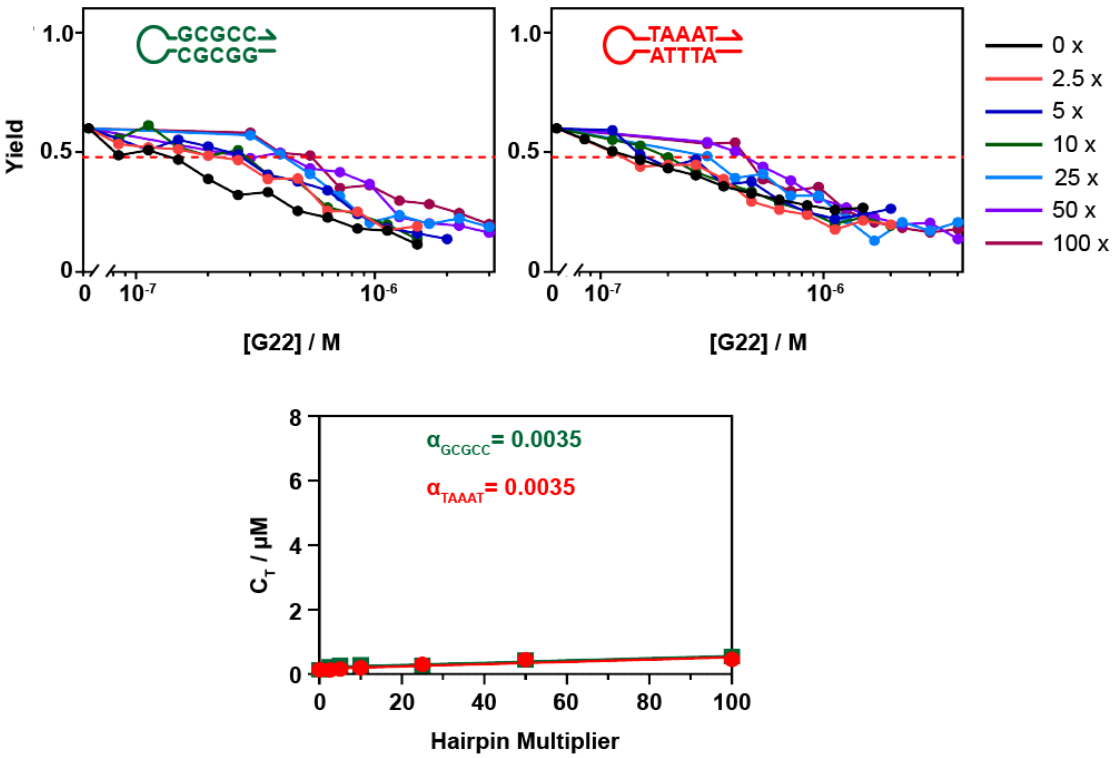

Fig. 11 | Determining the sequence selectivity of the newly discovered DNA binder G22 using GC and AT-rich sink probes.

4.2.6 Cytotoxicity study of charged binder G22 and neutral binder K45

MTT assays were constructed for three healthy cell lines and three cancerous cell lines to identify the cell toxicity behavior between these two binders (G22/K45) and cells. Neither of these novel DNA binders produced a significant cell growth inhibitory effect with all six cell lines (IC50 > 100 μM) (Fig. 12 and 13). These findings indicated that rational design on a structural basis to increase lipophilicity might be necessary to make these two compounds suitable drug leads, as cell killing effects are usually determined by both membrane penetrating ability and DNA binding affinity to a dsDNA binding agent.[13]

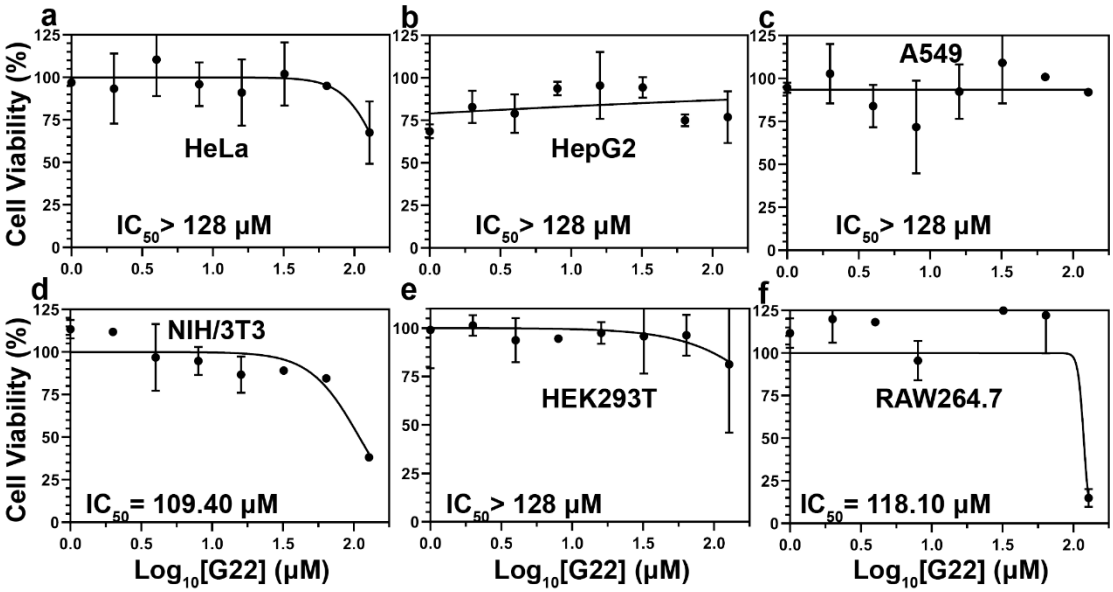

Fig. 12 | Cytotoxicity study (MTT assay) of G22 with three healthy cell lines and three neoplastic cell lines. Growth inhibition was researched for G22 against normal and cancerous cell lines, and there was no significant growth inhibition observed among all six lines of cells (**a-f**). The 50% inhibition concentration (IC_{50}) was 109.40 μM, above 128 μM and 118.10 μM for NIH/3T3, HEK293T and RAW264.7, respectively (healthy cell lines) and above 128 μM, above 128 μM and above 128 μM for HeLa, HepG2 and A549 respectively (neoplastic cell lines).

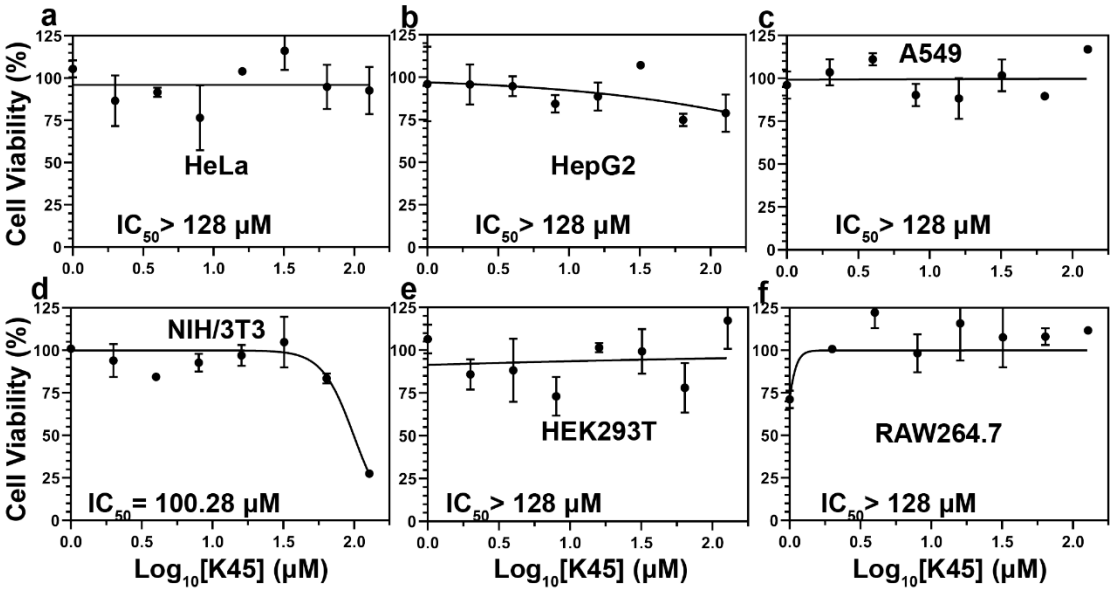

Fig. 13 | Cytotoxicity study (MTT assay) of K45 with three healthy cell lines and three neoplastic cell lines. Growth inhibition was researched for K45 against normal and cancerous cell lines, and there was no significant growth inhibition observed among all six lines of cells (**a-f**). The 50% inhibition concentration (IC_{50}) was 100.28 μM, above 128 μM and above 128 μM μM for NIH/3T3, HEK293T and RAW264.7, respectively (healthy cell lines) and above 128 μM, above 128 μM and above 128 μM for HeLa, HepG2 and A549 respectively (neoplastic cell lines).

4.3 Discussion

In Chapter 3, I proven that applying BIND individually could significantly reduce the false-negative rate, as BIND possessed low screening bias and its monitoring channel could be readily switched to avoid DNA binder fluorescence from overlapping. Using tandem BIND in HTS, small binder identification also misses all neutral hits and neutral DNA binders play an important role in defending us from infection, inflammation and malignancy. The FID HTS assay has long been reported for both charged and neutral binder identification but methods that apply FID individually usually suffers from high screening bias. In this chapter, I successfully merged BIND with FID and identified both charged and neutral binders from a chemical compound pool, in addition, I reported that this orthogonal HTS platform maintained both

advantages from these two HTS assays as follows: the screening window was large (Z' > 0.5)[14] and fluorescence overlapping from FID was avoided by BIND, while FID helped us rescue false-negative reported neutral binders from BIND displacement itself.

Both charged binder G22 and neutral binder K45 possessed low cytotoxicity to both healthy and neoplastic cell lines. The cytotoxicity to a DNA binder was determined by both duplexed DNA affinity and membrane penetration ability. Our findings indicated that either G22 or K45 needed rational designs to increase their membrane penetration ability as well as DNA binding affinity (especially to K45) to transform them into a capable drug lead for further medicinal chemistry research.

Theoretically and practically, I completed the last puzzle to formulate an HTS approach that could all-inclusively identify all kinds of small DNA binders without discriminating their charging status.

4.4 Experimental

Table 4.1. DNA sequences and modifications

DNA Names		Sequences
BIND probes	**C**	5’-Cy5-AGGTTGGTGAGTGATTGGAGGTT-3’
	P	5’-AATCACTCACCAACCT- Iowa Black FQ-3’
	I	5’-AACCT CCAATCACTCACCAA CCT-3’
Sink Probes	**5’-ATTTA-3’**	5’-CGATTTACAAAAAGTAAATCG-3’
	5’-AATTG-3’	5’-CGAATTGCAAAAAGCAATTCG-3’
	5’-CATTC-3’	5’-CGCATTCCAAAAAGGAATGCG-3’
	5’-ATCTT-3’	5’-CGATCTTCAAAAAG AAGATCG-3’
	5’-AAGTC-3’	5’-CGAAGTCCAAAAAGGACTTCG-3’
	5’-CGAAG-3’	5’-CGCGAAGCAAAAAGCTTCGCG-3’
	5’-CCGAG-3’	5’-CGCCGAGCAAAAAGCTCGGCG-3’
	5’-CGCGG-3’	5’-CGCGCGGCAAAAAGCCGCGCG-3’
Ligand Absorbance Probes	**LAP-1**	5’-GGTAGAGAACACGGACGAAACAT ACTGCATAGATAATGAAGC-3’
	LAP-2	5’-GCTTCATTATCTATGCAGTATGTT TCGTCCGTGTTCTCTACC-3’

4.4.1 Methods

High-throughput screening of small-molecule DNA binders using orthogonal BIND. Orthogonal tandem BIND reactions performed in parallel in 96-well microplates were used to establish the HTS assay. These assays were used to discover new DNA binders from a pool of 1170 compounds collected from Selleck’s express pick library. Briefly, the cy5 fluorescence signal of each BIND reaction mixture containing 20 nM CP and 10 nM I in 1 × TE buffer was maintained at its lowest level by adding EB at a final concentration equal to its CBC (1 μM) and incubated at 37 °C

for 10 min. A candidate compound at a final concentration of 30 μM was added to this reaction mixture. After another incubation at 37 °C for 2 hours, endpoint fluorescence was measured using a BioTek Cytation 5 Multimode Microplate reader at two pairs of excitation/emission wavelengths of 522 nm/593 nm and 640 nm/675 nm. The fluorescence signal in each well was normalized using the positive and negative controls as outlined above. Compounds with numeric values above the threshold (0.25) were considered positive hits and selected hits were subjected to subsequent thermodynamic characterization using BIND and thermal melting analysis.

Melting analysis of G22, K25 and K45. Briefly, a solution containing 200 nM CP and G22, K25, K45 and no drug candidate (N.C.) was mixed in 1x TE buffer containing 20 mM NaCl at a final volume of 50 μL. The solution was then analyzed using an Analytik Jena qTOWER3G quantitative PCR system by a temperature program including an initial incubation at 20 °C for 15 min and then increasing the temperature at a rate of 0.5 °C per minute until 90 °C. The fluorescence signal was recorded at a data acquisition rate of 1 data point per minute. Fluorescence excitation and emission wavelengths were set at 640 nm/675 nm.

Thermodynamic characterization of DNA-binder interactions using BIND. Endpoint fluorescence measurement was used to establish the BIND profile for measuring binding affinities and binding site sizes of DNA-binder interactions. Briefly, CP was diluted in 1 × TE buffer and then mixed with a given DNA binder at 37 °C for 5 min. Invader I was then added to this mixture to initiate the BIND reaction. The reaction mixture containing 10 nM I, 20 nM CP, and a given concentration of DNA

binder was incubated at 37 °C for 2 hours before an endpoint fluorescence measurement using a BioTek Cytation 5 Multimode Microplate reader by setting the excitation/emission wavelength at 640 nm/675 nm. The fluorescence signal was then normalized against the positive and negative controls as outlined above. The association binding constant Ka and binding site size n of each binder were then determined by fitting the fractional occupancy of bound binders using the McGhee and Von Hippel's binding isotherm equation as follows:

$$Y = \frac{n\cdot(C_{binder}-C_{DNA}\cdot\frac{Y}{n})\cdot K_a\cdot(1-Y)^n}{(1-Y+\frac{Y}{n})^{(n-1)}} \quad (1)$$

where Y is the fractional occupancy of the bound binder, C_{binder} is the total binder concentration at each sample, C_{DNA} is the concentration of base pairs in CP (e.g., 20 nM CP consists of 320 nM base pairs), K_a is the association constant and n is the binding site size. The value of Y was determined using the Equation Y = 1 – [(F – F_{CBC}) / (F_0 – F_{CBC})], where F is the normalized fluorescence signal of a given sample, F_{CBC} is the normalized fluorescence when the binder concentration equals its CBC and F_0 is the normalized fluorescence signal when no binder is added to the strand displacement system.

Binding enthalpy and binding entropy were determined by measuring Ka of a given biner using the BIND reaction at 27 °C, 30 °C, 32 °C, 35 °C and 37 °C and then fit using Van't Hoff's equation as follows:

$$ln\ K_a = -\frac{\Delta H}{RT} + \frac{\Delta S}{R} \quad (2)$$

where K_a is the association constant, ΔH is the binding enthalpy, R is the universal gas

constant, T is the temperature in Kelvin, and Δ*S*ias the binding entropy.

Determine sequence selectivity of DNA binders using BIND. The sequence selectivity of DNA binders was determined using a competitive BIND reaction between CP and stem-loop sink probes. Each sink prob was designed to contain an 8 bp stem domain of varying ATGC combinations and a 5 nt polydA loop domain. For a typical competitive BIND reaction, a given DNA binder was premixed with a sink probe in 1 × TE buffer at 37 °C for 2 hours. This reaction mixture was subsequently mixed with CP and I to initiate the BIND reaction using the protocol outlined above. The concentration ratios between the sink and CP probes were set to 2.5, 5, 10, 25, 50, and 100 in the competitive binding reaction. The threshold concentrations (C_T) that were defined as the binder concentration at 50% displacement yield at the S_N1 domain were then plotted against the sink/CP ratios to determine the selectivity factor α that was defined as the slope of the fitted linear curve.

DNA oligonucleotides. All DNA oligonucleotides were purchased from Integrated DNA Technologies (IDT, Coralville, IA, United States) and were purified by IDT using high-performance liquid chromatography (HPLC). Sequences and modifications are listed in Table 1.

Selleck's express pick library L3600. The 1170 compounds picked from Selleck's express pick library L3600 were generally provided by Dr. Deng, Department of Respiratory and Critical Care Medicine, Targeted Tracer Research and Development Laboratory, West China Hospital, Sichuan University, Chengdu, Sichuan, P.R. China, 610064.

Molecular docking. To visualize the binding mechanism between DNA and binders, specific binding models were obtained by performing molecule docking. Specifically, the binding modes were visualized by PyMOL software. The binding modes of G22 were simulated by the molecular docking software Autodock 4.2. In detail, the .mol files of binders were obtained through Chemdraw software, and .pdb files of DNA were obtained through PDB ID 108D. In the preliminary preparations for the molecular docking, the binders were successively hydrogenated, detected root, chosen torsion and finally converted into PDBQT files, while DNAs were similarly hydrogenated, removed water molecules, calculated gaseiger, assigned AD4 type, and finally converted to PDBQT files. The grid box was uniformly set to contain the entire DNA structure. During the docking process, the Lamarckian genetic algorithm was used for binder-DNA docking. Among them, the maximum number of energy evaluations was set to 2,500,000. The maximum number of generations was 27,000. The rate of gene mutation was 0.02. The rate of crossover was 0.8. The maximum number of top individuals who automatically survive was 1. Finally, we comprehensively evaluated and selected the optimal binding conformation of the binder and DNA according to the stable binding energy, which were visualized with PyMOL software.

Ligand absorbance research. K25 (20 μM) and K45 (10 μM) were dissolved in 1xTE buffer containing 100 mM NaCl with increasing concentrations of duplexed DNA structures (preheated and reannealed ss-DNA LAP-1 and ss-DNA LAP-2) titrated against fixed concentrations of ligands. Absorbance spectra of different equilibriums of DNA base pairs to ligand were acquired by Thermo Evolution 201 UV-vis

spectrophotometer between 200 nm and 500 nm. Characteristic peaks were identified and recorded for fitting of the Wolfe-Shimmer equation.

Cytotoxicity study (MTT assay) of G22 and K45 with three healthy and three neoplastic cell lines. Cells were seeded into 96-well plates (BIOFIL, catalog number TCP-011-096) at 1×10^4 cells per well and incubated for 12 h at 37 °C in 5% CO_2 to facilitate attachment. The cells were treated with different concentrations of compounds in DMEM with 10% FBS and then incubated for 24 h. The cells with no compounds added served as controls. After incubation, the old medium was removed, and the cells were washed with PBS once before cell medium was replaced with 120 μL of fresh medium with MTT (0.5 mg/mL). The cells were incubated for another 1.5 h at 37 °C in 5% CO_2. Next, the medium was replaced with 100 μL of DMSO and cell viability was determined by measuring the absorbance at 595 nm. The cell viability values were expressed as percentages and calculated as follows: Viability % = [Abs595 nm of treated sample) / [Abs595 nm of control] × 100%.

1. Dragan, A.I. et al. SYBR Green I: fluorescence properties and interaction with DNA. *J Fluoresc* **22**, 1189-1199 (2012).
2. Blumenfeld, C.M. et al. Drug capture materials based on genomic DNA-functionalized magnetic nanoparticles. *Nat Commun* **9**, 2870 (2018).
3. Pang, B. et al. Drug-induced histone eviction from open chromatin contributes to the chemotherapeutic effects of doxorubicin. *Nat Commun* **4**, 1908 (2013).
4. Wang, S. et al. Arginine-Rich Manganese Silicate Nanobubbles as a Ferroptosis-Inducing Agent for Tumor-Targeted Theranostics. *ACS Nano* **12**, 12380-12392 (2018).
5. Guo, C. et al. Molecular rectifier composed of DNA with high rectification ratio enabled by intercalation. *Nat Chem* **8**, 484-490 (2016).
6. Almaqwashi, A.A., Paramanathan, T., Rouzina, I. & Williams, M.C. Mechanisms of small molecule-DNA interactions probed by single-molecule force spectroscopy. *Nucleic Acids Res* **44**, 3971-3988 (2016).
7. Xiao, F., Chen, Z., Wei, Z. & Tian, L. Hydrophobic Interaction: A Promising Driving Force

for the Biomedical Applications of Nucleic Acids. *Advanced Science* **7** (2020).

8. Jones, S.F. et al. Hydrophobic Interactions between DNA Duplexes and Synthetic and Biological Membranes. *Journal of the American Chemical Society* **143**, 8305-8313 (2021).
9. Glass, L.S., Bapat, A., Kelley, M.R., Georgiadis, M.M. & Long, E.C. Semi-automated high-throughput fluorescent intercalator displacement-based discovery of cytotoxic DNA binding agents from a large compound library. *Bioorg Med Chem Lett* **20**, 1685-1688 (2010).
10. McGhee, J.D. Theoretical calculations of the helix-coil transition of DNA in the presence of large, cooperatively binding ligands. *Biopolymers* **15**, 1345-1375 (1976).
11. Benesi, H.A. & Hildebrand, J.H. A Spectrophotometric Investigation of the Interaction of Iodine with Aromatic Hydrocarbons. *Journal of the American Chemical Society* **71**, 2703-2707 (2002).
12. Hajian, R., Hossaini, P., Mehrayin, Z., Woi, P.M. & Shams, N. DNA-binding studies of valrubicin as a chemotherapy drug using spectroscopy and electrochemical techniques. *Journal of Pharmaceutical Analysis* **7**, 176-180 (2017).
13. Bhaduri, S., Ranjan, N. & Arya, D.P. An overview of recent advances in duplex DNA recognition by small molecules. *Beilstein J Org Chem* **14**, 1051-1086 (2018).
14. Zhang, J.H., Chung, T.D. & Oldenburg, K.R. A Simple Statistical Parameter for Use in Evaluation and Validation of High Throughput Screening Assays. *J Biomol Screen* **4**, 67-73 (1999).

Chapter 5

Conclusion and future works

In summary, we developed a new approach for tuning dynamic DNA nanotechnology, as well as two new HTS assays for duplexed DNA interacting small molecule discovery.

We designed, mathematically simulated, experimentally proved a brand-new DNA strand displacement reaction governed by duplexed DNA interacting small molecules (BIND). In this reaction, increasing the DNA binder concentration could switch the dominant DNA strand displacement reaction pathway from S_N1 to S_N2. We not only achieved this amazing phenomenon but also further developed this DNA binder introduced DNA strand displacement reaction into a comprehensive DNA binder characterization method through which almost all key binding parameters (binding affinity, binding site size, binding enthalpy and binding entropy as well as sequence specificity) could be reported by this single experimental design (Chapter 2).

We also found that only the duplexed DNA binding ligand could introduce a sigmodal structure of the strand displacement curve in this DNA strand displacement reaction. Based on this conclusion, we designed an HTS assay specifically for dsDNA interacting small molecule discovery and successfully identified 8 possible binding ligands from a pool of 700 chemical structures of different pathway inhibitors. We also thoroughly characterized one of the eight hits with BIND. We found that BIND-based HTS exhibited a lower screening bias than that of conventionally applied FID HTS

(Chapter 3).

Although BIND HTS had an overall lower false-negative rate in the identification of duplexed DNA interacting small molecule, none of the neutral DNA binders could be screened positive with this method as the neutral binder could not introduce S_N2 strand displacement promotion. Herein, we merged the FID with BIND mechanics and developed and validated an orthogonal HTS method for finding small DNA binders without discriminating their charging status. We have successfully identified 17 charged binders and a novel neutral binder. In particular, if no data were reported from the FIA channel, to the discovered novel neutral binder would have been missed. (Chapter 4).

Generally, we have witnessed a handful of DNA nanotechnologies that incorpate duplexed DNA interacting small molecules to apply their DNA binding and stabilizing traits. However, none of these technologies were designed to react in a metal ion-free buffer; thus, the individual effect that a small DNA binder exerted to a specific dynamic DNA nanotechnology reaction has never been thoroughly researched. In BIND, we scrutinized the interaction between DNA binders and DNA strands without interference from positively charged metal ions (counterion effect). We observed and systematically predicted and mathematically simulated a series of brand-new DNA strand displacement reactions controlled solely by a DNA binder; retrospectively, these novel DNA strand displacement reactions could be applied to thoroughly parse small-molecule DNA interactions. We further developed the following types of small DNA binder HTS methods, one was based on BIND alone which could be applied for positively charged DNA binder discovery; the other was an orthogonal HTS platform

merging BIND with the conventional method FID. The orthogonal HTS introduced later has much lower screening bias and solved one critical design flaw from BIND; it can be used to screen neutral binders rather than providing false-negative results from BIND individually. Although the small DNA binders have been used by humans for centuries to cure disease, very few methods have been developed for HTS assay application (FID might be the only example).

We hope our findings will further our knowledge of small molecule-DNA interactions, expand our toolbox to shape DNA structures and controll dynamic DNA reactions and contribute to identify novel small DNA binders to trace DNA and cure disease.

BIND and its HTS approaches derived from BIND have the following limitations: the dynamic DNA reactions in BIND do not sustain many positively charged metal ions since the presence of positively charged ions offsets the electrostatic repulsion between negatively charged DNA backbones through the counterion effect, and the hinderance of spontaneous dissociation between C and P neutralizes the S_N1 inhibition introduced by low concentrations of DNA binders so that the initial suppression region of DNA stand displacement in BIND does not appear. One of the possible solutions is to shorten the DNA strands and make them unstable even in the presence of high metal ion concentrations; thus, the initial inhibition introduced by the initial DNA binder could possibly be observed and parsed. On the other hand, BIND could not characterize binders with weak duplexed DNA stabilizing effects, which might be solved by analyzing the S_N1 inhibition region within the BIND curve tuned by the cooperative

inhibitory effect between characterized strong binders and characterized weak binders.

We could also expand BIND into protein-dsDNA or small binder-RNA interactions with the same algorithm, and the success of these transformations would benefit us in the search for specific segments of DNA interacting protein molecules or help expand our knowledge of RNA interacting small molecules and help characterize these two types of interactions.

From the humble beginnings of my PhD study years ago, we have forged a brand-new DNA nanotechnology method that could hopefully withstand time itself. Though countless chemical innovations rise and fall around us, we wish our BIND not only just survive, we wish out BIND prosper.